ISSN 2717-7203

JOURNAL OF ADVANCES IN MANUFACTURING ENGINEERING

JAME

Volume 6
Number 2
Year 2025 - December

YTÜ PRESS

www.jame.yildiz.edu.tr

ISSN 2717-7203

JOURNAL OF ADVANCES IN MANUFACTURING ENGINEERING

Volume 6 Number 2 Year 2025 - December

ISSN 2717-7203

JOURNAL OF ADVANCES IN MANUFACTURING ENGINEERING

Volume 6 Number 2 Year 2025 - December

Murat YAZICI

Department of Automotive Engineering, Bursa Uludağ University, Bursa, Türkiye

Mustafa Cemal ÇAKIR

Department of Mechanical Engineering, Bursa Uludağ University, Bursa, Türkiye

Navneet KHANNA

Institute of Infrastructure Technology Research and Management (IITRAM), India

Orhan ÇAKIR

Department of Mechanical Engineering, Yıldız Technical University, İstanbul, Turkiye

Tolga MERT

Department of Mechanical Engineering, Yıldız Technical University, İstanbul, Türkiye

Yusuf KAYNAK

Department of Mechanical Engineering, Marmara University, İstanbul, Türkiye

Abstracting and Indexing: EBSCO, TUBITAK TR Index, Bielefeld Academic Search Engine (BASE), ResearchBible, Directory of Research Journals Indexing (DRJI), Scilit, Google, Ideal Online, ASCI, DOAJ

Journal Description: The journal is supported by Yıldız Technical University officially, and is a blind peer-reviewed free open-access journal, published bimontly (June-December).

Publisher: Yıldız Technical University

Editor-in-Chief: Prof. Alper UYSAL

Language of Publication: English

Frequency: 2 Issues

Publication Type: Online e-version

Publisher: Kare Publishing

ISSN 2717-7203

JOURNAL OF ADVANCES IN MANUFACTURING ENGINEERING

JAME

Volume 6 Number 2 Year 2025 - December

CONTENTS

J Adv Manuf Eng, Vol. 6, Issue. 2, pp. 56–67, December, 2025

Journal of Advances in Manufacturing Engineering
Web page info: https://jame.yildiz.edu.tr
DOI: 10.14744/ytu.jame.2025.00007

Original Article

Cutting force estimation in turning of AISI 1117 free-cutting steel using machine learning algorithms

Kadir ÖZDEMİR[*1], Ulvi ŞEKER[2], Mustafa Cemal ÇAKIR[3]

[1]*Istanbul Health and Technology University, Faculty of Engineering and Natural Sciences Mechatronics Engineering, İstanbul, Türkiye*
[2]*Gazi UniversityFaculty of Technology, Ankara, Türkiye*
[3]*Department of Mechanical Engineering, Bursa Uludağ University Faculty of Engineering, Bursa, Türkiye*

ARTICLE INFO

Article history
Received: 22 March 2025
Revised: 10 July 2025
Accepted: 24 July 2025

Key words:
Cubic support vector machine, cutting forces, free cutting steel, gaussian process regression, machine learning, machining.

ABSTRACT

This research investigates how effectively machine learning algorithms can predict cutting forces during machining, offering a practical alternative to conventional experimental and numerical methods. The experiments included turning AISI 1117 steel with a cemented carbide insert on a CNC lathe while changing the cutting speed, feed rate, and depth of cut in a planned way. Cutting force data was collected using a Kistler 9257B dynamometer and used to train and test several regression-based machine learning models. These included cubic support vector machine (SVM), gaussian process regression (GPR), various forms of linear regression, decision trees, and ensemble techniques. Two modelling scenarios were analysed: one using cutting speed and feed rate as input variables, and the other using depth of cut as a third input. In the two-variable case, cubic SVM showed the best performance (R^2=0.93, root mean squared error [RMSE]=19.57), while GPR with a Matern 5/2 kernel achieved the highest accuracy in the three-variable model (R^2=0.99, RMSE<40). Model performance was assessed using metrics such as R^2, RMSE, mean squared error, and mean absolute error, with R^2 and RMSE being most effective for comparisons. The findings indicate that while cubic SVM is suitable for simpler, lower-dimensional data, GPR performs better in capturing complex, non-linear relationships among multiple variables.

Cite this article as: Özdemir, K., Şeker, U., & Çakır, M. C. (2025). Cutting force estimation in turning of AISI 1117 free-cutting steel using machine learning algorithms. *J Adv Manuf Eng*, 6(2), 56–67.

INTRODUCTION

This study aims to evaluate which learning algorithm provides the most accurate predictions using machine learning (ML) methods and to compare the algorithms that produce the best findings.

The finite element method has been the leading numerical methodology in this field for a long time. Recently, ML and artificial intelligence have become significant methodologies for handling engineering difficulties. The advantage of predictive or learning methodologies is in the ability to reduce the resolution times of problems that are difficult to address using the finite element method, enabling faster solution acquisition. Finite element software can integrate learning or predictive methodologies, either in conjunction to minimise solution time or separately to attain the solution. When precise modelling approaches and assumptions are used, numerical solution methods, such as the finite el-

***Corresponding author.**
*E-mail address: kadirzdemir@gmail.com

ement method, produce results that closely correspond to experimental data. Artificial intelligence or ML systems can use the finite element method to reproduce data. Concurrently, it can reduce the time and financial resources spent on studies by obtaining data that is inaccessible through experimental methods.

ML is a specialised field in artificial intelligence that involves creating models and algorithms to analyse current data using mathematical and statistical techniques. These models are then used to generate predictions about unknown data based on the patterns and insights derived from the analysis. The primary objective of ML is to provide precise estimations. Nevertheless, comprehending the prediction functions and linking them to a particular probability model may present challenges [1].

Machining processes, fundamental to manufacturing procedures, generate outputs including cutting forces, temperature, surface roughness, tool wear, and tool vibrations, all of which directly influence production quality. Researchers have increasingly utilised ML and artificial intelligence algorithms in recent years to predict and optimise these outputs. Researchers have conducted and continue to develop numerous studies in this field. While some researchers have evaluated the performance of individual ML algorithms, others have focused on hybrid approaches by combining multiple algorithms to achieve higher accuracy. These efforts contribute significantly to making manufacturing processes more efficient, predictable, and automated.

For instance, in a study focusing on the turning process of AISI 4340 alloy steel, gaussian process regression (GPR) was employed to predict cutting forces. The results showed that GPR was better than other methods like support vector machines (SVM) and artificial neural networks (ANN), with a mean absolute percentage error of 5.12% and a high coefficient of determination (R^2=0.9843). Moreover, the GPR model exhibited the shortest training time, completing in just 0.35087 seconds. These findings suggest that GPR can be effectively utilised by process engineers to estimate cutting forces prior to production, aiding in resource optimisation and the design of experiments aimed at achieving desired product quality [2].

Kumar et al. [3] did a study comparing different ML algorithms to predict cutting forces in turning operations using cutting fluids that are enriched with hybrid nanofluids. Their results emphasised the importance of fluid-based process parameters for enhancing prediction accuracy. Mikołajczyk et al. [4] suggested a method that compares multiple linear regression (MLR), SVM, and ANN to predict cutting forces when turning materials, using a large set of experiments with various tool shapes, feed rates, and cutting speeds. Their work involved an extensive experimental dataset covering different combinations of tool geometry, feed rate, and cutting speed. The results demonstrated that ANN models outperformed MLR and SVM in terms of prediction error and robustness across various machining conditions.

In their study, George et al. [5] employed ML algorithms to identify the most effective parameters for removing metal. They found that neural networks and ML are valuable resources for engineers, but their implementation in industrial settings requires innovative approaches to gather applicable data. Kant and Sangwan [6] employed ANN and support vector regression models to identify the optimal processing parameters. As a result, it was found that ANN produced more accurate results than the reinforcement learning model, and the learning methods used were very similar to the experimental findings. Yang et al. [7] employed the supported vector machine method to handle difficult-to-machine materials, namely AISI 304. In their work on optimising cutting settings, they discovered that the SVM method achieved a high level of accuracy.

Recent advancements in machining have demonstrated the growing relevance of ML for optimising cutting processes and predicting performance metrics, such as surface roughness, cutting forces, and tool wear. Dehghanpour Abyaneh et al. [8] investigated the grinding of UNS S34700 stainless steel under different coolant conditions using a hybrid modelling framework combining GPR, ANN, and genetic algorithms. Their models achieved high predictive accuracy (R^2≈0.98), showing that ML can effectively model complex grinding dynamics. Similarly, Hernández-González et al. [9] applied ANN to analyse the dry, high-speed turning of AISI 1045 steel, revealing that moderate cutting speeds minimise specific energy consumption and cutting forces while emphasising the role of optimal parameter selection. In another recent study, Das et al. [10] used multiple ML techniques—including polynomial regression, Random Forest, Gradient Boosting, and AdaBoost—to predict tool wear, cutting forces, and surface roughness during the tough turning of AISI D6 steel with an AlTiSiN-coated tool. Their models, particularly polynomial regression, achieved R^2 values above 0.90 and were coupled with metaheuristic optimisation to determine the optimal machining parameters. Pawanr and Gupta [11] investigated the dry turning of SDSS-2507 super duplex stainless steel using textured tools and applied ML to estimate mean roughness depth (Rz), validating the effect of feed rate and the efficacy of tool surface modifications under challenging machining conditions. Jouini et al. [12] studied dry and Cryo+MQL-assisted high-speed turning of hardened AISI 4340 and found that the feed rate was the most important factor affecting cutting forces and surface quality, while tool life was more affected by cutting speed, as demonstrated by Grey Relational Analysis. Sudarsan et al. [13] sought to improve the production process parameters in the CNC machining of aluminium alloy 7071 using the L27 orthogonal array developed by Taguchi and response surface methodology. Nevertheless, they did not intend to employ ML algorithms in their studies.

Numerous studies have focused on enhancing surface quality within the manufacturing sector. Recent studies have increasingly concentrated on enhancing surface integrity using roller burnishing, especially for aluminium alloys such as Al6061-T6. Somatkar, et al. [14] conducted an extensive assessment of process parameters—including burnishing speed, feed rate, and number of passes—and their effects on surface roughness, microhardness,

and residual stresses. The authors reiterated the importance of modelling tools, such as ANN and response surface methodologies, for optimising surface properties and accurately predicting results.

Dwivedi et al. [15] established a comprehensive modelling and optimisation framework for Al6061-T6, illustrating that enhanced surface smoothness and improved roundness may be achieved by precise modulation of penetration depth and burnished pressure. Their experimental methodology, utilising statistical methods, confirmed the efficacy of their predictive model, which is pertinent to machine learning-driven process control systems.

Somatkar et al. [16] conducted a comparative study examining the impact of lubrication conditions—dry versus nanofluid minimum quantity lubrication (MQL)—on surface quality. The results show that nanofluid MQL markedly improves microhardness and diminishes surface roughness in comparison to dry burnishing. These findings underline the importance of thermal and tribological parameters in surface integrity and pave the way for data-driven modelling of lubrication techniques in roller burnishing.

Beyond conventional experimental approaches, machine learning (ML) techniques have been increasingly applied to finite element simulation studies, particularly parameter estimation and surrogate modelling. This trend reflects the growing need to reduce the computational costs associated with traditional physics-based simulations in manufacturing. Hashemitaheri et al. [17] created SVR and GPR models that use data from finite element simulations to predict cutting forces and maximum tool temperatures during orthogonal machining. Their study demonstrated that ML models, particularly SVR, can match the predictive accuracy of numerical methods while enabling near real-time predictions. In the same way, Klippel et al. [18] suggested a ML system based on 2,500 virtual experiments using SPH to predict cutting and feed forces when machining Ti6Al4V. The model incorporated tool geometry variables such as rake angle, clearance angle, and cutting-edge radius, providing a fast and efficient alternative to SPH simulations. Although the ML model slightly underpredicted certain trends when compared with physical experiments, it proved highly effective for interpolating across a wide design space. These studies collectively highlight the synergy between physics-based simulations and data-driven models, where ML serves not only as a surrogate for rapid prediction but also as a tool for identifying trends and generalising simulation results for complex machining processes.

These studies collectively illustrate that ML-driven modelling achieves high predictive accuracy for machining outputs. Key parameters, including feed rate, cutting speed, and depth of cut, remain significant determinants of machining results. Enhancements in tool design, such as coatings and textures, provide quantifiable performance advantages when combined with ML. Furthermore, contemporary machining strategies increasingly integrate sustainability metrics, such as energy efficiency, by highlighting ML's contribution to performance prediction and optimising smart, sustainable manufacturing.

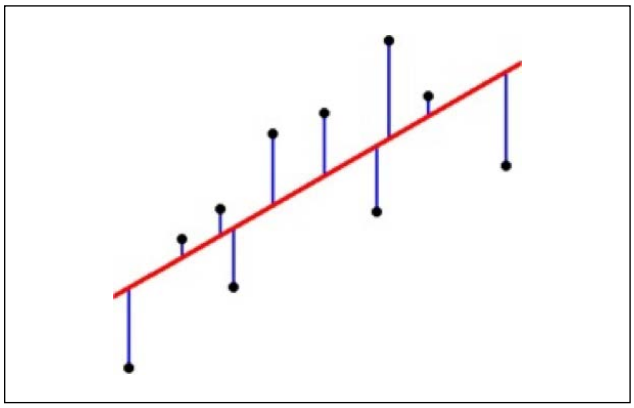

Figure 1. Visualising errors in regression. The vertical lines represent the error in our regression model, which is squared and summed to make our SSE [23].

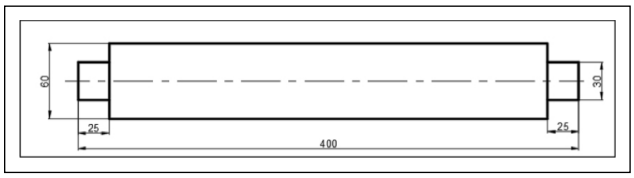

Figure 2. The workpiece used in the experiments [24].

Evaluation Criteria of Learning Algorithms

Once the experimental data has been transmitted to the regression learning algorithm in Matlab software, all learning algorithms may be executed concurrently, and the most optimal prediction method can be chosen. Estimation involves two crucial steps: data preparation and model comparison. The parameters used to evaluate and contrast models include accuracy, speed, resilience, scalability, and interpretability. R2, mean square error (MSE), root mean squared error (RMSE), and mean absolute error (MAE) are key performance measures used in the evaluation of ANN and ML techniques [19].

The coefficient R^2, which represents the explanatory coefficient of the model, is directly related to its predictive ability. The model's performance inversely correlates with the error metrics MSE, RMSE, and MAE. According to Jierula et al. [20], low values of MSE, RMSE, and mean absolute error MAE imply a high level of performance. Out of these performance indicators, R^2 is the coefficient used to determine the accuracy of the model. The coefficient's high value suggests a strong predictive link. According to Wang et al. [21], low values of MSE, RMSE, and MAE imply strong performance, with the level of performance being inversely proportional to the results of these error measures. For instance, when the RMSE is zero, it indicates a high level of performance [22].

Several regression models depend on distance metrics to determine convergence towards the optimal result. Determining the ideal result requires a quantitative analysis based on specific criteria. The often-employed metrics include the MAE, the MSE, or the square RMSE. MAE measures the absolute deviation of the predicted values (entries of the dataset) from the actual values in a

Table 1. Experimental cutting parameters [24]

Experiment number	Cutting speed (m/min.)	Cutting depth (mm)	Feed rate (mm/rev)
1	50	1-2	0.1
2			0.15
3			0.2
4			0.25
5			0.3
6	75	1-2	0.1
7			0.15
8			0.2
9			0.25
10			0.3
11	100	1-2	0.1
12			0.15
13			0.2
14			0.25
15			0.3
16	125	1-2	0.1
17			0.15
18			0.2
19			0.25
20			0.3
21	150	1-2	0.1
22			0.15
23			0.2
24			0.25
25			0.3

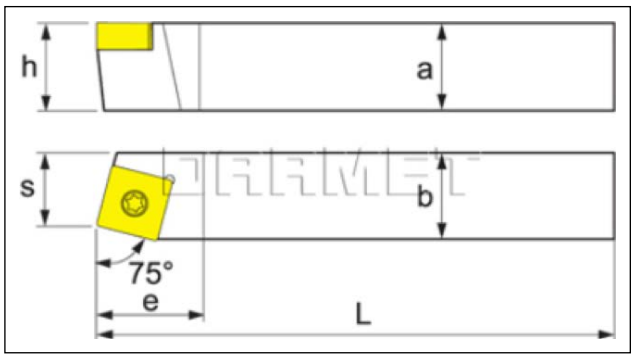

Figure 3. Schematic drawing of the cutting tool and tool holder used in the experiments [24].

regression problem. It is calculated by taking the average of the absolute differences between the predicted and actual values. When calculating negative errors, the absolute value of the distances is employed to ensure accuracy. Figure 1 accurately illustrates this scenario. Equation 1 displays the computation of MAE [23].

Table 2. Tool holder dimensions [24]

Parameter	Dimension (mm)
a	25
b	25
L	150
h	25
s	22
e	25

Table 3. Specifications of the JOHNFORD T35 CNC lathe

X axis	250 mm
Y axis	600 mm
Power	10 kW
Revolution speed	4000 dev/dak.
Hydraulic chuck diameter	250 mm
Precision	0.001 mm
Turret tool capacity	12

Table 4. Technical specifications of the Kistler 9257B dynamometer [24]

Force Range	-5…10 kN
Response	<0.01N
Sensitivity	
Fx, Fy	-7.5 pC/N
Fz	-3.5 pC/N
Linearity	1% FSO
Hysteresis	0.5% FSO
Natural frequency	3.5 kHz
Operating temperature	0…70°C
Capacitance	220 pF
Insulation resistance at 20°C	1013 Ω
Ground insulation	>108 Ω
Protection class	IP 67
Weight	7.5 kg

$$MAE = \frac{1}{n}\sum_{i=1}^{N}\left|y_i^{real} - y_i^{prediction}\right| \quad (1)$$

An alternative approach is to calculate the square of the distance, resulting in positive values. As the projected values approach the real values, the MSE decreases. The MSE, is calculated by taking the average of the squared errors of the model, as shown in Equation 2.

$$MSE = \frac{1}{n}\sum_{i=1}^{N}(y_i^{real} - y_i^{prediction})^2 \quad (2)$$

RMSE is a mathematical metric that calculates the square root of the MSE and converts it back to the original unit of measurement. RMSE quantifies the dispersion of predicting errors (Equation 3).

$$RMSE = \sqrt{MSE} \quad (3)$$

In this study, all parameters were evaluated, and the ML algorithms used were closer to the prediction.

MATERIAL AND METHOD

Workpiece

The experimental tests conducted in the laboratories of Gazi University, Faculty of Technology, utilised a workpiece with a diameter of 60 mm and a length of 400 mm. [24]. The workpiece material is AISI 1117 steel. The material's surface was initially machined with a depth of cut of 1 mm in case of hardening of the outer surface layer. The dimensions of the workpiece are illustrated in Figure 2. Experimental cutting parameters are given in Table 1.

Cutting Tool and Tool Holder

The cutting tool used in the experiments is a cemented carbide SCMW 12 M508-12F insert, compliant with ISO 1832 standards and without a chip breaker. It features a rake angle of 0° and a clearance angle of 7°. The tool holder is of type SSBCR 25 25 M12 with a 75° lead angle, suitable for the insert geometry. Figure 3 provides a schematic representation of the tool and holder, while Table 2 provides the dimensional specifications.

Experimental Setup

The experiments were conducted at the CNC Workshop of Gazi University, Faculty of Technical Education, using the JOHNFORD T35 CNC turning machine. The main specifications of the lathe are presented in Table 3 [24]. The cutting forces in the experiments were measured using a Kistler 9257B-type dynamometer, as seen in Figure 4. The technical features of this dynamometer are shown in Table 4. During the cutting process, signals produced by the tool were transmitted to a computer using an amplifier and transformed into actual force values using the Dynoware software package [24].

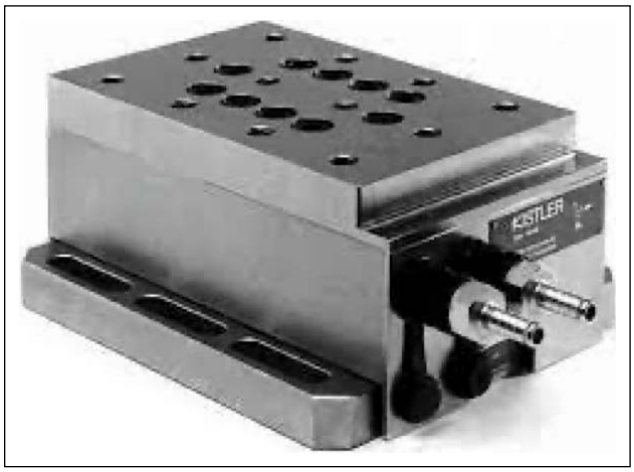

Figure 4. Kistler 9257B dynamometer [24].

Estimation of Cutting Forces by Learning Method

This part emphasises the prediction of cutting forces through the analysis of variations in cutting speed, feed rate,

Table 5. Comparison of learning algorithms in Matlab regression

Algorithms Used	RMSE	R^2	MSE	MAE
Linear regression (interactions linear)	23,441	0.91	549.48	18,607
Linear regression (linear)	22,089	0.9	48.93	18,642
Linear regression (robust linear)	22,358	0.91	499.89	18,716
Stepwise linear regression	22,089	0.91	487.93	18,642
Tree (medium tree)	74,713	0	5582.1	63,092
Tree (coarse tree)	74,713	0	5582.1	63,092
Tree (fine tree)	51,269	0.53	2628.5	45,503
SVM (linear SVM)	22,478	0.91	505.28	18,837
SVM (medium gaussian SVM)	33.09	0.79	1149.8	29,176
SVM (cubic SVM)	19,573	0.93	383.1	16,658
SVM (coarse gaussian SVM)	30,644	0.83	939.03	26,287
SVM (fine gaussian SVM)	73,152	0.04	5351.3	61,087
Gaussian process regression (squared exponential GPR)	22,013	0.91	484.57	18,652
Gaussian process regression (matern 5/2 GPR)	22,932	0.91	525.85	19,386
Gaussian process regression (rational quadratic GPR)	22,839	0.91	521.63	19,266
Gaussian process regression (exponential GPR)	22,561	0.91	509.14	19,988
Ensemble (boosted trees)	50,841	0.54	2584.8	44,141
Ensemble (bagged trees)	60,588	0.34	3670.9	51,621

SVM: Support vector machine; GPR: Gaussian process regression; RMSE: Root mean squared error; MSE: Mean square error; MAE: Mean absolute error.

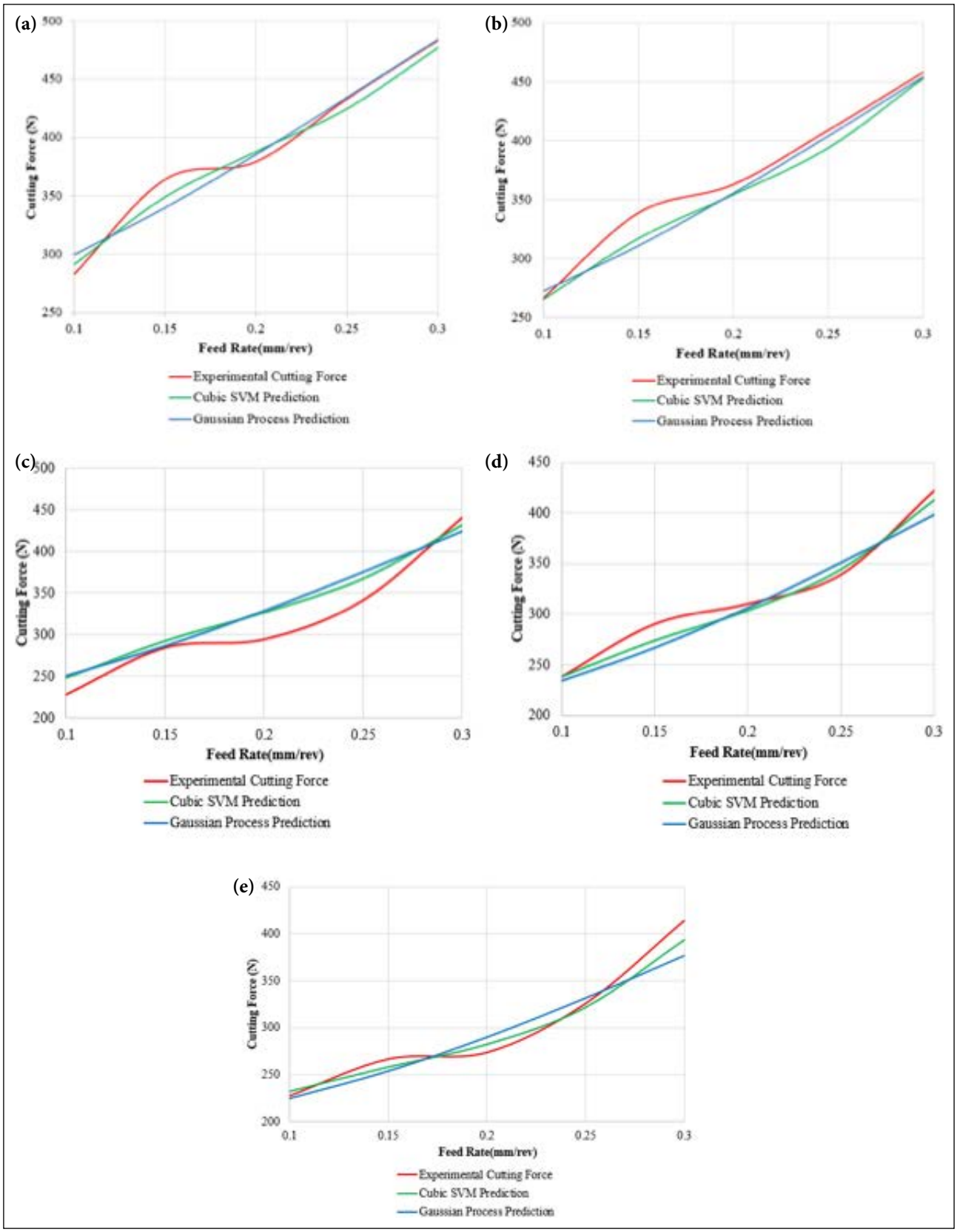

Figure 5. Feed rate & cutting force for the cutting speed of **(a)** 50 m/min **(b)** 75 m/min **(c)** 100 m/min **(d)** 125 m/min **(e)** 150 m/min.

and depth of cut. The depth of cut was initially maintained constant, but the feed rate and cutting speed were treated as independent variables. Subsequently, depth of cut was incorporated as a third independent variable in addition to the initial two. The prediction models were evaluated to determine which method most precisely mirrored the experimental

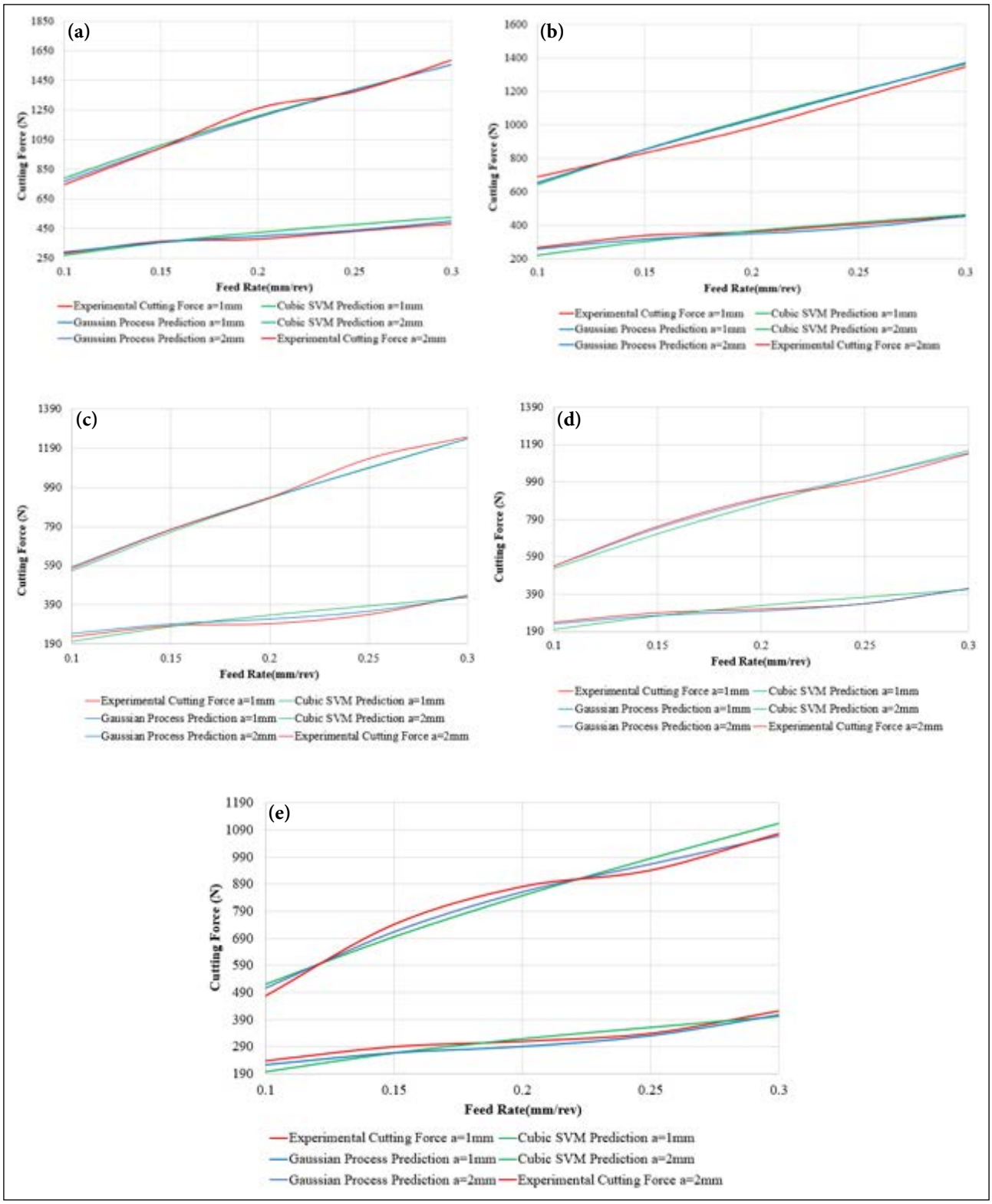

Figure 6. Feed rate & cutting force for various cutting speeds and depths of cuts **(a)** 50 m/min **(b)** 75 m/min **(c)** 100 m/min **(d)** 125 m/min **(e)** 150 m/min.

cutting forces, the dependent variable. The aim is to estimate cutting forces using only independent variables and to see if ML techniques produce more accurate results by comparing the predicted cutting force to experimentally acquired values. The efficacy of the learning algorithms was assessed utilising R^2, RMSE, MSE, and MAE, as previously mentioned.

Hyperparameter Tuning and Cross-Validation Methods

The success of ML algorithms depends not only on the choice of the model but also on the selection of appropriate hyperparameter values and model validation strategies. In this study, regression-based learning algorithms were implemented using MATLAB's Regression Learner interface, which provides

Table 6. Comparison between experimental and predicted cutting force results

Cutting speed (m/min)	Feed rate (mm/rev)	Experimental cutting force (N)	Cubic SVM prediction	Gaussian process prediction	Cubic SVM prediction error rate	Gaussian process prediction error rate
50	0.1	283	291.5	299.6	3.02	5.87
50	0.15	364	349.0	339.7	-4.12	-6.66
50	0.2	379	387.7	385.2	2.28	1.63
50	0.25	433	424.5	433.9	-1.97	0.20
50	0.3	483	476.5	483.5	-1.34	0.10
75	0.1	267	265.7	272.7	-0.49	2.14
75	0.15	339	317.3	311.1	-6.39	-8.24
75	0.2	363	354.4	355.4	-2.37	-2.09
75	0.25	409	393.9	403.8	-3.68	-1.28
75	0.3	458	453.0	453.8	-1.10	-0.93
100	0.1	229	248.4	250.5	8.46	9.40
100	0.15	285	292.8	286.4	2.74	0.49
100	0.2	295	327.0	328.7	10.83	11.44
100	0.25	342	367.8	375.7	7.55	9.87
100	0.3	441	432.5	425.1	-1.94	-3.60
125	0.1	238	237.9	234.3	-0.04	-1.56
125	0.15	290	273.8	267.0	-5.60	-7.93
125	0.2	310	303.6	306.6	-2.07	-1.10
125	0.25	339	344.4	351.3	1.60	3.64
125	0.3	422	413.3	399.1	-2.06	-5.43
150	0.1	228	232.5	224.8	1.99	-1.40
150	0.15	267	258.4	253.9	-3.20	-4.91
150	0.2	274	282.6	290.1	3.14	5.87
150	0.25	326	322.0	331.8	-1.22	1.77
150	0.3	414	393.8	377.0	-4.89	-8.94

SVM: Support vector machine.

automated tools for testing multiple hyperparameter configurations and selecting the optimal model setup. Specifically, the study explored and compared different kernel functions and associated parameter values for cubic SVM and GPR.

Although the hyperparameter tuning was not conducted manually by the user, the automated configuration and selection process provided by the Regression Learner interface was effectively meant to enhance model performance. In the case of SVM, kernel types such as linear, cubic, and Gaussian were evaluated, while for GPR, various kernel functions, including squared exponential, rational quadratic, and Matern 5/2, were tested.

Model performance was assessed using a cross-validation approach. The MATLAB Regression Learner applies 5-fold cross-validation by default, which objectively evaluates the generalisability of the model. In this method, the training dataset is divided into five equal parts, each serving as a test set in turn, and the average performance metrics are calculated and compared.

Results of the Estimation Utilizing two Independent Variables

This section presents a constant cutting depth of 1 mm. The cutting speed and feed rate are considered as independent variables, whereas the cutting force is regarded as the dependent variable. Regression and learning techniques from MATLAB are employed for analysis.

The review of Tables 5 and 6 and Figure 5 shows how well different ML algorithms predict cutting forces using two factors: cutting speed and feed rate. The cubic SVM was the most accurate of all the algorithms tested, with an R^2 value of 0.93 and the lowest RMSE of 19.57, outperforming both linear regression and tree-based models. The cubic SVM showed the best accuracy of all the algorithms tested, with an R^2 value of 0.93 and the lowest RMSE of 19.57, outperforming linear regression and tree-based models.

The prediction errors presented in Table 6 demonstrate that Cubic SVM consistently achieves errors below 10%, especially at both lower and higher cutting speeds.

Table 7. Learning algorithms and validation with Matlab regression

Algorithms used	RMSE	R^2	MSE	MAE
Linear regression (interactions linear)	46.92	0.99	2201.8	35,146
Linear regression (linear)	121.24	0.9	14699	95,669
Linear regression (robust linear)	125.55	0.9	15763	98,627
Stepwise linear regression	49,256	0.98	2426.1	36,959
Tree (medium tree)	210.43	0.71	44282	153.34
Tree (coarse tree)	390.13	0	343.35	343.35
Tree (fine tree)	164.63	0.82	27102	112.88
SVM (linear SVM)	142.58	0.87	20329	105.99
SVM (medium gaussian SVM)	105.38	0.93	11105	69,801
SVM (cubic SVM)	51,572	0.98	2659.7	40,816
SVM (coarse gaussian SVM)	168.22	0.81	28299	114.84
SVM (fine gaussian SVM)	363.17	0.13	131890	316.04
Gaussian process regression (squared exponential GPR)	43,163	0.99	1863.1	34,137
Gaussian process regression (matern 5/2 GPR)	39,782	0.99	1582.6	32,321
Gaussian process regression (rational quadratic GPR)	43,316	0.99	1859	34,112
Gaussian process regression (exponential GPR)	75,386	0.96	5683	49,352
Ensemble (boosted trees)	151.55	0.85	22968	99,037
Ensemble (bagged trees)	278.71	0.49	77680	243.28

SVM: Support vector machine; RMSE: Root mean squared error; MSE: Mean square error; MAE: Mean absolute error.

Figures 6a–e illustrate a linear increase in cutting force with respect to feed rate, with a steeper slope observed at higher cutting speeds, thereby confirming the impact of feed rate on force generation.

Trend Analysis Across Cutting Speeds

Figure 5 illustrates the correlation between feed rate and cutting force at various cutting speeds (50, 75, 100, 125, and 150 m/min). In all instances, the cutting force exhibits a linear rise with the feed rate, which is consistent with expected machining behaviour. The rate of increase is more obvious at higher cutting speeds, suggesting that feed rate significantly influences cutting force at increased speeds.

Model Performance Observation

At lower cutting speeds (like 50 m/min, Figure 5a, both models provide similar results, with Cubic SVM slightly performing better than GPR in terms of error (as shown in the first five rows of Table 6). At medium speeds (75–100 m/min, Figures 5b, Figure 5c, GPR shows more reliable results, especially when cubic SVM tends to overestimate or underestimate (for example, at 100 m/min and 0.2 mm/rev, Cubic SVM has an error of 10.83% while GPR has 11.44%). At higher speeds (125–150 m/min, Figures 5 (d and e)), both models provide reliable predictions, but GPR is better at handling small changes in the force response.

Error Rate Evaluation

Table 6 indicates that Cubic SVM consistently achieves a prediction error below 10%, demonstrating optimal performance at both very low and very high cutting speeds. GPR predictions demonstrate increased stability under different conditions, particularly at mid-range feed rates (e.g., 0.2–0.3 mm/rev). The most unfavourable prediction scenarios (e.g., 100 m/min at 0.2 mm/rev) demonstrate the sensitivity of Cubic SVM to particular input interactions, whereas GPR exhibits relative robustness.

Estimation Results Using Three Independent Variables

This part concentrates on predicting cutting forces by analysing variations in cutting speed, feed rate, and depth of cut. By incorporating the depth of cut as a third independent variable, several regression approaches are utilised to choose the ML strategy that achieves the greatest prediction accuracy.

As depth of cut is introduced as a third variable, Table 7 and Figures 6a through 6e reveal a shift in algorithm performance. GPR, using the Matern 5/2 kernel, performed better than Cubic SVM, reaching an R^2 of 0.99 and a low RMSE of 39.78. The figures demonstrate that even under more complex conditions, GPR offers more stable predictions. Tables 8, 9 further confirms this trend: while Cubic SVM's error rates range from 5% to 10%, GPR's prediction errors mostly stay under 4% for a depth of 1 mm and often below 3% for 2 mm depth, highlighting its robustness in higher-dimensional data environments. These tabular and graphical findings collectively demonstrate that cubic SVM is effective for simpler, two-variable models, whereas GPR provides more accurate and consistent predictions when dealing with three-variable, nonlinear machining scenarios.

Table 8. Result comparison for three parameters

Cutting speed (m/min)	Feed rate (mm/rev)	Experimental cutting force a=1mm (N)	Cubic SVM prediction a=1mm (N)	Gaussian process prediction a=1mm (N)	Cubic SVM prediction error rate	Gaussian process prediction error rate
50	0.1	283	269.4	289.2	-4.81	2.19
50	0.15	364	356.7	356.4	-2.01	-2.09
50	0.2	379	423.5	396.6	11.74	4.64
50	0.25	433	477.5	436.0	10.28	0.69
50	0.3	483	526.3	499.1	8.96	3.33
75	0.1	267	222.5	261.7	-16.67	-1.99
75	0.15	339	304.3	318.7	-10.24	-5.99
75	0.2	363	366.4	350.0	0.94	-3.58
75	0.25	409	416.4	387.6	1.81	-5.23
75	0.3	458	462.2	455.0	0.92	-0.66
100	0.1	229	204.4	242.8	-10.74	6.03
100	0.15	285	281.4	291.5	-1.26	2.28
100	0.2	295	339.6	317.2	15.12	7.53
100	0.25	342	386.5	356.9	13.01	4.36
100	0.3	441	429.8	432.3	-2.54	-1.97
125	0.1	238	200.5	233.3	-15.76	-1.97
125	0.15	290	273.6	278.0	-5.66	-4.14
125	0.2	310	328.5	300.4	5.97	-3.10
125	0.25	339	373.0	340.0	10.03	0.29
125	0.3	422	414.7	418.6	-1.73	-0.81
150	0.1	228	196.3	222.4	-13.90	-2.46
150	0.15	267	266.1	266.9	-0.34	-0.04
150	0.2	274	318.6	290.4	16.28	5.99
150	0.25	326	361.3	330.8	10.83	1.47
150	0.3	414	402.1	408.5	-2.87	-1.33

SVM: Support vector machine.

CONCLUSION

This study finds that ML methods, especially cubic SVM and GPR, are very promising for accurately predicting cutting forces in machining. The cubic SVM demonstrated superior performance with cutting speed and feed rate as the sole inputs, attaining a high R^2 and low RMSE. Incorporating depth of cut as a third factor improved the performance of GPR, particularly when using the Matern 5/2 kernel, making it more accurate and reliable than all other methods. Along with these two models, we also looked at different algorithms, such as several kinds of linear regression, decision trees (fine, medium, and coarse), and ensemble methods (boosted and bagged trees). These models typically exhibited reduced performance, especially in their ability to capture nonlinear and multivariable interactions. This study's results align with previous research by Kumar et al. [3] and Chen and Jeng [25], both of which highlighted the advantages of SVM and GPR models in machining applications.

The study indicates that the quantity and nature of independent variables significantly affect the generalisation capabilities and predictive accuracy of ML models. Models such as Cubic SVM demonstrate effective performance in low-dimensional settings characterised by stable variable interactions. As the number of input variables increases and their interactions grow more complex, particularly regarding the depth of cut, results projection becomes more difficult, necessitating the use of more adaptable and robust algorithms like GPR. This highlights the necessity of aligning model complexity with data structure in manufacturing contexts. This study identifies optimal models for predicting cutting force and contributes to the advancement of manufacturing science through computational intelligence.

Data Availability Statement

The authors confirm that the data that supports the findings of this study are available within the article. Raw data that support the finding of this study are available from the corresponding author, upon reasonable request.

Table 9. Result comparison for three parameters

Cutting speed (m/min)	Feed rate (mm/rev)	Experimental cutting force a=2mm (N)	Cubic SVM prediction a=2mm (N)	Gaussian process prediction a=2mm (N)	Cubic SVM prediction error rate	Gaussian process prediction error rate
50	0.1	745	789.7	767.2	9.49	3.58
50	0.15	993	1012.3	993.7	9.57	3.62
50	0.2	1260	1209.0	1200.9	9.68	3.65
50	0.25	1373	1387.5	1385.5	9.60	3.61
50	0.3	1586	1555.5	1557.3	9.58	3.66
75	0.1	691	646.4	655.8	9.60	3.68
75	0.15	832	856.0	852.4	8.95	3.69
75	0.2	983	1040.4	1030.2	8.63	3.46
75	0.25	1163	1207.5	1200.8	8.67	3.35
75	0.3	1348	1364.8	1371.0	8.71	3.09
100	0.1	574	563.5	582.4	8.73	3.06
100	0.15	772	760.8	773.9	8.21	2.95
100	0.2	937	933.7	936.8	8.12	2.96
100	0.25	1137	1090.1	1087.1	7.90	2.73
100	0.3	1248	1237.4	1238.0	7.76	2.68
125	0.1	540	526.4	539.2	7.62	2.59
125	0.15	752	712.1	741.7	6.28	2.48
125	0.2	905	874.3	896.0	5.78	2.15
125	0.25	996	1020.6	1018.6	5.78	1.86
125	0.3	1141	1158.8	1143.8	5.75	1.81
150	0.1	476	520.6	504.9	5.49	1.69
150	0.15	740	695.4	713.3	3.49	1.36
150	0.2	880	847.6	861.3	3.21	1.27
150	0.25	940	984.7	964.6	2.85	1.13
150	0.3	1076	1114.3	1069.3	2.89	1.14

SVM: Support vector machine.

Author's Contributions

Kadir Özdemir: Conception, Materials, Design, Data Processing, Supervision, Analysis and Interpretation, Literature Review, Writer, Critical Review.

Ulvi Şeker: Conception, Materials, Data Collection and Processing, Interpretation, Literature Review, Writer, Critical Review.

Mustafa Cemal Çakır: Conception, Materials, Design, Supervision, Analysis and Interpretation, Literature Review, Writer, Critical Review.

Conflict of Interest

The authors declared no potential conflicts of interest with respect to the research, authorship, and/or publication of this article.

Statement on the Use of Artificial Intelligence

Artificial intelligence was not used in the preparation of the article.

Ethics

There are no ethical issues with the publication of this manuscript.

REFERENCES

[1] Akay, E. C. (2018). Ekonometride yeni bir ufuk: Büyük veri ve makine öğrenmesi. Sosyal Bilimler Araştırma Dergisi, 7(2), 41-53. [Turkish]

[2] Alajmi, M. S., & Almeshal, A. M. (2021). Modeling of Cutting Force in the Turning of AISI 4340 Using Gaussian Process Regression Algorithm. *Applied Sciences, 11*(9), 4055. [CrossRef]

[3] Kumar, V., Dubey, V., & Sharma, A. K. (2023). Comparative analysis of different machine learning algorithms in prediction of cutting force using hybrid nanofluid enriched cutting fluid in turning operation. *Materials Today: Proceedings*, Inpress. [CrossRef]

[4] Mikołajczyk, T., Nowicki, Ł., & Górski, F. (2018). Artificial intelligence techniques in predicting cutting forces: A comparative study. *Mechanik, 91*(7), 569-572.

[5] George, K., Kannan, S., Raza, A., & Pervaiz, S. (2021). A hybrid finite element-machine learning backward training approach to analyze the optimal machining conditions. *Materials, 14*(21), 6717. [CrossRef]

[6] Kant, G., & Sangwan, K. S. (2015). Predictive modelling for energy consumption in machining using artificial neural network. *Procedia Cirp, 37*, 205-210. [CrossRef]

[7] Yang, C., Jiang, H. and Liu, B. (2020) Optimization design of cutting parameters based on the support vector machine and particle swarm algorithm. *Open Access Library Journal, 7*, 1-8. [CrossRef]

[8] Dehghanpour Abyaneh, M., Narimani, P., Javadi, M. S., Golabchi, M., Attarsharghi, S., & Hadad, M. (2024). Predicting surface roughness and grinding forces in UNS S34700 steel grinding: A machine learning and genetic algorithm approach to coolant effects. *Physchem, 4*(4), 495-523. [CrossRef]

[9] Hernández-González, L.W., Curra-Sosa, D. A., Pérez-Rodríguez, R., & Zambrano-Robledo, P. D. C. (2021). Modeling Cutting forces in high-speed turning using artificial neural networks. *TecnoLógicas, 24*(51), 43-61. [CrossRef]

[10] Das, A., Das, S. R., Panda, J. P., Dey, A., Gajrani, K. K., Somani, N., & Gupta, N. (2022). Machine learning based modeling and optimization in hard turning of AISI D6 steel with newly developed AlTiSiN coated carbide tool. *arXiv* preprint arXiv:2202.00596. [CrossRef]

[11] Pawanr, S., & Gupta, K. (2025). Analysis of surface roughness and machine learning-based modeling in dry turning of super duplex stainless steel using textured tools. *Technologies, 13*(6), 243. [CrossRef]

[12] Jouini, N., A. Ghani, J., Yaqoob, S., & Juri, A. Z. (2025). Optimized machining parameters for high-speed turning process: a comparative study of dry and Cryo+MQL techniques. *Processes, 13*(3), 739. [CrossRef]

[13] Sudarsan, D., Bovas Herbert Bejaxhin, A. & Rajkumar, S. (2025). Enhancing CNC turning efficiency of aluminium 7071 alloy using taguchi method and L27 array. *International Journal of Precision Engineering and Manufacturing, 26*, 177-194. [CrossRef]

[14] Somatkar, A. A., Dwivedi, R., & Chinchanikar, S. S. (2024). Enhancing surface integrity and quality through roller burnishing: a comprehensive review of parameters optimization, and applications. *Communications on Applied Nonlinear Analysis, 31*(1s), 151-169. [CrossRef]

[15] Dwivedi, R., Somatkar, A., & Chinchanikar, S. (2024). Modeling and optimization of roller burnishing of Al6061-T6 process for minimum surface roughness, better microhardness and roundness. *Obrabotka Metallov/Metal Working and Material Science, 26*(3), 52-65. [CrossRef]

[16] Somatkar, A., Dwivedi, R., & Chinchanikar, S. (2024). Comparative evaluation of roller burnishing of Al6061-T6 alloy under dry and nanofluid minimum quantity lubrication conditions. *Obrabotka Metallov/Metal Working and Material Science, 26*(4), 57-74. [CrossRef]

[17] Hashemitaheri, M., Mekarthy, S. M. R., & Cherukuri, H. (2020). Prediction of specific cutting forces and maximum tool temperatures in orthogonal machining by support vector and Gaussian process regression methods. *Procedia Manufacturing, 48*, 1000-1008. [CrossRef]

[18] Klippel, H., Sanchez, E. G., Isabel, M., Röthlin, M., Afrasiabi, M., Michal, K., & Wegener, K. (2022). Cutting force prediction of Ti6Al4V using a machine learning model of SPH orthogonal cutting process simulations. *Journal of Machine Engineering, 22*(1), 111-123. [CrossRef]

[19] Karasu, S., Altan, A., Saraç, Z., & Hacioğlu, R. (2018). Prediction of Bitcoin prices with machine learning methods using time series data. In *2018 26th signal processing and communications applications conference (SIU)* (pp. 1-4). IEEE. [CrossRef]

[20] Jierula, A., Wang, S., OH, T.-M., & Wang, P. (2021). Study on accuracy metrics for evaluating the predictions of damage locations in deep piles using artificial neural networks with acoustic emission data. *Applied Sciences, 11*(5), 2314. [CrossRef]

[21] Wang Y, Xu C, Wang Z, Zhang S, Zhu Y, Yuan J (2018) Time series modeling of pertussis incidence in China from 2004 to 2018 with a novel wavelet based SARIMA-NAR hybrid model. *PLoS One, 13*(12), e0208404. [CrossRef]

[22] Çınaroğlu, S. (2017). Comparison of machine learning regression methods to predict health expenditures. *Uludag Universitesi Mühendislik Fakültesi Dergisi, 22*(2), 179-200.

[23] Ross, S. M. (2017). Chapter 8-Estimation. In S. M. Ross, (Ed.), *Introductory Statistics* (4th ed., pp. 329-380). Academic Press. [CrossRef]

[24] Boy, M. (2004). *Kesme parametrelerine bağlı olarak talaş arka yüzey sıcaklığının deneysel olarak incelenmesi* [Yüksek Lisans Tezi]. Gazi Üniversitesi. [Turkish]

[25] Chen, C. S., & Jeng, Y. (2015). A data-driven multidimensional signal-noise decomposition approach for GPR data processing. *Computers & Geosciences, 85*, 164-174. [CrossRef]

J Adv Manuf Eng, Vol. 6, Issue. 2, pp. 68–76, December, 2025

Journal of Advances in Manufacturing Engineering
Web page info: https://jame.yildiz.edu.tr
DOI: 10.14744/ytu.jame.2025.00009

Original Article

The modal characteristics of the CFRP, GFRP and hybrid composites exposed to HCl environment and impact loadings

Betül SÖZEN COŞKUN*[1], Taner COŞKUN[2], Serkan KAPICI[2], Yavuz Selim TARİH[3], Ömer Sinan ŞAHİN[2]

[1]*Department of Mechanical Engineering, Selçuk University Faculty of Technology, Konya, Türkiye*
[2]*Department of Mechanical Engineering, Konya Technical University Faculty of Engineering and Natural Sciences, Konya, Türkiye*
[3]*Department of Mechanical Engineering, Bingöl University Faculty of Engineering and Architecture, Bingöl, Türkiye*

ARTICLE INFO

Article history
Received: 11 August 2025
Revised: 06 October 2025
Accepted: 07 October 2025

Key words:
Damping ratio, HCl environment, hybridization, modal characteristics, low-velocity impact.

ABSTRACT

Composite materials can be subjected to low-velocity impact (LVI) loadings at various velocities in their application areas, as well as corrosive environments, causing degradation in the mechanical and dynamic properties. When the literature is reviewed, LVI loadings, aging time, fiber material, and hybridization effects on vibration characteristics have all been examined separately, but no research has looked at these aspects together. Therefore, in the current study, Carbon Fiber-Reinforced Polymer (CFRP), Glass Fiber-Reinforced Polymer (GFRP) and Carbon/Glass Fiber-Reinforced Polymer (Hybrid) composites were manufactured utilizing the Vacuum-Assisted Hand-Layup Method (VAHLM) and then exposed to corrosive environments and Low-Velocity Impact (LVI) loadings, respectively. In this context, the fabricated composites were immersed in a 10% diluted HCl solution for 1 week and 1 month and then exposed to LVI loadings at 2 and 3 m/s impact velocities. After that, vibration tests were conducted, and thus the impacts of corrosive environments and LVI loadings, as well as fiber materials and hybridization, on the modal characteristics were examined experimentally as a novelty for the current study. The study's findings showed that the natural frequencies of CFRP and GFRP composites are 159.5 and 91.5, respectively, and that CFRP composites have approximately 75% higher natural frequencies than GFRP ones due to the high stiffness of carbon fibers. On the other hand, it was determined that hybrid composites had higher damping ratios than the others, which was ascribed to elevated energy absorption caused by the various interface characteristics of carbon/glass fibers. It was also discovered that no significant changes appeared in the dynamic responses following the corrosive environment exposure and LVI loadings, which was attributed to the composites' substantial impact and corrosion resistance.

Cite this article as: Sözen Coşkun, B., Coşkun, T., Kapıcı, S., Tarih, Y. S., & Şahin, Ö. S. (2025). The modal characteristics of the CFRP, GFRP and hybrid composites exposed to HCI environment and impact loadings. *J Adv Manuf Eng*, 6(2), 68–76.

INTRODUCTION

A corrosive environment leads to various damage mechanisms in composites such as debonding, crack propagation, delamination, swelling etc. Moreover, pre-existing damage in the composite is triggered by the effects of the corrosive environment and this accelerates the degradation of the dynamic properties. For these reasons, much research

***Corresponding author.**
*E-mail address: betulsozenn@gmail.com

has been conducted on the corrosion resistance of composites and it is aimed at determining the effects of a corrosive environment on vibration behaviour [1–12]. For example, Ramalingam et al. [2] examined the effects of aging on biocomposites' vibration characteristics. In this regard, the impacts of various aging conditions, particularly humidity, on the dynamic behaviour of composites were studied. According to the study, as aging time climbed, so did the damping factor, whereas natural frequency responses dropped. In another study [4], the effects of hydrothermal aging on composite vibration properties were investigated experimentally. Sea water and distilled water were chosen as aging environments, and thus the effects of these media on vibration responses were examined. Furthermore, the dynamic characteristics for the aramid, glass, and aramid/glass fiber-reinforced composites were explored, as well as the impacts of fiber material, hybridization, and aging on vibration responses. The study found that aging had no significant effect on first-mode natural frequency responses, but it did raise the damping responses of hybrid ones. Moreover, aging was shown to reduce storage and loss modulus responses. In the study conducted by Senthilrajan and Venkateshwaran [5], the effects of aging on vibration responses were investigated by considering various fiber lengths and weight percentages. The study concluded that fiber density and fiber/matrix bonding strength were extremely efficient on moisture resistance, and that rising fiber density and bonding strength reduced dynamic behaviour deterioration. It was also said that water molecules attacked the fiber-matrix interface, causing debonding, which resulted in a reduction in natural frequency responses due to aging. Cheour et al. [8] subjected flax fiber-reinforced composite specimens to room-temperature water aging, and then studied their damping and mechanical properties. According to the study, it was determined that water uptake caused a reduction in flexural modulus and an increment in loss factors. To test the reversibility of these changes, the same parameters were examined after the specimens had been dried, and it was discovered that the drying process was reversible in terms of loss factors but irreversible in terms of flexural modulus. It was also indicated that fiber orientation is vital to water uptake. Xu et al. [10] studied the effects of hygrothermal aging on the mechanical properties of composites and discovered that the saturated moisture contents of pure resin and composite at 70°C were about 0.32% and 0.19%, respectively. It was revealed that following moisture absorption, the tensile strengths of the pure resin and composite retained at 81.85% and 95.49%, respectively. In another study, Oğuz et al. [11] looked at how distilled water affected the flexural and impact properties of composites. In the study, the specimens were aged at 25 and 70 °C for 1000 hours, and it was stated that the reduction in impact and flexural strength rose with ascending temperature. In a similar study, Oğuz et al. [12] examined the effect of aging in seawater on the flexural and LVI responses of composite materials. The study concluded that damage such as fiber-matrix cracking and delamination in composites also increased as the temperature elevated.

Apart from that, composite materials are frequently subjected to LVI loadings in their application areas, and this causes some damage such as delamination, fiber breakage, and matrix cracks. Moreover, these structures can be subjected to vibration at various frequencies, distortions occur in their vibration responses due to LVI-induced damages and this poses a great danger for their usage areas. For all these reasons, various research have been done to determine the vibration characteristics of composites, or the effects of LVI loading on vibration responses [13–19]. In their study, Coskun et al. [13] applied LVI loading on polyamide fiber-reinforced composites before performing an experimental investigation into the variations in vibration characteristics. The study found that using polyamide fibers resulted in a specific damping capacity of approximately 11.5%, and it was concluded that thermoplastic fibers greatly improve damping responses when compared to synthetic ones. It is also deduced that the change in vibration responses is restricted since the LVI loading acts on a limited area. In another study [15], Coskun et al. [13] integrated various thermoplastic veils into carbon and fiber-reinforced composites as interlayers, and investigated their vibration responses after LVI loading. As a consequence of the study, it was determined that loss factor responses decreased due to LVI loading and this was greater for CFRP composites compared to GFRP composites. In another study, Duan et al. [18] performed experimental LVI tests at various energy levels, examining the dynamic responses of composite materials. C-Scan tests were also used to analyse the delaminated areas following LVI loadings. Furthermore, frequency-sweep vibration tests were performed, and the damage characteristics of composites exposed to LVI stress were determined. The study found that matrix damage and delamination were the most common damage processes in composites. The results also showed that the delamination area and first-order frequency had a linear correlation, that the stiffness reduced as the delaminated area rose, and that this phenomenon resulted in a reduction in frequency responses.

Studies on the impact of aging on vibration characteristics have found that extending aging time reduces the natural frequency responses of composite materials, which is associated with stiffness loss. On the other hand, LVI loading has resulted in a reduction in natural frequencies, which has been linked to stiffness loss with damage. Furthermore, it was determined that aging and LVI loading led to more damage and friction surfaces, resulting in greater damping responses. When studies in the literature are reviewed, it is noticeable that studies that examine the vibration responses of composites exposed to corrosive environments or LVI loadings are commonly found. However, it is seen that the effects of LVI and aging on vibration responses are not examined together, and this stands out as a deficiency in the literature. Moreover, the fact that the effects of LVI and corrosive environment are not examined in terms of fiber material or hybridization constitutes another motivation for the current study. For that reason, as part of the present study, CFRP, hybrid and GFRP composites were exposed to

Table 1. Some details for the CFRP, GFRP and hybrid composites

Specimens	Length (mm)	Width (mm)	Thickness (mm)	Weight (g)	Density (kg/m^3)
CFRP	150.1	100.2	3.2	68.09	1414.77
Hybrid	149.9	100.1	3.08	72.88	1576.97
GFRP	150.1	100.1	3.03	80.03	1757.91

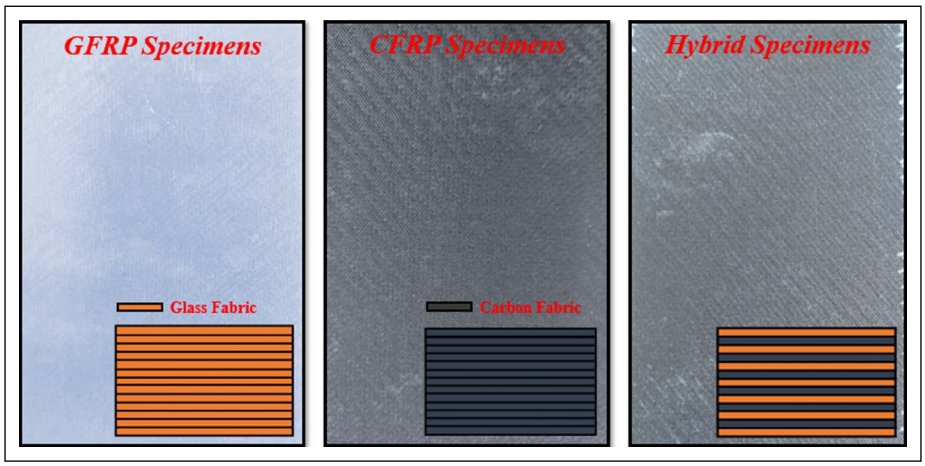

Figure 1. Visualization of the fabricated CFRP, GFRP and hybrid composites and their stacking sequence.

aging in a HCI environment for 1 week and 1 month, and then impacts were applied to the aged specimens at 2 various velocities, 2 and 3 m/s. Then, modal tests of synthetic fiber-reinforced composites exposed to corrosive environments and LVI loadings were performed under fixed-free boundary conditions, and thus changes in vibration responses were examined and gained to the literature.

MATERIAL AND METHODS

In the current study, CFRP, GFRP, and hybrid composites were fabricated and then subjected to accelerated aging, LVI loading, and vibration tests to examine the impacts of fiber material, hybridization, LVI loading, and corrosive environment on modal characteristics. In synthetic fiber-reinforced composites, 3k twill (0°/90°) carbon and twill (0°/90°) E-Glass fabrics with areal densities of 245 g/m^2 and 300 g/m^2, respectively, were employed as reinforcement materials, and thus the impacts of fiber material on dynamic responses have been studied. On the other hand, a combination of 75% LR160 resin and 25% LH160 hardener by weight was prepared as matrix material, and then the resin system was impregnated into the fabrics using the VAHLM method. The resin-impregnated fabrics were kept under vacuum at 80°C for 1 hour, and thus, by removing the air bubbles from the system, specimens with the minimum void content were fabricated. After that, the cured composite panels were machined into 100x150 mm dimensions following the ASTM D-7136 LVI test standard. CFRP and GFRP composites employed 13 layers of carbon and glass fiber, respectively, whereas hybrid composites were produced using 6 carbon and 7 glass fibers. Table 1 shows some details such as final thickness, length, density etc. On the other hand, CFRP, GFRP and hybrid composite specimens and their stacking sequences are shown in Figure 1.

Following specimen fabrication, accelerated aging was employed to evaluate the influence of corrosive environments on CFRP, hybrid and GFR composites. In this regard, composites were placed in a 10% diluted HCl solution and subjected to a corrosive environment for one week and one month. Thus, it was possible to examine the impact of aging time and fiber material on vibration responses. Apart from that, composite specimens were impacted at two distinct velocities, 2 m/s and 3 m/s, to ascertain how LVI loadings affected vibration characteristics following corrosive exposure. In LVI tests, a 5.6 kg hemispherical tip impactor was dropped from the 20.4 and 45.9 cm heights for the impacts with 2 and 3 m/s velocities, respectively, and thus 11.2 and 25.2 J impact energy was transferred to the composite specimens. The experimental studies were carried out in accordance with the ASTM D-7136 standard, utilizing the support fixture depicted in Figure 2, with the boundary conditions set to pinned-support at four points. In LVI tests, force variations are detected as electrical signals thanks to the loadcell, and then the relevant signals are converted into force-time data using a data acquisition system and software. On the other hand, the experimental setup included anti-rebound equipment to avoid multiple impacts, and thus it can be examined how the vibration responses altered when only one impact was applied to the specimens. Figure 2 depicts the process followed to assess the effects of material effects, LVI loadings, and corrosive environments on the dynamic characteristics of composites.

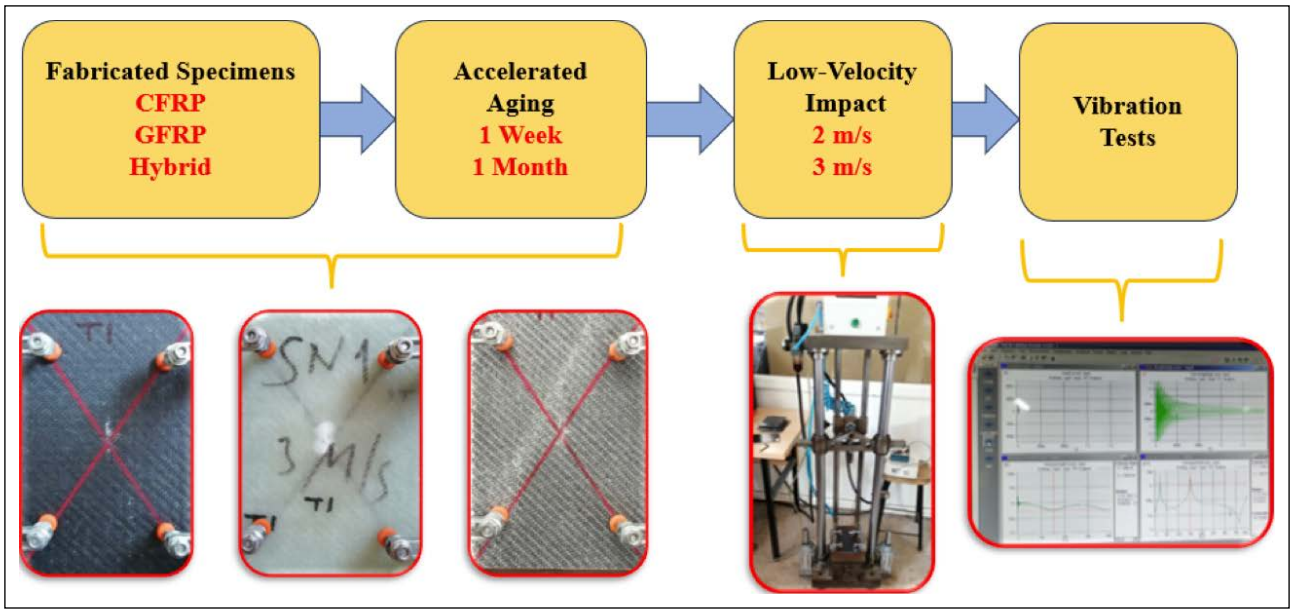

Figure 2. Flowchart for the current study.

Figure 3. Experimental setup for the vibration tests.

Vibration tests were performed to examine variations in dynamic properties following exposure to corrosive environments and LVI loadings, and thus damping ratio and natural frequencies for CFRP, hybrid and GFRP composites were acquired experimentally. As shown in Figure 3, experimental studies were conducted under fixed-free boundary conditions, and amplitude-frequency data were collected from composites pushed to vibrate with an impact hammer utilizing a laser doppler in a non-contact manner. Tests were conducted using a laser Doppler vibrometer, with a 25 kHz sampling frequency and approximately 65600 data points collected for each test. A 0.5 kg impact hammer with a force sensor sensitivity of 2.25 mV/N was used in the experimental studies, and composite samples were excited with a medium-hard polymer tip. While the window method was used to eliminate spectrum leakage before the FFT analyses, and frequency response functions (FRF) were used to fit curves and thus provide natural frequency and damping ratio responses. In this way, natural frequency responses were calculated for CFRP, hybrid and GFRP composites, and the impacts of aging time, LVI loadings, and fiber material on natural frequency were experimentally studied. On the other hand, amplitude-time data were collected for composites, and damping ratio responses were calculated using the free decay method [20] based on the hybridization, fiber material, aging time, and LVI velocity. To avoid degrading effects, vibration tests were carried out at room temperature and atmospheric pressure, and at least 3 repetitions were performed for each specimen type. Moreover, average responses and standard deviations for dynamic responses were obtained; thus, the results were found to be repeatable and reliable.

Table 2. Natural frequency and damping ratio responses for the control and non-immersed composites

	Natural Frequency (Hz)	Standard Deviation	Damping Ratio (%)	Standard Deviation
Control				
GFRP	91.5	4.929503018	0.366666667	0.029337121
Hybrid	120.0	8.221921916	0.63	0.057896459
CFRP	159.8	6.298809411	0.267833333	0.049696747
Non-Immersed (3 m/s)				
GFRP	91.1	3.090082703	0.456222222	0.099261999
Hybrid	111.3	2.179449472	0.435333333	0.094615009
CFRP	154.2	1.952562419	0.238333333	0.062044339
Non-Immersed (2 m/s)				
GFRP	90	5.006246099	0.437111111	0.132642795
Hybrid	117.5	1.5612495	0.889111111	0.092303846
CFRP	157.8333333	2.277608395	0.284888889	0.070223651

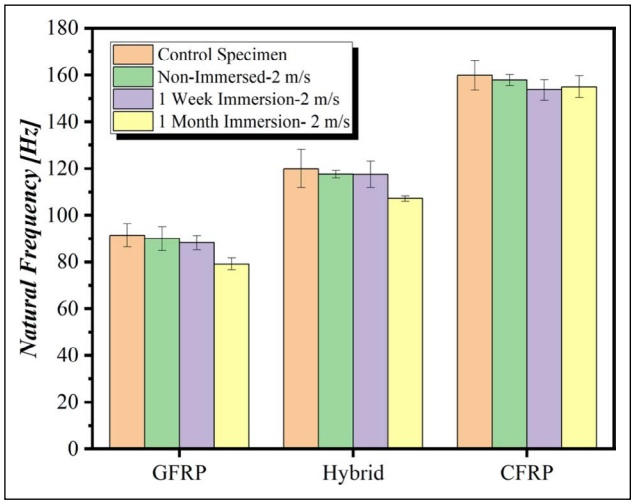

Figure 4. Natural frequency responses for the CFRP, hybrid and GFRP composites subjected to a corrosive environment (2 m/s impact velocity).

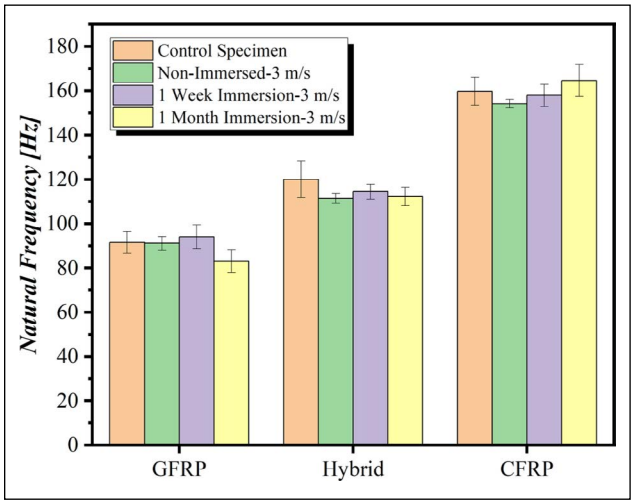

Figure 5. Natural frequency responses for the CFRP, hybrid and GFRP composites subjected to a corrosive environment (3 m/s impact velocity).

RESULTS AND DISCUSSIONS

In the present study, experimental studies were conducted to assess the effects of fiber material, impact velocity, and exposure time to corrosive environments on dynamic responses. In this context, vibration responses for CFRP, hybrid and GFRP composites were obtained and comparatively examined concerning aging time and impact velocity. Figures 4 and 5 show the natural frequency responses of CFRP, hybrid and GFRP composites subjected to 2 and 3 m/s LVI loadings, respectively, varying with exposure time to the HCl environment. Moreover, numerical results for the damping ratio and natural frequencies are shown in Table 2–4. When the findings are evaluated, it is clear that GFRP and CFRP composites exhibit the lowest and highest natural frequency responses, respectively. For example, when the impact of the fiber material is taken into account for the control specimens, the natural frequencies for GFRP and CFRP ones are observed as 91.5 and 159.8 Hz, respectively, and thus, an approximately 75% increment in natural frequencies took place compared to glass fiber-reinforced ones thanks to the carbon fiber utilization. The rise in natural frequency responses is frequently associated with high stiffness, and the responses found in the present study are attributed to the fact that carbon fabrics are stiffer than glass ones. On the other hand, the natural frequency for the hybrid control specimens was determined to be 120 Hz, and it was established that the hybrid composites had a 31% higher natural frequency than the GFRP ones. The related results were interpreted as the hybrid composites exhibited the characteristics of both fabrics and had stiffness between the GFRP and CFRP composites as expected.

When the natural frequencies for the control and non-immersed specimens were examined, a slight drop was observed, but no significant changes took place since the damaged area was localized and limited. This situation was

Table 3. Natural frequency and damping ratio responses for the 1-week immersed composites

	Natural Frequency (Hz)	Standard Deviation	Damping Ratio (%)	Standard Deviation
1 Week Immersion (3 m/s)				
GFRP	94.1	5.352828951	0.444333333	0.085777328
Hybrid	114.4	3.342695187	0.608222222	0.055703830
CFRP	157.9	4.94834428	0.311555556	0.031321363
1 Week Immersion (2 m/s)				
GFRP	88.33333333	3.041381265	0.503333333	0.10459565
Hybrid	117.4444444	5.62052291	0.403333333	0.094597833
CFRP	153.6111111	4.342938074	0.252444444	0.057591473

Table 4. Natural frequency and damping ratio responses for the 1-month immersed composites

	Natural Frequency (Hz)	Standard Deviation	Damping Ratio (%)	Standard Deviation
1 Month Immersion (3 m/s)				
GFRP	83.1	5.122119787	0.532222222	0.069524776
Hybrid	112.2	4.21389896	0.423111111	0.050851363
CFRP	164.6	7.270564704	0.309111111	0.083914308
1 Month Immersion (2 m/s)				
GFRP	79.16666667	2.537222891	0.434888889	0.091769336
Hybrid	107.1111111	1.21906157	0.387	0.05652212
CFRP	155	4.562071898	0.261222222	0.055352908

interpreted as the LVI loading did not affect the composite structure too much, while the reductions in the natural frequencies were interpreted as a slight degradation in the material stiffness. On the other hand, when the impacts of the corrosive environment on modal properties were examined, it was concluded that aging had no substantial impact on natural frequencies. This situation demonstrates that the carbon/glass fiber-reinforced composites' corrosion resistance was quite high, since neither the structural integrity nor the stiffness of the relevant structures deteriorated significantly. Apart from that, when the natural frequency responses for various impact velocities are compared in Figures 4 and 5, it becomes apparent that raising the impact velocity from 2 m/s to 3 m/s has no significant effect on the findings. This demonstrates that the relevant impact velocities are insufficient to cause substantial deterioration in structural integrity, as well as no significant degradation in the dynamic properties of composites subjected to local damage. When the relevant studies in the literature are examined, it is stated that the change in the modal responses is not significant in the case of a limited impact area. For example, Srihi et al. [21] investigated vibration responses following LVI and discovered that, while there was a reduction in natural frequencies as energy increased, the reduction was fairly minimal in some modes. In another work, Katunin et al. [22] investigated the damage analysis and modal responses of various composite structures and discovered that modal parameters were not significantly sensitive to minor damage in local areas.

In their application areas, composite materials can be subjected to vibration loadings at various frequencies, and structures can exhibit vibration with extremely large amplitudes in the case of resonance. This situation induces critical stresses, causing components to lose functionality and get damaged. On the other hand, inherent damping is a crucial material property and can be defined as the amount of energy absorbed within the material [23]. In the case of resonance, vibration movement is reduced in materials with relatively higher inherent damping in a shorter time, reducing the probability of damage. On the other hand, composite materials may be subjected to a variety of corrosive environments in their application areas, which can cause a degradation in vibration properties, particularly in the damping ratio. For that reason, in the present study, vibration tests have been conducted to assess the effects of impact velocity and aging time on the damping ratios, and related responses were presented comparatively for CFRP, GFRP and hybrid composites in Figures 6 and 7. When damping properties are evaluated, it becomes apparent that the LVI loadings induce a slight increase in damping ratios, but no substantial changes take place. This situation demonstrates that the impact and aging cause little structural integrity deterioration; however, raises in damping ratios are attributed to composite damages, resulting in a slight rise in energy absorption. When the studies on the relevant modal characteristics are eval-

Table 5. T-test responses obtained for the vibration properties

Material	Response	Group 1	Group 2	T-statistic	P-Value	Significance
GFRP	Natural Freq.	Control	1 Week Immersion (3 m/s)	-2.23	0.0412	Yes
GFRP	Damping Ratio	Control	1 Month Immersion (3 m/s)	2.45	0.0278	Yes
Hybrid	Damping Ratio	Control	Non-Immersed (3 m/s)	-2.31	0.0325	Yes
CFRP	Natural Freq.	Control	1 Month Immersion (2 m/s)	2.58	0.0189	Yes
CFRP	Damping Ratio	Control	1 Week Immersion (2 m/s)	-3.12	0.0093	Yes
Other Combinations	–	–	–	–	p≥0.05	No

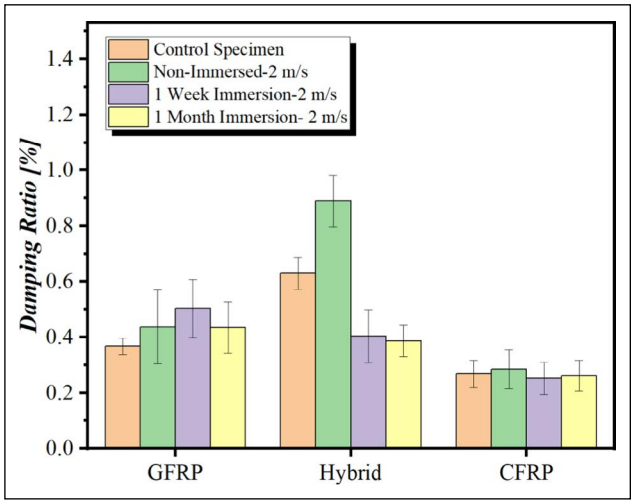

Figure 6. Damping ratio responses for the CFRP, hybrid and GFRP composites subjected to a corrosive environment (2 m/s impact velocity).

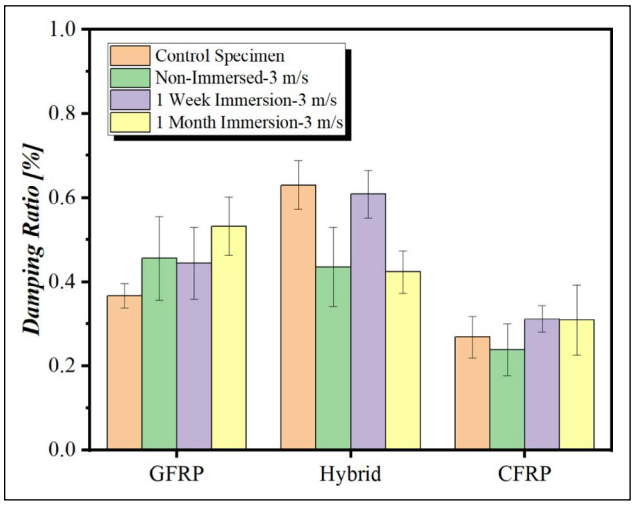

Figure 7. Damping ratio responses for the CFRP, hybrid and GFRP composites subjected to a corrosive environment (3 m/s impact velocity).

uated, it is obvious that the amount of change in the responses varies based on the moisture absorption, and that there were no substantial changes in the responses when the absorption was inadequate. For example, Namrata et al. [24] discovered that moisture absorption in the composite raised due to the aging effect, which somewhat elevated the samples' mass while partially reducing their natural frequencies. However, they reported that high water absorption resulted in a considerably more profound reduction. In another study conducted by Mayya et al. [25], it was stated that moisture absorption is one of the most important parameters affecting the mechanical properties of marine structures, and that pH change and moisture absorption weaken the stiffness and bending properties.

On the other hand, when the impacts of fiber material on composite damping were evaluated, hybrid composites were shown to have higher damping ratios than GFRP and CFRP ones. This was attributable to the various interface characteristics of glass and carbon fibers, resulting in an increment in internal energy distribution. Apart from that, unusual fluctuations in damping responses were detected, which were attributable to structural differences in the composites, experimental disturbances, and production-related variations. A t-test was used to assess the significance of the vibration data, and thus p values were obtained from relevant tests, taking into account composite materials, accelerated aging, and LVI effects. When the data were evaluated, as indicated in Table 5, it was discovered that the responses were significant and the findings were reliable.

CONCLUSION

In the current study, CFRP, GFRP and hybrid composites were produced and subjected to vibration tests to determine the impacts of fiber material, LVI loading and corrosive environments on the vibration characteristics of composites. In addition to the control specimens, the dynamic responses for composites subjected to various impact velocities and immersed in 10% diluted HCl environments were experimentally achieved and presented comparatively. The following are some significant outcomes from the present study:

- Natural frequency responses for GFRP, hybrid, and CFRP control specimens were found to be 91.5, 120, and 159.8 Hz, respectively, and the utilization of carbon fibers resulted in a 75% increment in natural frequencies when compared to GFRP. The relevant findings demonstrate that CFRP composites exhibit the highest natural frequency, which is ascribed to the relatively greater stiffness of carbon fibers. On the other hand, hybrid ones were observed to exhibit the common characteristics of both composites and, as expected, exhibited a natural frequency between CFRP and GFRP composites.
- It was determined that there was no significant change in the dynamic characteristics of the composites exposed to the HCl environment. This was ascribed to the excellent corrosion resistance of synthetic fiber-reinforced composites and thus no significant changes in the structural integrity.
- Examining how LVI loading affects the natural frequencies reveals that there is a slight reduction due to the impact, but no notable alterations take place because the damaged area is limited and local. Similarly, it was determined that there were no significant changes in the vibration responses as a consequence of ascending the impact velocity from 2 m/s to 3 m/s, and this was interpreted as the impacts at the relevant velocities did not cause significant degradation in the material stiffness.
- When the damping ratios for CFRP, GFRP, and hybrid composites were examined, the hybrids demonstrated the highest damping ratios. The relevant responses were attributed to the differences in interface characteristics between glass and carbon fabrics, which were interpreted as enhanced energy absorption within the structure.

Data Availability Statement

The authors confirm that the data that supports the findings of this study are available within the article. Raw data that support the finding of this study are available from the corresponding author, upon reasonable request.

Author's Contributions

Betül Sözen Coşkun: Methodology, investigation, visualization, writing – original draft, editing.

Taner Coşkun: Methodology, investigation, visualization, writing – original draft, editing.

Serkan Kapici: Experimental tests, specimen fabrication.

Yavuz Selim Tarih: Experimental tests.

Ömer Sinan Şahin: Conceptualization, validation, editing.

Conflict of Interest

The authors declared no potential conflicts of interest with respect to the research, authorship, and/or publication of this article.

Financial Disclosure

This work is supported by the Coordinatorship of Scientific Research Projects of Konya Technical University (Project Number: 201010035).

Statement on the Use of Artificial Intelligence

Artificial intelligence was not used in the preparation of the article.

Ethics

There are no ethical issues with the publication of this manuscript.

REFERENCES

[1] Fan, W., Li, J. L., Chen, L., Wang, H., Guo, D. D., & Liu, J. X. (2016). Influence of thermo-oxidative aging on vibration damping characteristics of conventional and graphene-based carbon fiber fabric composites. *Polymer Composites, 37*(9), 2871-2883. [CrossRef]

[2] Ramalingam, R., Hemath, M., Rangappa, S. M., Siengchin, S., & Chellapandi, P. S. D. (2022). Aging effects on free vibration and damping characteristics of polymer-based biocomposites: A review. *Polymer Composites, 43*(6), 3890-3901. [CrossRef]

[3] Coskun, T., Sozen, B., Kapıcı, S., & Sahin, O. S. (2024). Mechanical and dynamic characteristics for the CFRP, GFRP, and hybrid composites exposed to HCl environment. *Journal of Reinforced Plastics and Composites*. [Epub ahead of pint] doi: 10.1177/07316844241301. [CrossRef]

[4] Doğan, N. F., Oğuz, Z. A., & Erkliğ, A. (2023). An experimental study on the hydrothermal aging effect on the free vibration properties of hybrid aramid/glass/epoxy composites: Comparison of sea water and distilled water. *Polymer Composites, 44*(10), 6902-6912. [CrossRef]

[5] Senthilrajan, S., & Venkateshwaran, N. (2019). Ageing and its influence on vibration characteristics of jute/polyester composites. *Journal of Polymers and the Environment, 27*(10), 2144-2155. [CrossRef]

[6] Coskun, T., Sozen, B., & Sahin, O. S. (2024). Dynamic responses and damage/element composition analysis of thermoplastic polyamide reinforced epoxy composites exposed to HCl environment. *Polymer Composites, 45*(14), 13378-13391. [CrossRef]

[7] Mlyniec, A., Korta, J., Kudelski, R., & Uhl, T. (2014). The influence of the laminate thickness, stacking sequence and thermal aging on the static and dynamic behavior of carbon/epoxy composites. *Composite Structures, 118*, 208-216. [CrossRef]

[8] Cheour, K., Assarar, M., Scida, D., Ayad, R., & Gong, X. L. (2016). Effect of water ageing on the mechanical and damping properties of flax-fibre reinforced composite materials. *Composite Structures, 152*, 259-266. [CrossRef]

[9] Tian, W., & Hodgkin, J. (2010). Long-term aging in a commercial aerospace composite sample: Chemical and physical changes. *Journal of Applied Polymer Science, 115*(5), 2981-2985. [CrossRef]

[10] Xu, X., Zhang, B., Shi, F., Liu, K., Peng, G., Gao, L., Gao, J., & Du, Y. (2025). Study on the influence of hygrothermal aging on the mechanical properties of carbon fabric/polyetheretherketone composites. *Polymers, 17*(6), Article 724. [CrossRef]

[11] Oğuz, Z. A., Erkliğ, A., & Bozkurt, Ö. Y. (2021). Degradation of hybrid aramid/glass/epoxy composites hydrothermally aged in distilled water. *Journal of Composite Materials, 55*(15), 2043-2060. [CrossRef]

[12] Oğuz, Z. A., Erkliğ, A., & Bozkurt, Ö. Y. (2021). Effects of hydrothermal seawater aging on the mechanical properties and water absorption of glass/aramid/epoxy hybrid composites. *International Polymer Processing, 36*(1), 79-93. [CrossRef]

[13] Coskun, T., Yar, A., Demir, O., & Sahin, O. S. (2022). Effects of low-velocity impact on vibration behaviors of polyamide fiber-reinforced composites. *Journal of the Brazilian Society of Mechanical Sciences and Engineering, 44*(1), Article 13. [CrossRef]

[14] Akbaş, Ş. D. (2018). İki malzemeli kompozit bir kirişin serbest ve zorlanmış titreşimlerinin incelenmesi. *Politeknik Dergisi, 21*(1), 65-73. [CrossRef]

[15] Tarih, Y. S., Coskun, T., Yar, A., Gundogdu, Ö., & Sahin, Ö. S. (2023). The influences of low-velocity impact loading on the vibration responses of the carbon/glass fiber-reinforced epoxy composites interleaved with various non-woven thermoplastic veils. *Journal of Applied Polymer Science, 140*(15), e53728. [CrossRef]

[16] Çağdaş, İ. U. (2020). The influence of axial compression on the free vibration frequencies of cross-ply laminated and moderately thick cylinders. *J Polytehnic, 23*(1), 45-52. [CrossRef]

[17] Kösedağ, E., & Ekici, R. (2021). Free vibration analysis of foam-core sandwich structures. *Politeknik Dergisi, 24*(1), 69-74. [CrossRef]

[18] Duan, M., Yue, Z., & Song, Q. (2020). Investigation of damage to thick composite laminates under low-velocity impact and frequency-sweep vibration loading conditions. *Advances in Mechanical Engineering, 12*(10), 1687814020965042. [CrossRef]

[19] Daşdemir, A. (2021). Frequency response of an initially stressed slab made from three compressible materials. *J Polytehnic, 24*(1), 275–282. [Turkish] [CrossRef]

[20] Kadioglu, F., Coskun, T., & Elfarra, M. (2018). Investigation of dynamic properties of a polymer matrix composite with different angles of fiber orientations. In *IOP Conference Series: Materials Science and Engineering, 369*(1), Article 012037. [CrossRef]

[21] Srihi, K., Zergoune, Z., Massé, N., Genc, G., & El Hafidi, A. (2022). Modal behavior of post low velocity impact flax/epoxy composite structures. *Vibroengineering Procedia, 43*, 46-51. [CrossRef]

[22] Katunin, A. (2015). Nondestructive damage assessment of composite structures based on wavelet analysis of modal curvatures: State-of-the-art review and description of wavelet-based damage assessment benchmark. *Shock and Vibration, 2015*(1), Article 735219. [CrossRef]

[23] Kayaaslan, M., Coskun, T., Sahin, O. S., Unlu, U. M., & Kadioglu, F. (2022). Mechanical and dynamic responses of unidirectional/woven carbon fiber reinforced thermoset and thermoplastic composites after low velocity impact. *Polymers and Polymer Composites, 30*, 1–11. [CrossRef]

[24] Namrata, B., Pai, Y., Nair, V. G., Hegde, N. T., & Pai, D. G. (2024). Analysis of aging effects on the mechanical and vibration properties of quasi-isotropic basalt fiber-reinforced polymer composites. *Scientific Reports, 14*(1), Article 26730. [CrossRef]

[25] Mayya, H. B., Pai, D., Kini, V. M., Pai, Y., & Nair, V. G. (2021). Effect of marine environmental conditions on physical and mechanical properties of fiber-reinforced composites-A review. *Journal of the Institution of Engineers (India) Series C, 102*, 843-849. [CrossRef]

J Adv Manuf Eng, Vol. 6, Issue. 2, pp. 77–85, December, 2025

Journal of Advances in Manufacturing Engineering
Web page info: https://jame.yildiz.edu.tr
DOI: 10.14744/ytu.jame.2025.00010

Original Article

Non-destructive testing of glass fiber reinforced polypropylene matrix polymeric composites produced by additive manufacturing

Alperen DOĞRU*

Ege University, Aviation Higher Vocational School, İzmir, Türkiye

ARTICLE INFO

Article history
Received: 16 March 2024
Revised: 14 October 2025
Accepted: 16 October 2025

Key words:
Non-destructive testing (NDT), material extrusion-based additive manufacturing (MEX), polymeric composites, polypropylene.

ABSTRACT

Material extrusion-based additive manufacturing (MEX) is an innovative method that has become widely used in the production of polymeric materials. With this method, final products have started to be produced beyond prototype production. However, inherent characteristics of the MEX process can lead to production-related discontinuities that, if undetected, may reduce part performance and cause safety risks or unexpected failures. Non-destructive Testing (NDT) methods, which have been applied in the industry for many years, are crucial in the detection of these discontinuities. To detect discontinuities in thermoplastic composites produced by MEX and to examine the application examples of these methods, samples containing 30 wt% glass fiber with polypropylene matrix were produced in the study. Discontinuities were artificially created in some samples, and the performance of non-destructive testing methods in detecting these discontinuities was measured. 0.1, 0.2, and 0.4 mm layer thicknesses were produced, and the effects of layer thicknesses on ultrasonic sound waves, thermal change rates monitored by thermal camera, and the detection of discontinuities in the sample were examined. In the ultrasonic inspection method, it was found that the increase in layer thickness improves the sound echo transmission and makes it difficult to detect discontinuities in samples with a layer thickness of 0.1 mm. Thermal imaging results revealed that layer thickness did not significantly affect the overall temperature distribution, but the discontinuity detection was more visible in the AL tape region with high thermal conductivity than in the PTFE tape region, and the rate of temperature change was slower in the AL tape region. Discontinuities were detected in NDT controls with ultrasonic inspection and thermal imaging, and it was shown that similar discontinuities can be detected with these techniques.

Cite this article as: Doğru, A. (2025). Non-destructive testing of glass fiber reinforced polypropylene matrix polymeric composites produced by additive manufacturing. *J Adv Manuf Eng*, 6(2), 77–85.

INTRODUCTION

Polymeric composites are lightweight, durable, and economical materials widely used in many areas of our daily lives [1, 2]. These materials offer high mechanical performance play an important role various reinforcing elements integrated into the polymer matrix [3]. In sectors such as aerospace and automotive, composites are preferred to increase fuel efficiency by reducing the weight of vehicles and to meet high strength requirements as well as lightness. Polymeric composites, which have a wide range of applications from sports equipment to medical devices, electronic devices to building materials, energy saving and environmental sustainability. These properties have made them an indispensable part of modern engineering and design [4, 5].

***Corresponding author.**
*E-mail address: alperen.dogru@ege.edu.tr

Within polymeric composites, thermoplastics are increasingly emerging as a preferred matrix material. Due to their properties such as thermoformability, recyclability, and high impact resistance, thermoplastics are used in many industries [6, 7]. Their faster processability compared to conventional thermoset matrices reduces production costs and offers an environmentally friendly alternative [8]. Reinforcing thermoplastics such as polypropylene (PP), polyamide (PA), and polyetheretherketone (PEEK) with glass fiber or carbon fiber offers an ideal solution for applications requiring high strength and stiffness. In addition, the reshape ability of thermoplastic matrix composites contributes to the reduction of waste generated during production and sustainable production processes [9].

Thermoplastic composites are produced by a variety of methods and techniques, including injection molding, extrusion, thermoforming, spinning, and rolling. These methods are selected depending on the size and type of reinforcement material in the composite and the design requirements, and the production scale of the composite product [10–13]. In recent years, additive manufacturing methods have attracted attention as an innovative approach to the production of thermoplastic composites [14]. Additive manufacturing allows composite parts with complex geometries to be produced. The advantages of additive manufacturing include minimized material waste, easy implementation of customized designs, and speed in prototype production [15]. Material extrusion-based additive manufacturing (MEX) is the preferred method for thermoplastic composite production. In this method, the use of thermoplastic compounds formed by reinforcing carbon, glass, etc., fibers makes it possible to produce high-performance and lightweight structural parts. This method opens the door to revolutionary applications in the aerospace, automotive, and medical sectors [16, 17].

High-performance thermoplastic matrices such as polyamide (PA), polyetheretherketone (PEEK), polypropylene (PP), and polycarbonate (PC) are generally preferred in the production of thermoplastic composites for engineering applications. These matrix materials are chosen for their properties, such as high temperature resistance, chemical resistance, and mechanical strength. Fibers such as carbon fiber, glass fiber, and Kevlar are widely used as reinforcement materials. These reinforcements increase the strength and stiffness of the composites while at the same time providing a weight advantage. However, in extrusion-based methods, the bonding quality at the matrix-reinforcement interface, homogeneous material distribution, and interlayer adhesion are aspects that need to be improved [18, 19].

Discontinuities such as insufficient extrusion, layer separation, and interfacial bonding problems can occur in thermoplastic composites produced by material extrusion-based additive manufacturing. If these discontinuities are not detected, the mechanical performance of the produced parts is severely reduced, and unexpected failures may occur during use [20]. Failure to recognize such discontinuities can pose safety risks, especially in critical engineering applications. Non-destructive testing (NDT) methods can be used in the manufacturing process to detect discontinuities. For example, methods such as infrared thermography, ultrasonic inspection, and X-ray computed tomography are effective tools for detecting the quality of adhesion between layers and internal discontinuity [21].

Table 1. GF30-PP mechanical properties (XSTRANDTM 3D Printing Filaments, [25])

Properties	Value	Standard
Tensile Modulus (MPa)	6500	ISO 527 (1 mm/min)
Tensile Strength-Yield (MPa)	60	ISO 527 (1 mm/min)
Elongation-Break (%)	1.6	ISO 527 (1 mm/min)
Flexural Modulus (MPa)	4300	ISO 178 (2 mm/min)
Flexural Modulus-Yield (MPa)	83	ISO 178 (2 mm/min)

Ng et al. [22] developed an acceptance criteria model for quality control checks of MEX-manufactured parts using the 2-dimensional (2D) X-ray NDT technique. Preliminary studies have shown that 2D X-ray imaging can detect embedded discontinuities in MEX-manufactured parts. Hernandez-Contreras et al. [23] similarly focused on discontinuity angles to predict the mechanical properties of MEX fabricated parts using NDT. Computer tomography (CT) scanning was used to measure and analyze discontinuities in tensile test specimens produced by MEX in three different directions. The relationship between the mechanical properties of yield strength (σ) and Young's modulus (E) of the specimens and the detected discontinuity structures was analyzed. Butt et al. [24] also performed ultrasonic examination of graphene-reinforced PLA composites produced by MEX at different print speeds and bed temperature values, and correlations between sound transmission times, hardness, and mechanical properties were determined.

The novelty of this study lies in evaluating the detectability of potential discontinuities—such as artificial holes and delamination-like defects between layers—in glass fiber-reinforced thermoplastic composites produced via MEX using NDT methods. The influence of different types of discontinuities and manufacturing parameters on the performance of NDT techniques was experimentally analyzed through comparative assessments. In this regard, the study aims to contribute to quality control practices for additively manufactured composite materials.

MATERIALS AND METHODS

Material

Xstrand GF30-PP filament from Owens Corning was used in the study. PP matrix filament with 30 wt% glass fiber reinforced has 0.94 g/cm^3 density, 167 °C melting point, 120 °C heat deflection temperature [25]. The mechanical properties of the GF30-PP material used are given in Table 1.

Polytetrafluoroethylene (PTFE) film and aluminum tape (Al Tape) were used to create artificial discontinuities in polymeric composite samples produced by MEX. PTFE films are Aldrich brand, product number GF00775122, and the thickness is 10 microns. Aluminum tape is Aluminum Foil Tape 425 product of the 3M brand. AL tape is thick at 0.12 mm.

Table 2. Fixed MEX production parameters

Parameter	Value
Nozzle temperature (°C)	260
Ambient temperature(°C)	30–35
Bed temperature (°C)	80
Bed modification	Paper tape
Print speed (mm/s)	70
Infill degree (°)	0
Infill percent (%)	100

Production

All sample part productions were carried out with the Ultimaker brand model 3 MEX device. A 0.6 mm diameter CC nozzle with hardened sapphire material was used in the production of 30 wt% glass fiber reinforced thermoplastic composite parts. The fixed parameters used for production are given in Table 2. Paper tape was applied to the glass bed plate to increase the adhesion of the first layer, and production was carried out in this way. All parts were fabricated with 3 different layer thicknesses (0.1/0.2/0.4 mm) using these fixed parameters.

During the production, the ambient temperature was recorded with a Fischer Scientific brand 06-664-11 model Traceable Digital Thermometer. The measured minimum and maximum values are given in Table 2.

To test the performance of the non-destructive detection of discontinuities in polymeric composites produced by MEX, parts containing discontinuities were produced. In this context, a rectangular prism measuring 20 x 30 x 10 mm with a 3 mm diameter hole on it, shown in Figure 1 (a), and a plate measuring 20 x 100 x 3.2 mm, shown in Figure 1 (b), were produced in 3 different layer thicknesses. The drawings of the produced samples were designed in the Autodesk Fusion 360 computer-aided design (CAD) program.

Images of rectangular prisms with a 3 mm diameter hole produced at different layer thicknesses are given in Figure 2. The 3 mm diameter hole is positioned to represent an artificial discontinuity. Some of the rectangular prisms do not contain any discontinuity for comparison.

Table 3. Layers where discontinuities are positioned

Layer thickness	Number of layers	Layers where the tape is positioned
0.1	32	16
0.2	16	8
0.4	8	4

PTFE and AL tapes with a width of 20 mm were placed on the plates produced by MEX in different layer thicknesses, as shown in Figure 3 (a), and the dimensions of the plates and the location of the tapes are shown in Figure 3 (b). Images of samples produced with different layer thicknesses and containing PTFE and AL tape discontinuities are given in Figure 3 (c).

The CURA computer-aided manufacturing (CAM) program was used for adjusting production parameters, and the pause command was added to the G-code file created for production in the relevant layers to position artificial discontinuities in the layers. Position of layers where discontinuities are shown in Table 3. Accordingly, for 3.2 mm thick plates, the pause command was applied after producing layer 16 since the parts produced with a layer thickness of 0.1 mm consist of 32 layers, layer 8 since the parts produced with a layer thickness of 0.2 mm consist of 16 layers and finally layer 4 since the parts produced with a layer thickness of 0.4 mm consist of 8 layers.

The production steps are shown in Figure 4. After step 1, PTFE and AL tapes for artificial discontinuity were positioned in these layers that reached exactly midpoints, like step 2, and after production continued. Produced in 3 different layer thicknesses, some parts of the plates are free of discontinuity, and some parts also have layer separation created with PTFE tape and AL tape, as shown in step 3.

Testing

Ultrasonic and thermographic non-destructive testing methods were used to identify discontinuities and to examine the effect of layer thickness on discontinuity detection.

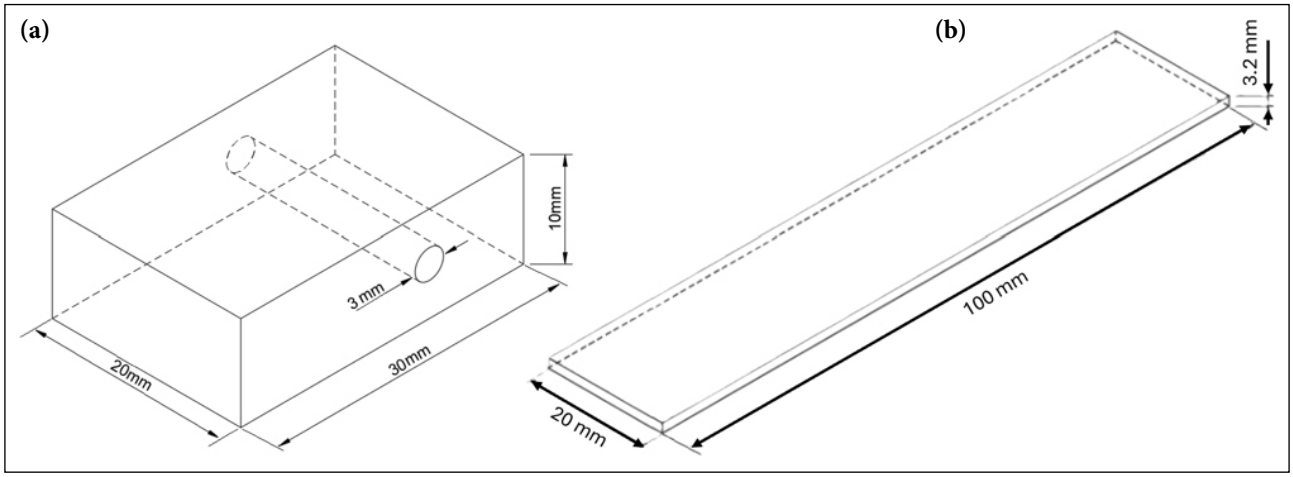

Figure 1. Composite Test Samples produced by MEX.

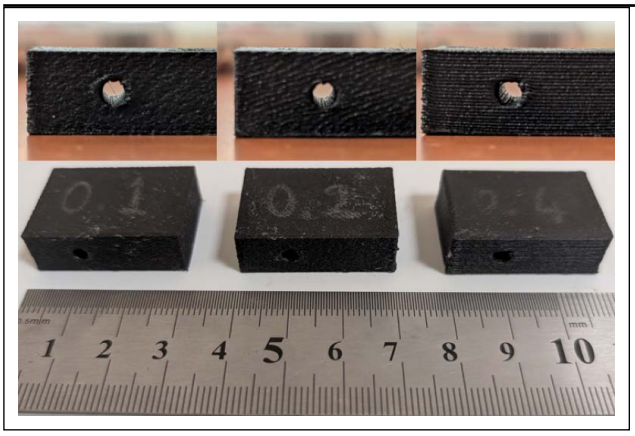

Figure 2. Rectangular prisms with a 3 mm diameter hole produced at different layer thicknesses.

The detection performance of discontinuities in a rectangular prism part with a 3 mm diameter artificial discontinuity produced in different layer thicknesses was performed by ultrasonic inspection. Ultrasonic inspection was performed with a Digital Ultrasonic Flaw Detector from Tru-test. Polymer materials generally have a low acoustic impedance, and high-frequency ultrasonic waves are very damp in these materials. Therefore, Tru-Sonics' BD-412 model with a frequency of 4 MHz and a 12 mm crystal size with a ceramic surface was used in the tests.

Thermal imaging was performed with the UNI-T brand UTi120T thermal imaging camera. The camera resolution is 120*90 pixels, the temperature sensitivity is +/-2 °C, and the frame rate is 25 Hz. The samples were heated to 60 °C in a Nucleon NKD-250 oven before thermal imaging. All thermographic measurements were performed at room temperature, and the ambient temperature was recorded with a Fisher Scientific thermometer. The change from 60 °C to room temperature was monitored and recorded at 30-second intervals. With the images obtained, the thermal temperature changes of the artificial discontinuities created in the specimens were analyzed.

RESULTS AND DISCUSSIONS

Ultrasonic Testing

The images obtained because of ultrasonic testing on rectangular prism samples with a 3 mm diameter hole produced at different layer thicknesses are shared in Figure 5. The graphs on the left in Figure 5 belong to the region with a 3 mm diameter hole created for artificial discontinuity. The graphs on the right in Figure 5 are obtained from the discontinuity-free region. The tests were performed at 10 dB, with a 2 mm delay signal and filtering signals below 30%. The horizontal axis in the graphs shows the distance of the measured echoes to the probe in mm. A 2 mm delay was applied due to interference echoes coming from the area where the probe is in contact with the sample, so the horizontal axis starts at 2 mm. The signals on the vertical axis represent the intensity of the echoes generated by the 10dB sound, reflected from the inner region of the material. In this section, signals below 30% were filtered out for an optimized image of the echoes.

No sound echo was detected in the region where the discontinuity was in each sample, at a depth of 5 mm. With a 0.4 mm layer thickness, the thickness of the rectangular prisms produced in layers was obtained accurately. In the perfect region, the thickness was measured as 10.1 mm, close to the part thickness of 10 mm. In the region containing the discontinuity, the thickness was measured to be 9.8 mm. This is an acceptable tolerance considering the sensitivity of the ultrasonic inspection method and the sound transmission capabilities of polymeric materials [26, 27]. In the echoes from the region containing the discontinuity, It was found that the 3 mm diameter hole region was located at a depth of 5 mm. After the discontinuity, it was observed that the thickness was slightly under-measured due to the loss of echoes. Similarly, the location of the discontinuity in the rectangular prism specimens with 0.2 mm and 0.1 mm layer thickness is seen in the 5 mm depth region. In specimens with a 0.2 mm layer thickness, a thickness of 9.6 mm was

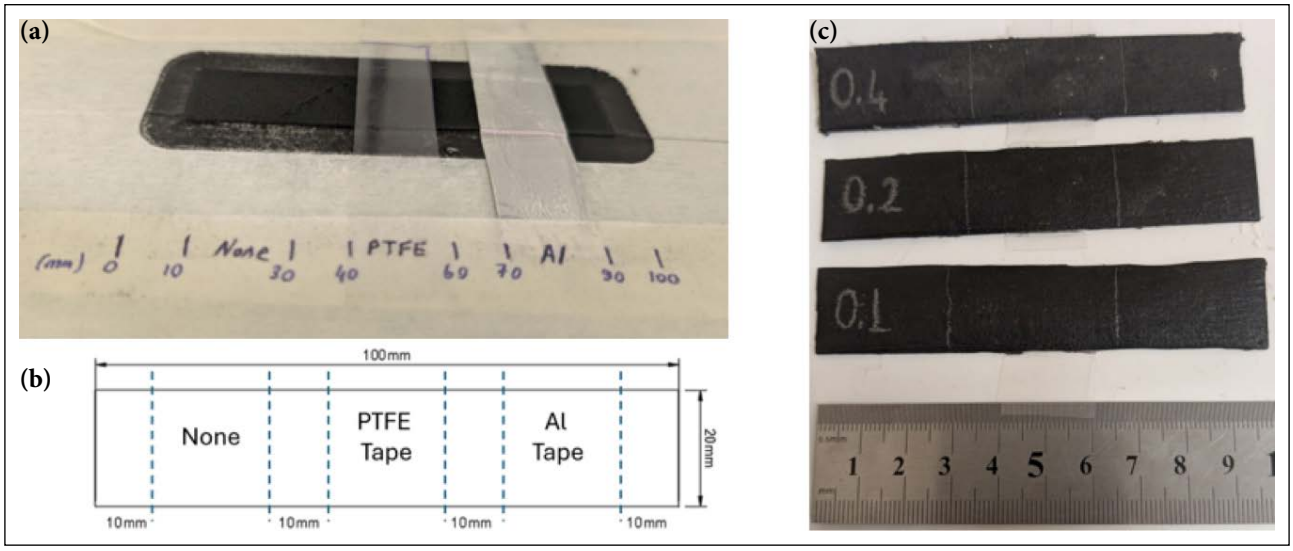

Figure 3. **(a)** The artificial discontinuity location in the plates produced by MEX **(b)** Dimensions of plates and location of tapes **(c)** Production of the plates by MEX.

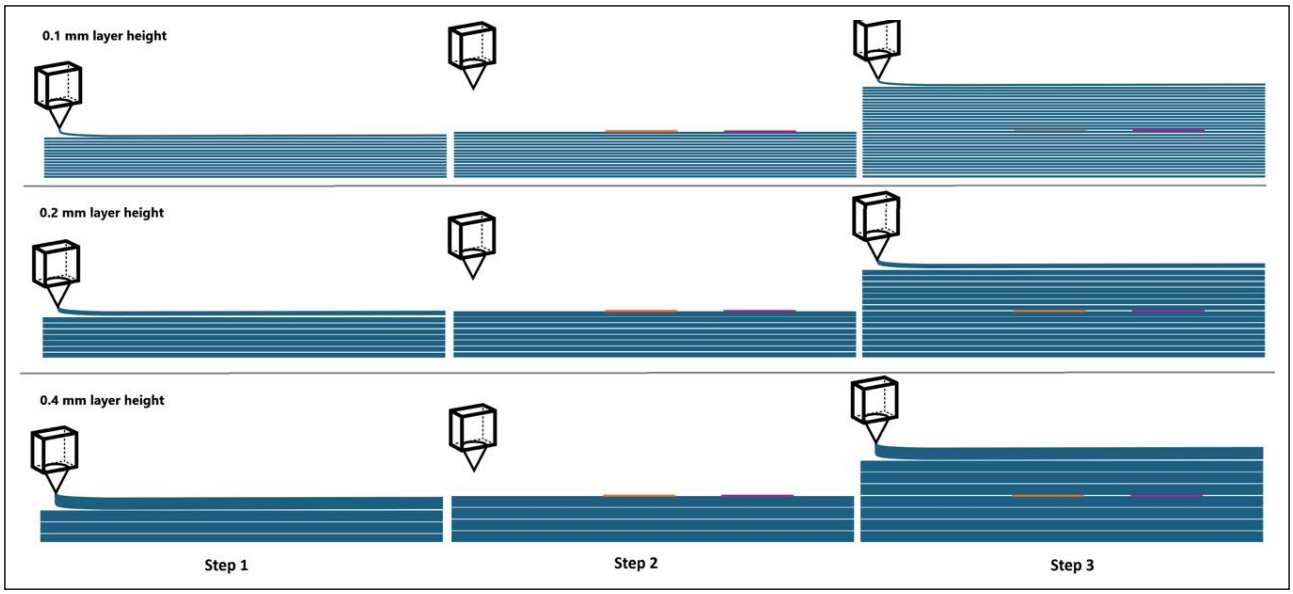

Figure 4. Plates production steps by MEX.

measured in the discontinuity-free zone at the same settings. However, in specimens with a 0.1 mm layer thickness, the thickness in the discontinuity-free zone was measured as 8.5 mm. Butt et al. [24] conducted a study on sound transmission in graphene-reinforced PLA composites produced by MEX with a 0.2 mm layer thickness. In their study, they stated that the production parameters did not significantly affect the sound transmission rate. Similarly, the results show that production parameters affect sound transmission. For example, while the measurements taken from the region without discontinuity in the samples with 0.4 mm and 0.2 mm layer thickness have close values, the number of echoes taken in the samples with 0.1 mm layer thickness decreased, and the thickness value was measured as 8.5 mm. In the region containing a 3 mm hole, the thickness was measured as 8.3 mm; similarly, it was observed that the thickness was slightly lower due to the loss of echo after the discontinuity. The artificial discontinuity was located between the measured thickness values, which allowed it to be detected. However, it would be difficult to detect a deeper discontinuity in samples with a layer thickness of 0.1 mm. This may be due to the layer joints formed by the raw material extruded in layers in MEX production. The junction area of each layer has a negative effect on sound transmission, and the presence of more layers in the samples with a layer thickness of 0.1 mm prevented the echoes traveling along the material from reaching the bottom surface. The specimens with a layer thickness of 0.4 mm had fewer layers and fewer losses at the layer joints, allowing more echoes to be detected for thickness measurements. Samples with 0.2 mm layer thickness showed no significant change, while samples with 0.1 mm layer thickness showed more negative effects. The study conducted by Fayazbakhsh et al. [20] is the first study in which high-resolution images were prepared for parts produced by MEX. In this study, PLA samples containing defects (gaps) were imaged using ultrasonic testing. The study supports the suitability of parts produced by MEX for non-destructive testing. Similarly, the results obtained in the study have shown that discontinuities can be detected in parts produced by MEX using non-destructive testing methods. The results, which were determined for different layer thicknesses by ultrasonic testing, similarly demonstrated the usability of this method in polymeric composites produced by MEX.

Thermal Testing

In Figure 6, time-dependent heat change images of the sample plates produced in different layer thicknesses are shared. The image processing algorithm was run to measure the maximum and minimum temperature values measured in the rectangular region on the screen, and these temperature values were measured in °C. In addition, the temperature value at the point where the PTFE tape was positioned at the center point was also measured. In this way, the temperature values in the AL tape region, in the discontinuity-free region, and in the PTFE tape region were recorded starting from 60 °C until room temperature.

All samples were kept at 60 °C for 24 hours and then imaged at regular intervals until they cooled down at room temperature, respectively. When the temperature changes were examined, no effect was observed due to the layer thickness difference. As seen in Figure 7, all samples tended to cool at similar rates. The data in this graph were created by averaging the maximum temperature values measured on the plate for the relevant minute. The temperature change (ΔT) obtained from the PTFE tape region is 35.8 °C for a 0.4 mm sample, 34.8 °C for a 0.2 mm sample, and 34 °C for a 0.1 mm sample after 7 min. The ΔT obtained in the AL tape region is 34.6 °C for a 0.4 mm sample, 33.9 °C for a 0.2 mm and 33.6 °C for a 0.1 mm sample after 7 min. Changes in layer thickness, although small, affected temperature changes. Increasing layer thickness in both the PTFE and AL tape regions increased ΔT. The presence of more layers in samples with lower layer thicknesses and the interfacial gaps between these layers affected temperature changes.

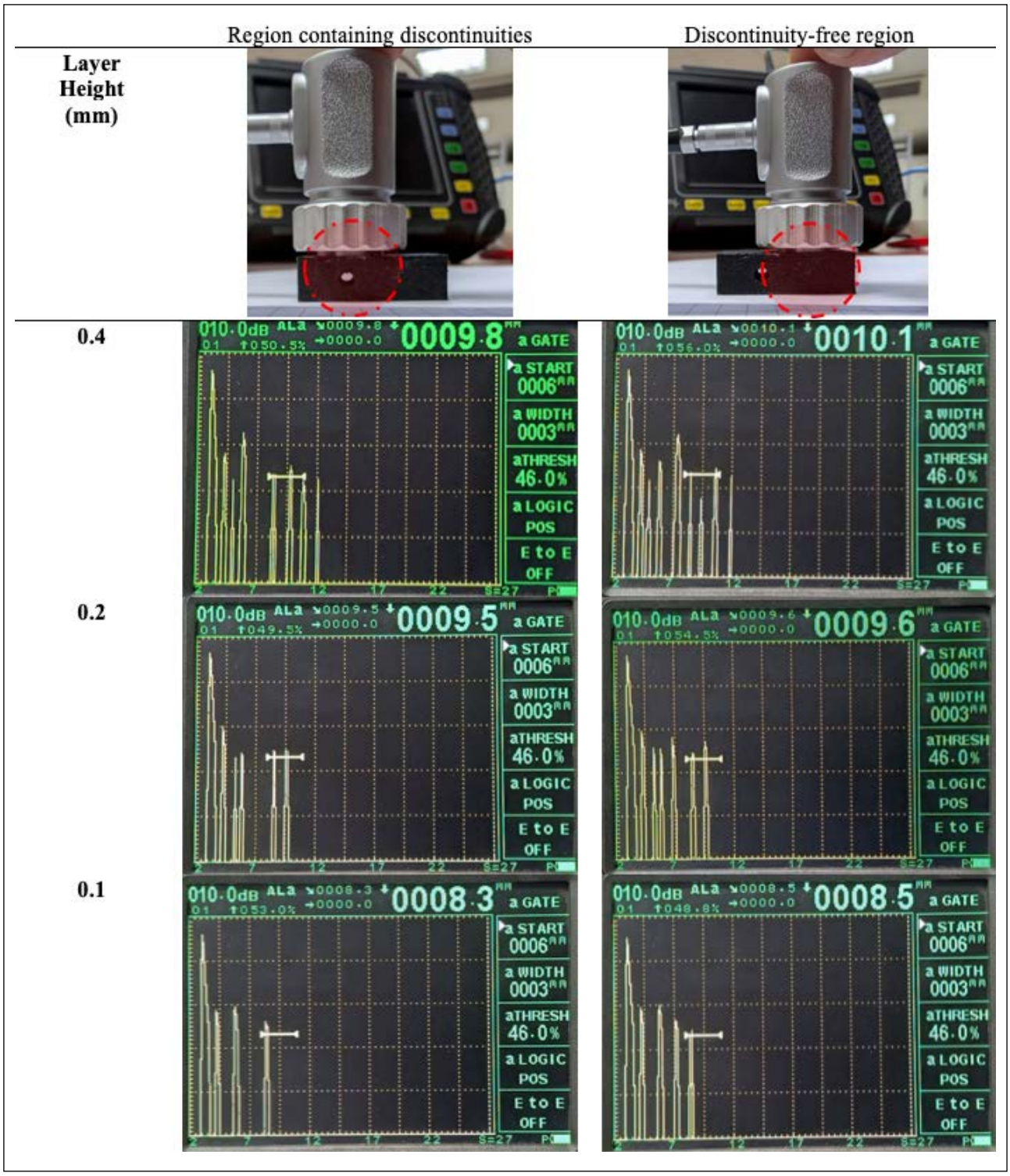

Figure 5. Ultrasonic test results.

When the effect of PTFE and AL tapes on thermal imaging was examined to simulate layer separation, which is one of the important discontinuities encountered in MEX production, it was seen that the highest temperatures were measured in these areas due to the thermal conductivity of AL tape. The temperature values measured in the regions with PTFE tape were not as high as the AL tape values. However, when the temperature values taken from the regions containing PTFE tape corresponding to the midpoint in the measurements are examined, it is seen that the temperature change in these regions also differs compared to the regions without discontinuity. This situation showed that the temperature changes were slower in the regions where thermal conduction was interrupted, where there was layer separation. When the ΔT values were analyzed, a lower temperature change was measured for each layer thickness in AL tape samples. The measured ΔT values varied for both PTFE and AL tape samples depending on the

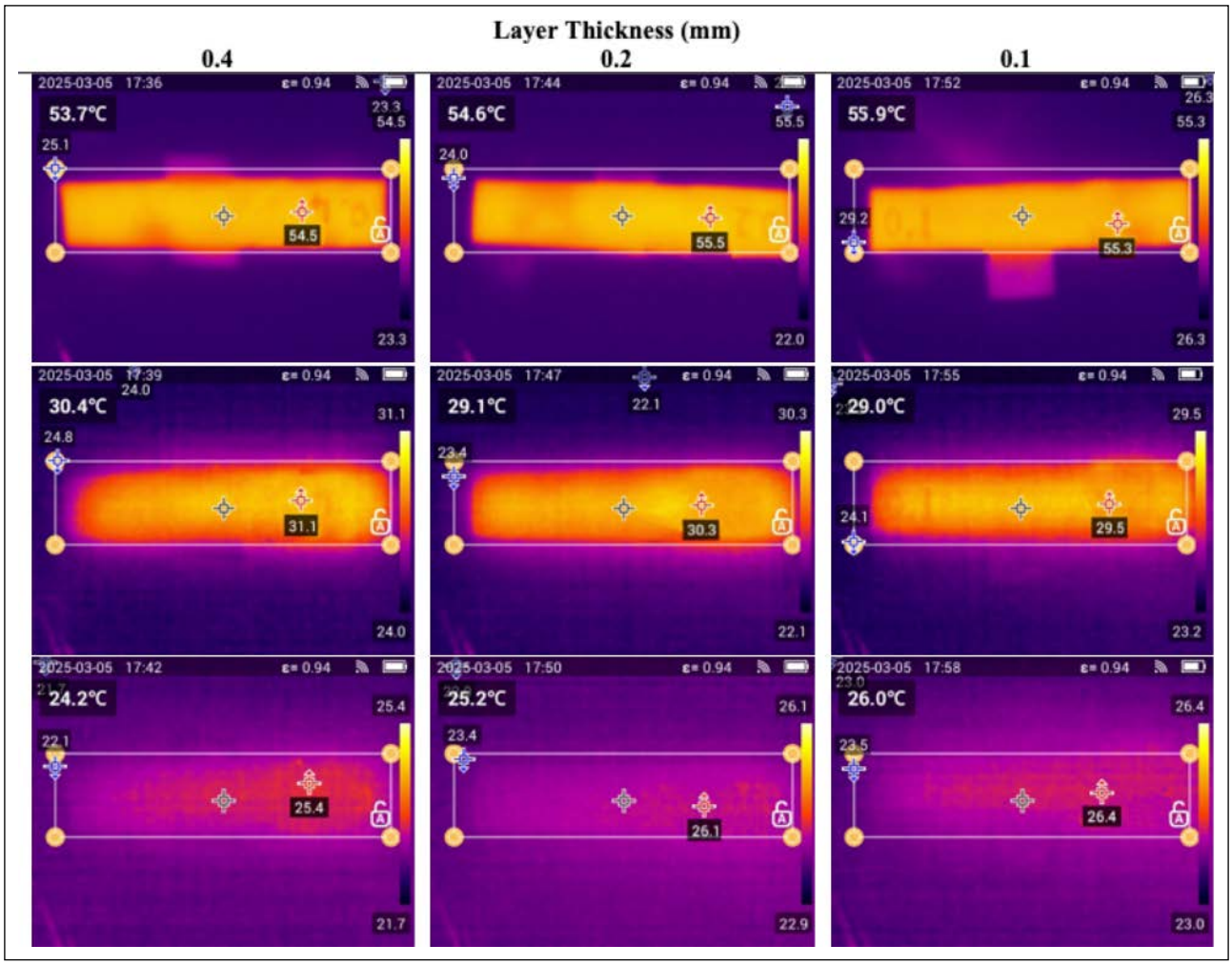

Figure 6. Thermal camera images.

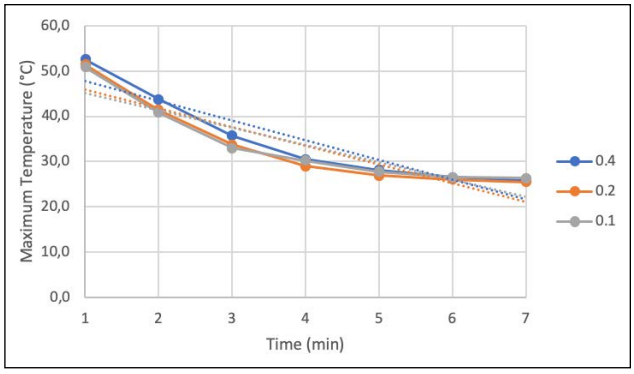

Figure 7. Measured thermal temperature changes.

layer thickness. In both regions, this change is seen as an increasing ΔT with increasing layer thickness. In all samples, slower temperature changes were measured in the regions with AL tape, while a lower temperature gradient was measured in the regions with PTFE tape compared to the regions without discontinuity. This indicates that the thermal conductivity at the points where the layers of the sample plates are in contact is higher than in the regions with layer separation, and that similar discontinuities can be detected by thermal imaging.

CONCLUSION

In this study, the performance of ultrasonic testing and thermal imaging techniques in detecting artificial discontinuities in 30 wt% glass fiber-reinforced polypropylene composites produced by MEX was evaluated for layer thicknesses of 0.1, 0.2, and 0.4 mm.

Ultrasonic detection performance:

- Artificial discontinuities with a 3 mm diameter and 5 mm depth were successfully identified in all samples.
- Measured-to-actual thickness deviations were 1% for 0.4 mm, 5% for 0.2 mm, and 15% for 0.1 mm layer thicknesses.
- Thinner layers (0.1 mm) caused significant signal attenuation and reduced echo clarity, limiting defect detectability.

Thermal imaging performance:

- Layer thickness variation had no major effect on overall temperature distribution.
- The temperature difference (ΔT) in PTFE regions was 35.8 °C (0.4 mm), 34.8 °C (0.2 mm), and 34.0 °C (0.1 mm).
- In Al tape regions, ΔT values were 34.6 °C, 33.9 °C, and 33.6 °C for 0.4, 0.2, and 0.1 mm, respectively.
- Thicker layers showed slightly higher ΔT values, indicating improved thermal conduction stability.

Overall, ultrasonic testing proved more sensitive to internal discontinuities, whereas thermal imaging effectively identified surface and near-surface delaminations. Both methods demonstrated complementary capabilities. The quantitative findings underline that optimal layer thickness and proper NDT technique selection are essential for reliable defect detection and structural integrity assessment in MEX-produced composites.

Data Availability Statement

The author confirm that the data that supports the findings of this study are available within the article. Raw data that support the finding of this study are available from the corresponding author, upon reasonable request.

Conflict of Interest

The author declared no potential conflicts of interest with respect to the research, authorship, and/or publication of this article.

Statement on the Use of Artificial Intelligence

Artificial intelligence was not used in the preparation of the article.

Ethics

There are no ethical issues with the publication of this manuscript.

REFERENCES

[1] Oladele, I. O., Omotosho, T. F., & Adediran, A. A. (2020). Polymer-based composites: An indispensable material for present and future applications. *International Journal of Polymer Science*, *2020*, 1-14. [CrossRef]

[2] Kangishwar, S., Radhika, N., Sheik, A. A., Chavali, A., & Hariharan, S. (2022). A comprehensive review on polymer matrix composites: Material selection, fabrication, and application. *Polymer Bulletin*, *80*, 47-87. [CrossRef]

[3] Rajak, D. K., Pagar, D. D., Menezes, P. L., & Linul, E. (2019). Fiber-reinforced polymer composites: Manufacturing, properties, and applications. Polymers, *11*, Article 1667. [CrossRef]

[4] Ahmad, J. (2009). Introduction to polymer composites (pp. 1-35). In *Machining of Polymer Composites*. Springer. [CrossRef]

[5] Seydibeyoğlu, M. Ö., Doğru, A., Kandemir, M. B., & Aksoy, Ö. (2020). Lightweight composite materials in transport structures (pp. 103-130). In *Lightweight Polymer Composite Structures*. CRC Press. [CrossRef]

[6] Karuppasamy, A., Rexliene, J., Dhandapani, A., Balaji, V., Praveen, R., Sridhar, J., Krishnasamy, S., Kumar Thiagamani, S. M., & Mutjukumar, C. (2023). Recyclability of lightweight and sustainable materials (pp. 79-96). In *Lightweight and Sustainable Composite Materials: Preparation, Properties and Applications*. WP Woodhead Publishing. [CrossRef]

[7] Engelmann, S. (2023). Basics of thermoforming and thermoplastics (pp. 5-11). In *Advanced Thermoforming: Methods, Machines and Materials, Applications, Automation, Sustainability, and the Circular Economy*. John Wiley & Sons. [CrossRef]

[8] Valente, M., Rossitti, I., & Sambucci, M. (2023). Different production processes for thermoplastic composite materials: Sustainability versus mechanical properties and processes parameter. *Polymers, 15*, Article 242. [CrossRef]

[9] Tarih, Y. S., Coskun, T., Yar, A., Gündoğdu, Ö., & Şahin, Ö. S. (2023). The influences of low-velocity impact loading on the vibration responses of the carbon/glass fiber-reinforced epoxy composites interleaved with various non-woven thermoplastic veils. *Journal of Applied Polymer Science, 140*, Article e53728. [CrossRef]

[10] Akdoğan, A., & Vanlı, A. S. (2020). Natural fiber thermoplastic composites in terms of new production technologies: A review. *Pamukkale University Journal of Engineering Sciences, 26*, 30-36. [CrossRef]

[11] Muralisrinivasan, N. S. (2024). Polymers (pp. 5-25). In *Thermoforming: Processing and Technology*. John Wiley & Sons. [CrossRef]

[12] Ilyas, R. A., Sapuan, S. M., Harussani, M. M., Hakimi, M. Y. A. Y., Haziq, M. Z. M., Atikah, M. S. N., Asyraf, M. R. M., Ishak, M. R., Razman, M. R., Nurazzi, N. M., Norrahim, M. N. F., Abral, H., & Asrofi, M. (2021). Polylactic acid (PLA) biocomposite: Processing, additive manufacturing and advanced applications. *Polymers, 13*, Article 1326. [CrossRef]

[13] Vaidya, U. K., & Chawla, K. K. (2008). Processing of fibre reinforced thermoplastic composites. *International Materials Reviews, 53*, 185-218. [CrossRef]

[14] Wang, Y., Ding, Y., Yu, K., & Dong, G. (2024). Innovative polymer-based composite materials in additive manufacturing: A review of methods, materials, and applications. *Polymer Composites, 45*, 15389-15420. [CrossRef]

[15] Zhou, L., Miller, J., Vezza, J., Mayster M, Raffay M, Justice, Q., Al Tamimi, Z., Hansotte, G., Sunkara, L. D., & Bernat, J. (2024). Additive manufacturing: A comprehensive review. *Sensors, 24*, Article 2668. [CrossRef]

[16] Altıparmak, S. C., Yardley, V. A., Shi, Z., & Lin, J. (2022). Extrusion-based additive manufacturing technologies: State of the art and future perspectives. *Journal of Manufacturing Processes, 83*, 607-636. [CrossRef]

[17] Oleff, A., Küster, B., Stonis, M., & Overmeyer, L. (2021). Process monitoring for material extrusion additive manufacturing: A state-of-the-art review. *Progress in Additive Manufacturing, 6*, 705-730. [CrossRef]

[18] Doğru, A., Seydibeyoğlu, M. Ö., & Ayranci, C. (2024). The effect of interface enhancement on the mechanical properties of fibre-reinforced PA6 matrix composites in material extrusion-based additive manufacturing. *Progress in Additive Manufacturing, 10*, 361-374. [CrossRef]

[19] Xavier, S. F. (2023). Applications (pp. 787-886). In *Thermoplastic Polymer Composites: Processing, Properties, Performance, Applications and Recyclability*. John Wiley & Sons. [CrossRef]

[20] Fayazbakhsh, K., Honarvar, F., Amini, H., & Varvani-Farahani, A. (2021). High frequency phased array ultrasonic testing of thermoplastic tensile specimens manufactured by fused filament fabrication with embedded defects. *Additive Manufacturing, 47*, Article 102335. [CrossRef]

[21] Khosravani, M. R., & Reinicke, T. (2020). On the use of X-ray computed tomography in assessment of 3D-printed components. *Journal of Nondestructive Evaluation, 39*, 1-17. [CrossRef]

[22] Ng, F. L., Tran, T. Q., & Liu, T. (2022). A methodology to develop part acceptance criteria model using non-destructive inspection technique for FDM printed part. Materials Today: *Proceedings, 70*, 310-316. [CrossRef]

[23] Hernandez-Contreras, A., Ruiz-Huerta, L., Caballero-Ruiz, A., Moock, V., & Siller, H. R. (2020). Extended CT void analysis in FDM additive manufacturing components. *Materials, 13*, Article 3831. [CrossRef]

[24] Butt, J., Bhaskar, R., & Mohaghegh, V. (2022). Non-destructive and destructive testing to analyse the effects of processing parameters on the tensile and flexural properties of FFF-printed graphene-enhanced PLA. *Journal of Composites Science, 6*, Article 148. [CrossRef]

[25] Prospector. (2025). XSTRANDTM 3D printing filaments material technical datasheet. *UL Prospector*. https://www.ulprospector.com/plastics/en/datasheet/404042/xstrand-gf30-pp Accessed on Nov 21, 2025.

[26] Duchene, P., Chaki, S., Ayadi, A., & Krawczak, P. (2018). A review of non-destructive techniques used for mechanical damage assessment in polymer composites. *Journal of Materials Science, 53*, 7915-7938. [CrossRef]

[27] Yang, H., Yang, L., Yang, Z., Shan, Y., Gu, H., Ma, J., Zeng, X., Tian, T., Ma, S., & Zhanjun, W. (2023). Ultrasonic detection methods for mechanical characterization and damage diagnosis of advanced composite materials: A review. *Composite Structures, 324*, Article 117554. [CrossRef]

J Adv Manuf Eng, Vol. 6, Issue. 2, pp. 86–93, December, 2025

Journal of Advances in Manufacturing Engineering
Web page info: https://jame.yildiz.edu.tr
DOI: 10.14744/ytu.jame.2025.00008

Original Article

Comparative study of machine learning and ensemble learning approach on tool wear classification

Muhammet Ali AYKANAT*[1], Rifat KURBAN[2]

[1]*Department of Electrical and Computer Engineering, Abdullah Gül University, Kayseri, Türkiye*
[2]*Department of Computer Engineering, Abdullah Gül University, Kayseri, Türkiye*

ARTICLE INFO

Article history
Received: 15 January 2025
Revised: 02 May 2025
Accepted: 29 September 2025

Key words:
Classification, ensemble learning, machine learning, machine tools, tool wear prediction.

ABSTRACT

Tool wear is a critical challenge in machining operations, significantly affecting production quality, operational efficiency, and maintenance costs. Traditional approaches, such as sensor-based monitoring and material coatings, have limitations in accurately and proactively predicting tool wear in dynamic manufacturing environments. To address these challenges, this study explores the application of machine learning and ensemble learning methods to improve the reliability and accuracy of tool wear classification. We implemented five different algorithms: K-Nearest Neighbors (KNN), Decision Trees, Random Forests, LightGBM, and XGBoost, to predict the tool condition as "worn" or "unworn." Despite high individual model performances, each exhibited certain weaknesses, motivating the development of an ensemble learning approach. A soft voting classifier, combining KNN, Random Forest, and LightGBM, was proposed to overcome these shortcomings by leveraging the strengths of multiple models. Experimental results demonstrated that the ensemble method achieved superior performance, with an accuracy of 0.9968 on the unseen test dataset. This research highlights the potential of ensemble learning to provide robust, accurate, and generalizable solutions for tool wear prediction, contributing to smarter, more proactive maintenance strategies in manufacturing environments.

Cite this article as: Aykanat, M. A., & Kurban, R. (2025). Comparative study of machine learning and ensemble learning approach on tool wear classification. *J Adv Manuf Eng*, 6(2), 86–93.

INTRODUCTION

Tool wear is a critical issue in machining operations as it directly impacts the workpiece's quality and the machining process's efficiency [1]. The gradual loss of material from the cutting tool due to friction and other factors not only affects the tool itself but also leads to changes in the machined surface and the overall performance of the machine tool Understanding and effectively managing tool wear is essential to maintaining production quality, reducing production time, and minimizing economic losses associated with tool replacement and poor workpiece quality [2].

Researchers have explored various traditional methods and technologies to address tool wear problems without resorting to machine learning or artificial intelligence. One approach involves using sensor fusion strategies to monitor cutting tool wear [2]. By integrating data from different sensors that capture information on tool conditions during machining processes, operators can make informed decisions regarding tool replacement and maintenance to ensure consistent workpiece quality and production efficiency. Additionally, the application of Ti/AlTiN multilayer coatings on cutting tools has been investigated to mitigate the crater wear process and improve the tribological properties of

***Corresponding author.**
*E-mail address: muhammetali.aykanat@agu.edu.tr

the tools [3]. These coating technologies offer a preventive measure against wear, enhancing the durability and performance of cutting tools in machining operations. On the other hand, leveraging machine learning techniques for tool wear classification has shown promising results in enhancing the accuracy and efficiency of wear monitoring systems. Studies have demonstrated using support vector machine (SVM) algorithms coupled with time and frequency domain analysis to correlate sound signals generated during cutting processes with tool wear conditions [4]. Training machine learning models on these acoustic signatures makes it possible to classify tool wear states in real time, enabling proactive maintenance and replacement strategies to be implemented.

Furthermore, the integration of machine learning classification models, such as convolutional neural networks (CNNs), has been explored for online tool wear classification during machining processes [5]. By utilizing real-time cutting force measurements and CNN approaches, researchers have achieved significant accuracy rates in classifying tool wear states, enabling timely identification and mitigation strategies to be deployed [5]. Additionally, the use of pre-trained CNNs for vision-based tool wear classification has been investigated, highlighting the importance of timely identification and classification of wear conditions to guide tool replacement decisions and minimize wear-related issues [6].

In conclusion, the problem of tool wear in machine tools is a multifaceted issue that requires a comprehensive approach for effective management. While traditional methods like sensor fusion and coating technologies offer preventive measures against wear, the use of machine learning and artificial intelligence techniques provide advanced capabilities for real-time wear monitoring and classification. By combining these approaches, manufacturers can optimize tool usage, enhance production efficiency, and ensure consistent quality in machining operations.

In this study, various machine learning algorithms are implemented to address the tool wear problem. By leveraging the capabilities of machine learning, it becomes possible to predict tool wear with higher accuracy and reliability compared to traditional methods. The algorithms used in this study include K-Nearest Neighbors (KNN), Decision Tree, Random Forest, LightGBM, and XGBoost, each known for their unique strengths in handling different aspects of data. These models are compared in terms of their predictive accuracy to identify the most effective approach for tool wear prediction. Additionally, ensemble learning techniques are employed to combine the strengths of multiple models, aiming to achieve more robust and reliable results. Ensemble learning, through methods like voting classifiers, enhances the overall performance by mitigating the weaknesses of individual models, thus providing a more comprehensive solution to the tool wear problem.

MATERIALS AND METHODS

Dataset

The dataset, originating from the University of Michigan's System-level Manufacturing and Automation Research Testbed (SMART) published in April 2018, 18 different machining experiments performed on wax blocks (2" x 2" x 1.5") with S shape using a CNC milling machine [7]. The general data from each of the 18 distinct experiments encompass the experiment number, the material used (wax), the feed rate, and the clamping pressure. Each experiment's outputs include the condition of the tool (unworn or worn) and whether the tool passed a visual inspection. Time series data were collected from the 18 experiments at a sampling rate of 100 ms and are individually documented in files named experiment_01.csv to experiment_18.csv. Each file contains measurements from the CNC machine's four motors (X, Y, Z axes, and spindle). These experiments varied tool conditions, feed rates, and clamping pressures to investigate their effects on machining performance. The aggregated dataset comprised 25,286 observations and 52 features, of which 12 were categorical, and 40 were numerical.

Proposed Method

The proposed method, given in Figure 1, leverages a machine learning and ensemble learning approach to solve the given problem. This methodology comprises three main steps: data preprocessing, model implementation, and ensemble approach.

Data preprocessing is a crucial step that involves handling outliers and missing values, encoding categorical variables, standardizing the features, and performing stratified data splitting. Outlier handling ensures that extreme values do not skew the model's performance while addressing missing values, which prevents the introduction of bias. Encoding categorical variables transforms them into a numerical format suitable for machine learning algorithms. Standardization ensures that the features have a mean of zero and a standard deviation of one, essential for the proper convergence of many machine learning algorithms. Stratified splitting ensures that the train and test sets have similar distributions of the target variable, maintaining the representativeness of the data.

Five different machine learning models are implemented to identify the best solution: K-Nearest Neighbors (KNN) [8], Decision Tree [9], Random Forest [10], LightGBM [11], and XGBoost [12]. Each base model undergoes hyperparameter optimization and is evaluated using 5-fold cross-validation on the training set to ensure robust performance and prevent overfitting. KNN is known for its simplicity and effectiveness in classification tasks [13]. Decision Trees provide interpretability by creating a tree-like structure of decisions [14]. Random Forest, an ensemble of Decision Trees, improves performance through averaging, which reduces variance and prevents overfitting [15]. LightGBM and XGBoost are gradient-boosting frameworks that build models sequentially, with each new model correcting errors made by the previous ones [11, 12]. These methods are compelling for large datasets and have been shown to achieve high predictive accuracy [16, 17].

The ensemble approach employs a voting classifier, evaluated on the test set. The voting classifier combines KNN, Random Forest, and LightGBM as voters. Ensemble methods are known to improve predictive performance by combining the strengths of multiple models [18]. This approach reduces the

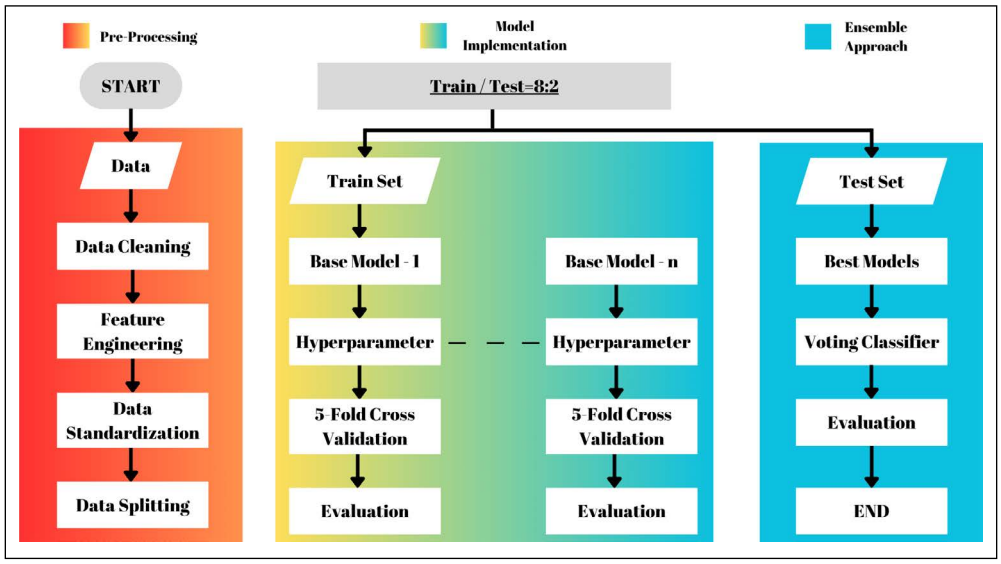

Figure 1. An architecture of proposed method.

likelihood of overfitting and increases robustness and generalization [19]. By aggregating the predictions of diverse models, the ensemble method can achieve higher accuracy and better generalization compared to individual models [20, 21].

RESULTS AND DISCUSSION

Data Preprocessing

The dataset comprised 18 experimental CSV files and one training file containing tool status labels categorized as "worn" or "unworn". The initial step involved merging the 18 experimental files into a single dataset. This merged dataset included features from the experimental files along with additional columns for exp_no, feedrate, clamp_pressure, and tool_condition extracted from the training file.

The aggregated dataset consisted of 25,286 observations and 52 features. Among these features, 12 were categorical, and 40 were numerical.

Outliers were detected in 27 features and addressed using the Interquartile Range (IQR) method to ensure a more robust dataset for analysis.

To prepare the dataset for machine learning algorithms, we meticulously applied label encoding to the tool_condition feature. This process converted the categorical labels "worn" and "unworn" into numerical values, ensuring the accuracy of the data. One-hot encoding was then applied to the other categorical features to avoid any ordinal relationships being implied by the model.

After implementing the encoding, the shape of the dataset was transformed to (25,286, 61), reflecting the addition of new columns from the one-hot encoding process. To standardize the dataset, Min-Max scaling (1) was applied to all features, bringing them into the range [0, 1]. The exp_no feature was subsequently dropped to prevent potential issues with high correlation.

$$X' = \frac{X - X_{min}}{X_{max} - X_{min}}$$

These preprocessing steps resulted in a clean, normalized, and well-structured dataset ready for subsequent machine learning model development and analysis. After pre-processing, the whole dataset was shuffled and split into different CSV files named train and test to ensure the model did not see the data.

Base Model

Before the training phase, the dataset was stratified and split into training and testing sets with an 80-20 ratio, ensuring that both sets' class distribution of the tool_condition labels was preserved. A fixed random state was used to ensure the reproducibility of the results.

Five different machine learning models, KNN, DT, RF, LightGBM, and XGBoost, respectively, were implemented to predict the tool condition of the dataset.

To assess the models' performance and their ability to generalize to unseen data, a 5-fold cross-validation was conducted on the training set. This strategy ensured that each model was trained and validated on different portions of the data, providing a solid evaluation of the model's effectiveness. The results of this evaluation are presented in Table 1.

Hyperparameter Optimization

The same split data and model were used to implement hyperparameter optimization. A 5-fold cross-validation was performed during the training phase to evaluate the models. Hyperparameter optimization was then conducted using the following ranges in Table 2. The hyperparameters' ranges were found and decided by trial and error.

The performance of each model was evaluated based on accuracy, F1-score, and ROC_AUC on the test set. The results of the best models after hyperparameter optimization with the train set are summarized in Table 3.

Model Evaluation

Accuracy measures how correct a model's predictions are overall. It is calculated as the ratio of correctly predicted instances to the total number of instances in the dataset. The formula for accuracy is:

Table 1. Base model train phase results

Model	Accuracy	F1_Score	ROC_AUC
KNN	0.8901	0.8952	0.9539
Decision Tree	0.986	0.9866	0.986
Random Forest	0.9923	0.9926	0.9998
LightGBM	0.9941	0.9944	0.9994
XGBoost	0.9942	0.9945	0.9998

Table 2. Models and their hyperparameter ranges

Model	Hyperparameter	Range
KNN	Number of neighbors	2 to 50
Decision Tree	Maximum depth	1 to 20
	Minimum sample split	2 to 30
Random Forest	Maximum depth	8 to 15
	Minimum sample split	15 to 20
	Number of estimators	200, 300
LightGBM	Learning Rate	0.01 to 0.1
	Number of estimators	300, 500
XGBoost	Learning rate	0.01 to 0.1
	Maximum depth	5 to 8
	Number of estimators	100, 200

Table 3. Models and their hyperparameter results

Model	Accuracy	F1_Score	ROC_AUC	Best parameters
KNN	0.9081	0.9124	0.9576	{'n_neighbors': 3}
Decision Tree	0.9859	0.9865	0.9901	{'max_depth': 19, 'min_samples_split': 7}
Random Forest	0.991	0.9914	0.9997	{'max_depth': None, 'min_samples_split': 15, 'n_estimators': 300}
LightGBM	0.9957	0.9959	0.9996	{'learning_rate': 0.1, 'n_estimators': 300}
XGBoost	0.9946	0.9949	0.9998	{'learning_rate': 0.1, 'max_depth': 8, 'n_estimators': 200}

$$Acc = \frac{TP+\mathrm{TN}}{All}$$

Accuracy is a valuable metric when the classes are balanced, as it provides a straightforward measure of how often the model is correct.

The F1-Score, which is the harmonic mean of precision and recall, serves as a metric that balances false positives and false negatives. It is particularly beneficial for imbalanced datasets because it takes into account both precision (the correctness of positive predictions) and recall (the capability to identify all positive cases). The formula for the F1-score is:

$$F1_{Score} = 2\,x\,\frac{\mathrm{Precision}\times\mathrm{Recall}}{\mathrm{Precision}+\mathrm{Recall}}$$

where

$$Precision = \frac{TP}{TP+\mathrm{FP}}$$

$$Recall = \frac{TP}{TP+\mathrm{FN}}$$

The receiver Operating Characteristic (ROC) and the Area Under the Curve (AUC) are fundamental concepts in evaluating the performance of binary classification models in machine learning and statistics.

The ROC curve is a graphical representation that illustrates the diagnostic ability of a binary classifier system as its discrimination threshold is varied. It is a plot of the True Positive Rate (TPR) (also called sensitivity) against the

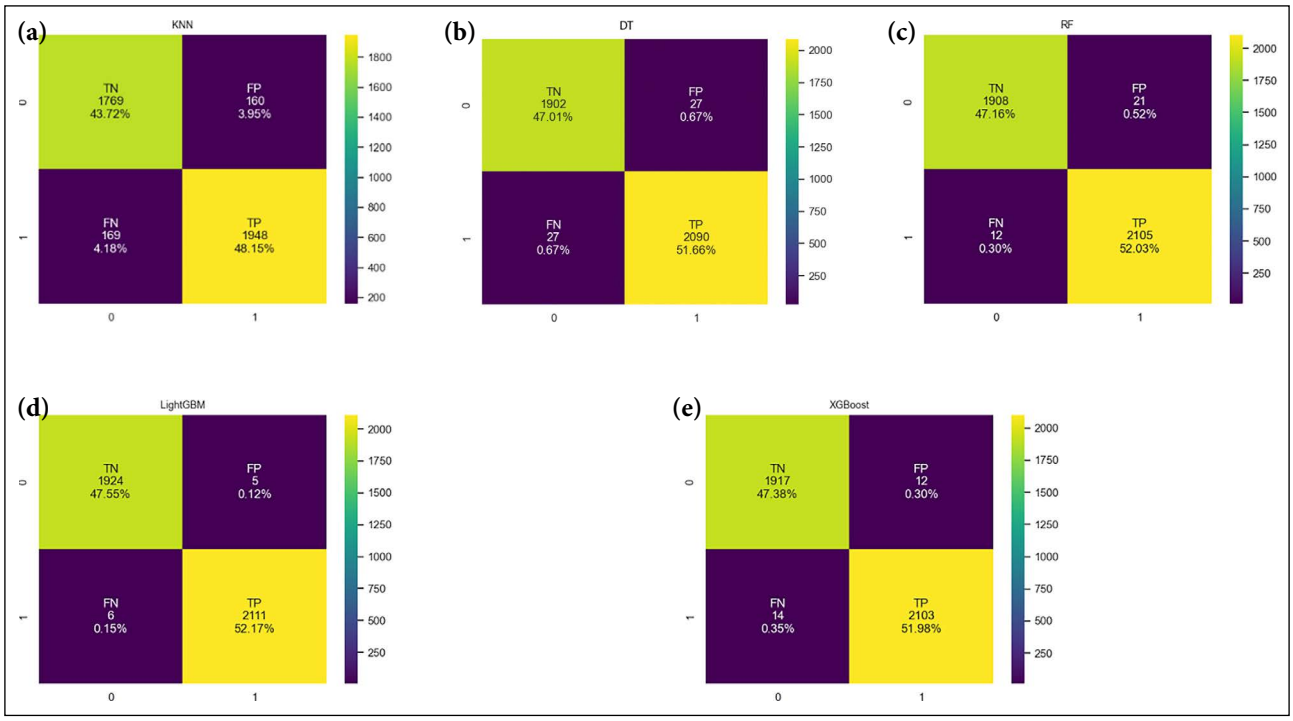

Figure 2. Confusion matrix of 5 models on train-validation sets. KNN **(a)**, DT **(b)**, RF **(c)**, LightGBM **(d)**, XGBoost **(e)**.

False Positive Rate (FPR) (also called false-alarm-rate). So, it is a commonly used summary for assessing the tradeoff between sensitivity and specificity [22]. In mathematical terms, the ROC described as:

$$TPR = \frac{TP}{TP+\mathrm{FN}}$$

$$FPR = \frac{FP}{FP+\mathrm{TN}}$$

The AUC is that summarizes how well a classification model separates positive and negative classes. It is derived from the ROC curve, which plots the true positive rate against the false positive rate at different thresholds. That's why it called ROC_AUC. When the ROC_AUC is 1.0, it indicates that the model perfectly separates the classes, making accurate predictions without any mistakes. An ROC_AUC of 0.5 means the model has no discriminative power and performs as if it were guessing randomly, with no better performance than chance. When the ROC_AUC is less than 0.5, the model performs worse than random guessing, making more incorrect predictions than correct ones, and thus is considered worse than random. The higher the AUC, the better the model is at correctly distinguishing between the classes. Mathematical formula for ROC_AUC is:

$$ROC\_AUC = \int TPR \times d(FPR)$$

where TPR is true positive rate, FPR is false positive rate

Accuracy was selected as the primary evaluation metric for this study because the dataset is close to balanced, with 13,308 instances labelled as "worn" (52.63%) and 11,978 instances labelled as "unworn" (47.37%). In a balanced dataset, accuracy provides a clear and straightforward measure of model performance, as it equally considers the correct predictions of both classes. Additionally, since there is no significant class imbalance, the potential issues of overemphasizing either precision or recall (which the F1-score addresses) are minimized.

Accuracy Comparison of Models on Train-Validation Phase

Prediction results are obtained from the test set and classification report results are given in Table 4.

Experiment results are given in Table 4 and Figure 2 and show that most of the models have good enough accuracy to handle tool wear classification. LightGBM and XGBoost are significantly accurate classifications compared to others.

Ensemble Learning

In ensemble learning, a soft voting classifier is an advanced technique that merges the probabilistic outputs of several machine learning models to determine the final prediction. This classifier makes decisions based on the combined probabilities provided by all the contributing models. The soft voting classifier operates through the following steps:

Base model training: Multiple base classifiers, denoted as $C_1, C_2, .. , C_n$ are independently trained on the same dataset. These classifiers can be homogeneous (same algorithm) or heterogeneous (different algorithms)

Probability Prediction: For given input data x, each classifier C_j produces a predicted probability vector:

$$P_i = [p_{i1}, p_{i2}, .., p_{ij}]$$

where p_{ij} is the predicted probability that belongs to classifier C_j and j is the total predicting class number.

Table 4. Models and their prediction results on train-validation phase

Model	Tool condition	Accuracy	F1_Score	Support
KNN	Unworn	0.9187	0.9149	1929
	Worn		0.9221	2117
Decision Tree	Unworn	0.9867	0.9860	1929
	Worn		0.9872	2117
Random Forest	Unworn	0.9918	0.9914	1929
	Worn		0.9922	2117
LightGBM	Unworn	**0.9973**	**0.9971**	1929
	Worn		**0.9974**	2117
XGBoost	Unworn	0.9936	0.9933	1929
	Worn		0.9939	2117

Table 5. Models and their prediction results on the test phase

Model	Tool condition	Accuracy	F1_Score	Support
KNN	Unworn	0.9203	0.9139	2332
	Worn		0.9259	2725
Random Forest	Unworn	0.9905	0.9897	2332
	Worn		0.9912	2725
LightGBM	Unworn	0.9968	0.9966	2332
	Worn		0.9971	2725
Voting Classifier	Unworn	**0.9970**	**0.9968**	2332
	Worn		**0.9972**	2725

The formula for the soft-voting classifier final decision:

$$\hat{y} = \arg max \sum_{j\ 1}^{m} p_{ij}$$

where $p_{ij} = P_i(\mathrm{C} \mid \mathrm{x})$ is probability for each class C given an input x.

For a classifier task with m models and C classes, each model j outputs a probability distribution $P_i(\mathrm{C} \mid \mathrm{x})$ for each given class C. This approach effectively leverages the strengths and mitigates the weaknesses of individual models, leading to enhanced overall performance.

In this study, KNN, RF, and LightGBM models are utilized as constituent models for the soft voting classifier. KNN is a non-parametric method that classifies a sample by looking at the predominant class among its nearest neighbors. RF is an ensemble approach that utilizes a collection of decision trees to boost predictive accuracy and prevent overfitting by averaging the predictions from several trees. LightGBM is a gradient-boosting framework that utilizes tree-based algorithms, renowned for its efficiency and outstanding performance. To improve performance, 3 different substructures of the machine learning model were selected. The combined use of these diverse models in a soft voting classifier resulted in an exceptional performance on the train-validation phase, achieving an accuracy of 0.9953, an F1 score of 0.9955, and an ROC AUC of 0.9996. Even though the voting classifier model could not reach the training-validation phase, it shows that the voting classifier model is not as effective as LightGBM (0.9972). We need to evaluate the test data to make a final decision. To handle this, all models, including the voting classifier, are saved to make predictions on the test set, which is taken during the data pre-processing phase.

Test results are given in Table 5 and show that even if the model achieves good results in the training-validation phase, it may lose performance on test data that it has not yet encountered. While gradient-based models, like LightGBM, often demonstrate strong performance during the training and validation phases, there is a possibility that their effectiveness may diminish when applied to new, unseen test data. This phenomenon can arise due to the model's reliance on specific patterns learned from the training data, which may not generalize well to other datasets. In contrast, non-parametric models such as K-Nearest Neighbors (KNN) tend to excel in these situations. KNN operates on the principle of proximity, making predictions based on the closest training data points to a given test instance. This flexibility allows KNN to adapt to the underlying structure of the data more effectively, often resulting in improved performance when faced with previously unencountered data. Thus, as can be seen from Table 5, while both model types have their strengths and weaknesses, the voting classifier can eliminate model weaknesses if it contains diverse types of machine learning models.

CONCLUSION

This research highlights the ability of machine learning algorithms to accurately predict tool wear in machining operations. By utilizing aggregated dataset we systematically explored the effectiveness of machine learning and ensemble learning techniques for tool wear classification in machining operations. Through rigorous experimentation with multiple algorithms—K-Nearest Neighbors (KNN), Decision Trees, Random Forests, LightGBM, and XGBoost—we demonstrated that advanced learning methods can accurately differentiate between worn and unworn tool states. LightGBM and XGBoost emerged as the leading individual models, achieving superior classification performance on training phase. Furthermore, by employing a soft voting ensemble composed of KNN, Random Forest, and LightGBM, we achieved an exceptional test accuracy of 99.70% on unseen test data, underscoring the robustness and reliability of ensemble strategies in industrial predictive maintenance contexts.

These findings highlight the potential of machine learning to enhance tool monitoring, allowing manufacturers to implement proactive maintenance strategies. By improving prediction accuracy, companies can reduce costs associated with tool replacement and improve production efficiency.

Future research may focus on integrating real-time data with different types of materials and exploring additional algorithms to further enhance predictive capabilities with fewer features. Overall, this study provides a promising framework for leveraging advanced analytics in manufacturing to optimize operational performance.

Data Availability Statement

The underlying data repository is publicly available on kaggle [7].

Author's Contributions

Muhammet Ali Aykanat: Conception, Design, Supervision, Data Processing, Analysis, Interpretation, Literature Review, Writer.

Rifat Kurban: Conception, Design, Supervision, Interpretation, Writer, Critical Review.

Conflict of Interest

The authors declared no potential conflicts of interest with respect to the research, authorship, and/or publication of this article.

Statement on the Use of Artificial Intelligence

During the preparation of this work the author(s) used ChatGPT-4 in order to improve grammar and style. After using this tool/service, the authors reviewed and edited the content as needed and take full responsibility for the content of the published article.

Code Availability

Code is publicly available and link is provided in reference [23].

Ethics

There are no ethical issues with the publication of this manuscript.

REFERENCES

[1] Ni, J., Liu, X., Meng, Z., & Cui, Y. (2023). Identification of tool wear based on infographics and a double-attention network. *Machines, 11*(10), Article 927. [CrossRef]

[2] Mahardika, M., Taha, Z., Suharto, D., Mitsui, K., & Aoyama, H. (2006). Sensor fusion strategy in the monitoring of cutting tool wear. *Key Engineering Materials, 306*, 727-732. [CrossRef]

[3] Kadhim, K. J., Abbas, A. A., & Hussein, M. A. H. (2018). Effect Ti/AlTiN multilayer coating on the crater wear process of cutting tool and tribological properties. *Al-Khwarizmi Engineering Journal, 13*(4), 58-68. [CrossRef]

[4] Kothuru, A., Nooka, S. P., & Liu, R. (2017). Cutting process monitoring system using audible sound signals and machine learning techniques: An application to end milling. In *Proceedings of the International Manufacturing Science and Engineering Conference, 3*, V003T04A050. [CrossRef]

[5] Terrazas, G., Martínez-Arellano, G., Benardos, P., & Ratchev, S. (2018). Online tool wear classification during dry machining using real time cutting force measurements and a CNN approach. *Journal of Manufacturing and Materials Processing, 2*(4), Article 72. [CrossRef]

[6] Kumar, A. S., Agarwal, A., Jansari, V. G., Desai, K. A., Chattopadhyay, C., & Mears, L. (2023). Vision-based tool wear classification during end-milling of Inconel 718 using a pre-trained convolutional neural network. In *ASME International Mechanical Engineering Congress and Exposition, 3*, V003T03A016. [CrossRef]

[7] Sun, S. (2018). CNC mill tool wear. Available at: https://www.kaggle.com/datasets/shasun/tool-wear-detection-in-cnc-mill Accessed on Oct 3, 2025.

[8] Cover, T., & Hart, P. (1967). Nearest neighbor pattern classification. *IEEE Transactions on Information Theory, 13*(1), 21-27. [CrossRef]

[9] Quinlan, J. R. (1986). Induction of decision trees. *Machine Learning, 1*(1), 81-106. [CrossRef]

[10] Breiman, L. (2001). Random forests. *Machine Learning, 45*(1), 5-32. [CrossRef]

[11] Ke, G., Meng, Q., Finley, T., Wang, T., Chen, W., Ma, W., Ye, Q; & Liu, T. Y. (2017). *Lightgbm: A highly efficient gradient boosting decision tree*. Advances in Neural Information Processing Systems 30. Curran Associates Inc Publisher.

[12] Chen, T., & Guestrin, C. (2016). XGBoost: A scalable tree boosting system. In *Proceedings of the ACM SIGKDD International Conference on Knowledge Discovery and Data Mining, 785*-794. [CrossRef]

[13] Peterson, L. E. (2009). K-nearest neighbor. *Scholarpedia, 4*(2), 1883. [CrossRef]

[14] Safavian, S. R., & Landgrebe, D. (1991). A survey of decision tree classifier methodology. *IEEE Transactions on Systems, Man, and Cybernetics, 21*(3), 660-674. [CrossRef]

[15] Liaw, A., & Wiener, M. (2002). Classification and regression by randomForest. *R news, 2*(3), 18 –22.

[16] Dietterich, T. G. (2000). Ensemble methods in machine learning. In *Multiple Classifier Systems* (pp. 1-15). Springer Berlin Heidelberg. [CrossRef]

[17] Zhou, Z.-H. (2012). *Ensemble methods: Foundations and algorithms* (Vol. 14). [CrossRef]

[18] Rokach, L. (2010). Ensemble-based classifiers. *Artificial Intelligence Review, 33*(1), 1-39. [CrossRef]

[19] Polikar, R. (2006). Ensemble based systems in decision making. *IEEE Circuits and Systems Magazine, 6*(3), 21-45. [CrossRef]

[20] Kuncheva, L. (2014). *Combining pattern classifiers: Methods and algorithms: Second edition* (Vol. 47). [CrossRef]

[21] Opitz, D., & Maclin, R. (1999). Popular ensemble methods: An empirical study. *Journal of Artificial Intelligence Research, 11*, 169-198. [CrossRef]

[22] Hastie, T., Tibshirani, R., & Friedman, J. (2009). *The elements of statistical learning: Data mining, inference, and prediction* (2nd ed.). Springer. [CrossRef]

[23] Aykanat, M. A., & Kurban, R. CNC-tool-wear-detection. Available at: https://github.com/MAAykanat/CNC-Tool-Wear-Detection Accessed on Oct 03, 2025.

J Adv Manuf Eng, Vol. 6, Issue. 2, pp. 94–110, December, 2025

Journal of Advances in Manufacturing Engineering
Web page info: https://jame.yildiz.edu.tr
DOI: 10.14744/ytu.jame.2025.00011

Original Article

Mapping and evaluating the enablers of additive manufacturing for sustainable supply chains using ISM–MICMAC and DEMATEL methodologies

Cihat ÖZTÜRK*, Nurullah GÜLEÇ

Department of Industrial Engineering, Ankara Yıldırım Beyazıt University, Faculty of Engineering and Natural Sciences, Ankara, Türkiye

ARTICLE INFO

Article history
Received: 13 August 2025
Revised: 21 November 2025
Accepted: 05 December 2025

Key words:
Additive manufacturing, sustainability, supply chain management, ISM-MICMAC, DEMATEL.

ABSTRACT

Additive Manufacturing (AM) has been attracting attention in recent years as an innovative production technology that can enhance sustainability in supply chains. Offering maximum material utilization, this technology can reduce waste generated during production. Furthermore, its ability to produce close to the point of consumption makes it environmentally significant. Unlike traditional techniques, it produces layer-by-layer only in the required areas. This enables manufacturing processes that are demand-driven, flexible, and compatible with circular economy principles. This study reveals the factors and obstacles that facilitate the integration of AM into sustainable supply chains. It also aims to assess three-dimensional sustainability impacts. The research explored the interactions between sustainability elements using the ISM (Interpretive Structural Modeling)–MICMAC (Cross-Impact Matrix Multiplication Applied to Classification) and DEMATEL (Decision-Making Trial and Evaluation Laboratory) methods. The results demonstrate that AM-induced enablers play a critical role in influencing the sustainability of supply chains. It is also emphasized that fully realizing this potential requires policy support, stakeholder collaboration, and investments in energy-efficient technologies and environmentally friendly materials. Future research is recommended to focus on the integration of AM with Industry 4.0 technologies and the establishment of legal and economic incentive mechanisms to accelerate its widespread adoption.

Cite this article as: Öztürk, C., & Güleç, N. (2025). Mapping and evaluating the enablers of additive manufacturing for sustainable supply chains using ISM–MICMAC and DEMATEL methodologies. *J Adv Manuf Eng*, 6(2), 94–110.

INTRODUCTION

In modern manufacturing, however, economic efficiency itself has ceased to be a sufficient indicator of performance. Other dimensions, such as environmental and social sustainability of the supply chain, have taken a central place when designing and managing production systems. Herein, AM appears to be one of the most promising technologies with the potential to revolutionize not only sustainable production but also supply chain management [1].

Conventional machining methods carve the parts from large blocks, whereas AM constructs the parts layer by layer, using only the material actually needed [2]. This drastically reduces waste and allows considerable efficiency in resource usage.

Efficiency, flexibility, and the ability to realize tailor-made designs in material use are also among the key features of AM. This leads to supply chains that can be agile and responsive to demand [3]. The ability to produce close to the point of need reduces transportation requirements

***Corresponding author.**
*E-mail address: cozturk@aybu.edu.tr

and, consequently, reduces the overall carbon footprint. In line with the guiding principles of the circular economy, AM allows for materials that are recyclable. This ensures minimum post-production waste, therefore paving ways for sustainable methods of production.

Of course, large-scale use of AM in supply chains is not without its challenges. In particular, institutional investment remains at a low level, technical know-how is lacking, and organizational culture is resistant to change-all factors slowing integration. Besides, even though AM is designed to be much less wasteful of material, its high energy consumption and limited recyclability of certain feedstock materials raise considerable concerns about environmental performance. Technology's transformative impact on traditional supply chains also brings critical risks around cost management, potential process disruptions, and scalability challenges.

The present research identifies the factors of sustainability that need to be prioritized in implementing AM so that its positive impact on sustainable development can be maximized. We analyze the environmental, economic, and social dimensions of the impact of AM, starting from the specific factors that drive this impact. Further, we identify how these factors are interconnected and influence each other. For this purpose, 15 domain experts were involved to map the causal relationship among the identified factors using ISM and MICMAC. The developed causality map makes it crystal clear which underlying driver/s will most effectively enhance the contribution of AM towards sustainability.

The second step was to measure, using linguistic scales, the strength of these causal relationships by the same group of experts. We analyzed their judgments by the DEMATEL method and hence could identify the most critical factors in sustainability and the strength of influence of each factor on others. This will thus indicate where the efforts for improvement must be made.

Ultimately, this research goes further than the simple identification of environmental benefits of AM, since it provides a wide perspective on how AM is able to redesign supply chain processes, and delivers insights that can be used to shape industrial strategies oriented toward sustainable development.

The rest of the paper is organized as follows: first, a review of the literature on the intersection of sustainability and AM, especially within supply chain contexts, is done. Next, the description of the research methods, including justification for why ISM-MICMAC and DEMATEL have been chosen, will follow. Then comes the explanation of the implementation process, including data collection, expert judgments, and analytical steps. Finally, we will present in-depth discussions based on the findings by emphasizing the key enablers of sustainability, their inter-relationships, and implications for theory and practice.

LITERATURE REVIEW

Increasing environmental concerns have motivated manufacturing firms to adopt new or innovative technologies that enable them to produce in an environmentally sustainable manner, reducing resource consumption, global warming, and waste generation [4, 5]. In this industrial scenario, fostered by Industry 4.0, AM technologies play a central and revolutionary role, offering many economic advantages along with potential sustainability [4–8]. AM is the process of producing objects from a three-dimensional model by assembling raw material layer by layer, without molds, tooling, or dies; this is in opposition to traditional methods of manufacturing [9]. Scientific literature on the adoption of AM finds completion in systematic reviews focusing specifically on three aspects of sustainability: environmental, economic, and social [4, 10, 11].

Research interest in the intersection of AM and SC has grown significantly over the past years, increasing the number of publications between 2013–2021 [10, 11]. Studies in this topic typically employ a systematic literature review methodology and conduct an extensive search in databases such as Scopus or Web of Science [4, 10, 12]. The identified literature reported that a high percentage of research was conducted in Europe - %61 and North America, while limited in developing countries like Africa [11]. The most represented academic journals on the subject are: International Journal of Production Economics, Journal of Manufacturing Technology Management, and Additive Manufacturing [10, 12]. Even though most research in this area covers the "Make" dimension inside the SCOR framework, the most covered industries are aerospace, industrial goods, consumer goods, and automotive sectors [10, 11].

From the point of view of economic sustainability, remarkable advantages of firms arise from AM technology. Unlike traditional manufacturing, it overcomes the economies of scale since, with AM, the unit cost of the product does not depend on the volume of production [4, 13]. The utilization of AM provides a potential for shorter production times and, therefore, lower production costs and energy consumption [4, 14]. The decrease in processing waste results in positive monetary value [4, 15]. Moreover, the AM-based digital warehouses decrease significantly the cost of raw material storage and inventory [10, 16, 17]. Relocation of the production site closer to the customer reduces or totally eliminates transportation and distribution costs [4, 18]. However, due to high equipment costs and low machine turnaround times associated with AM, shifting the economies of scale currently still holds many challenges [19–21].

The most important benefits of AM concern environmental sustainability. AM produces complex-shaped products with a minimum of material waste [16, 22]. It helps to improve the circular economy, which involves less waste and less CO_2 emissions [4, 23]. These technologies have many environmental benefits, such as little waste of raw materials, energy, and emissions during manufacturing [24, 25]. Designing the whole product life cycle from a sustainable point of view supports this advantage [26, 27]. Reduction of weight in particular reduces environmental impact caused during the product usage phase [28, 29]. Additionally, AM can recycle its own waste material

and also waste from other manufacturing techniques that are not AM. However, ecological balance can be affected negatively by the high energy requirements of some AM processes [30–33].

Social sustainability and supply chain resilience are increasingly important issues in the AM literature. Research on the social impacts of AM is still limited [4]. There are two key issues: worker conditions and opportunities for localized production. While AM has the potential to improve workers' health by reducing exposure to harsh environments, hazardous materials remain a concern [4]. Furthermore, the potential to relocate production to technologically advanced countries creates instability in countries reliant on industrial production [4, 34]. On the contrary, although AM is expected to reduce labor intensity and create new job opportunities [35], it also offers a risk of negative employment impacts [4]. On the other hand, after global disruptions like COVID-19, AM has again come up as a solution for supply chain resilience [12, 36]. AM enhances supply chain flexibility, reduces lead times, and decreases requirements for safety stock [37–40]. However, high material costs, a lack of material standardization, and energy-intensive processes hinder widespread adoption [11, 12, 40].

Although the impacts of AM on sustainable supply chains are widely discussed in the literature, the existing studies generally remain one-dimensional analyses and fail to explore the hierarchical relationships of the technological, economic, environmental, and social enablers through a holistic system approach. While most explain the benefits of AM at a conceptual level or assess them through case studies of specific sectors, the interdependence structures, impact-degree relationships, and causal links of the drivers (enablers) that enable AM in sustainable supply chains have not yet been systematically mapped. The literature discusses AM's contribution to sustainability from an environmental or economic point of view; however, there is a remarkable gap with regard to prioritization of key enablers, measurement of impact-dependency levels, and strategic roadmap developments.

In this respect, the combined use of decision analysis methods like ISM-MICMAC and DEMATEL offers sound methodological support for an approach which is fundamentally lacking in the literature. These methods will enable us to define the roles of the enablers within a hierarchical structure, such as drivers, dependent and linked, or autonomous variables of AM, in detail, and will make it possible to quantify the causal relationships between them in amplitude. Therefore, a pertinent deficit in the literature consists of the fact that the enabling factors allowing the integration of AM into sustainable supply chains have never been modeled in a systemic way, their relational structures have never been explained, and the determination of managerial priorities has never been performed in an empirical way. It is for this reason that this study, while contributing to the theoretical literature in this subject area, develops an integrated framework for use in industrial applications, strategic decisions support being granted.

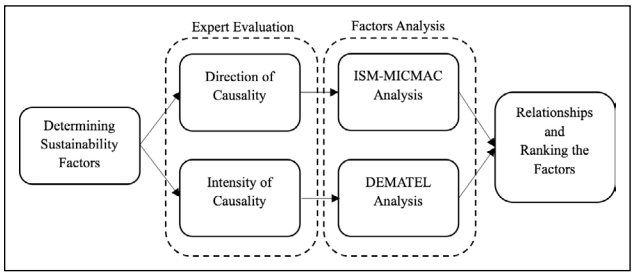

Figure 1. Proposed methodology.

MATERIALS AND METHODS

In this study, the methodological framework shown in Figure 1 was used to identify the key sustainability factors that strengthen the contribution of AM practices to sustainability, as well as to evaluate how the AM approach influences progress toward sustainable development.

In the first step of the proposed methodology, criteria for sustainability were determined by using the literature so that AM could be evaluated by experts. To determine the impact of the resulting sustainability criteria and sub-criteria on AM's sustainability, it is necessary to uncover their hidden inter-relationship effects. In this context, in the second step, expert opinions were obtained through a survey to determine the inter-relationship effects of the sub-criteria and the direction of the impact. In the third step, the obtained expert opinions were analyzed using the ISM method to determine the direction of the relationships and impacts, and the intensity of the relationships was determined using the DEMATEL method. In the final step, the criteria were ranked according to the results obtained, and it was determined which criteria should be given the most importance and developed within the framework of AM's sustainability.

Determining the Sustainability Factors

In the first step of proposed methodology, factors driven by AM and have effect of sustainability are determined. The impacts of AM within the framework of sustainability can be systematically examined under three interrelated dimensions: economic, environmental, and social sustainability. Economically, AM contributes to cost efficiency through reduced material usage, minimized inventory requirements, and streamlined production processes. From an environmental point of view, AM is highly beneficial in reducing material waste, enabling more energy-efficient processes for production, and lastly, allows the manufacture of products locally, thus reducing carbon emissions. The social perspective sees AM fostering inclusivity, increasing the ability to produce highly customized products, and facilitating the adoption of decentralized production methods that can help augment regional manufacturing capabilities. This is able to create new, high-skilled jobs in areas relating to advanced technologies. From both ecological and social standpoints, AM is more than just a novelty in manufacturing; it is also a driver of sustainable industrial change. Figure 2 summarizes the role of AM in terms of the main dimensions of sustainability.

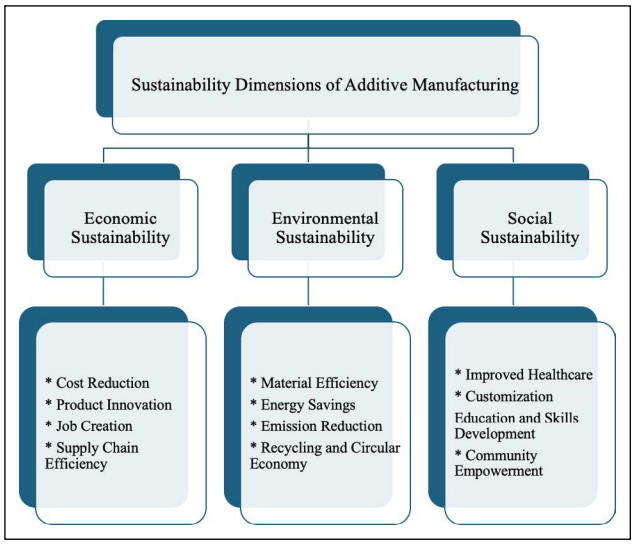

Figure 2. Sustainability dimensions of additive manufacturing.

When we look at it from a sustainable manufacturing point of view, AM brings some clear economic benefits. It changes the way traditional production works and also opens up new job opportunities [41]. Out of the three main pillars of sustainability, the economic side is where its impact can be seen the most. In this context, the key ways in which AM contributes to economic sustainability can be outlined as follows:

- Cost Reduction: AM helps cut material waste, supports demand-driven production that reduces the need for large inventories, and decreases transportation costs by making it possible to manufacture products closer to where they are needed [42].
- Product Innovation: AM makes it possible to produce complex, highly customized designs that traditional manufacturing methods cannot easily achieve. This design freedom opens the door to new markets and niche opportunities, encouraging the creation of innovative products.
- Job Creation: The widespread adoption of AM technology increases the demand for skilled professionals in fields such as design, engineering, and machine operation. This contributes to the creation of employment opportunities in advanced manufacturing sectors, supporting economic growth [42].
- Supply Chain Efficiency: AM facilitates the production of parts closer to their point of use, thereby simplifying supply chains, reducing lead times, and decreasing dependence on offshore manufacturing, ultimately enhancing operational efficiency.

AM contributes to environmental sustainability through its resource-efficient processes and potential for emission reduction [43]. The environmental sustainability benefits of AM can be examined through the following key factors:

- Material Efficiency: AM minimizes waste by using only the exact amount of material required for the product, significantly reducing material waste in comparison to traditional manufacturing processes [44].
- Energy Savings: In industries such as aerospace and automotive, the production of lightweight components using AM reduces energy consumption throughout the product's lifecycle [45].
- Emission Reduction: Localized production facilitated by AM reduces the need for long-distance transportation, which in turn lowers greenhouse gas emissions, contributing to a decrease in the overall environmental footprint [45].
- Recycling and Circular Economy: AM makes it easier to use recycled and even biodegradable materials, which helps support a circular economy where materials are used again instead of being thrown away. This approach moves manufacturing closer to a more sustainable, closed-loop model [43].

AM has a big impact on society by helping improve quality of life, making technology more accessible, and supporting sustainable developmen [46]. We can look at its social impact through a few main aspects:

- Improved Healthcare: AM makes it possible to produce custom medical devices like prosthetics and implants, which can greatly improve patient care and make important healthcare services more accessible [47, 48].
- Customization: AM allows efficient production of customized solutions for many areas, like consumer goods, architecture, and mobility, helping meet the changing and varied needs of society [49].
- Education and Skills Development: The proliferation of AM technology has spurred the development of educational and training programs that equip individuals with the necessary skills to thrive in the future workforce, preparing them for emerging industry demands [50].
- Community Empowerment: By decentralizing manufacturing processes, AM empowers local communities to independently produce goods, thereby fostering self-reliance, resilience, and economic autonomy [51].

Expert Evaluations

In the proposed methodology, expert opinions were obtained for the determination of the sustainability effectiveness of the applications. In this context, experts were asked to compare the sub-criteria in pairs in order to determine their influence on each other. A group of experts with academic and professional backgrounds in the fields of sustainable supply chain management, logistics operations, and AM was called upon to assess the impact of AM on sustainable supply chains using established criteria through pairwise comparison methods. A total of 15 experts were engaged in the pairwise comparison of the criteria.

The academic participants are scholars in sustainability, supply chain management, logistics, operations management, and AM, with a particular focus on the integration of emerging technologies within supply chains.

The majority of the professional participants belong to different industries and encompass practitioners with expertise in supply chain operation practices. The sample also encompasses individuals with experience related to practices of AM and technological integration.

Both groups exhibited a satisfactory level of expertise concerning AM, sustainability principles, and sustainable supply chain management.

Application Steps of Proposed Methods

In this stage, ISM was used to identify relationships among the variables. The facilitators were then classified into different groups using the MICMAC analysis in the form of a driver-dependency diagram. The ISM methodology presents the variables in the form of hierarchical levels of relationship. Similarly, the MICMAC method divides these variables into four classes of variables based on their driving power and dependency characteristics: autonomous (inactive) variables, dependent (affected) variables, link (both affecting and affected) variables, and independent (affected) variables. Lastly, the DEMATEL method is used to analyze facilitators of sustainability on different dimensions. This leads to a cause-and-effect diagram showing the cause-and-effect relationship of factors.

The study used both ISM–MICMAC and DEMATEL methods. Both techniques have been considered powerful tools in solving complex problems that include a lot of interdependent variables [52]. They can be used in investigations of relationships among AM-supported sustainable supply chain management facilitators. The ISM–MICMAC method provides a hierarchical structure by investigating drivers and interdependencies in the facilitators. This provides a clearer view of how these facilitators that affect the dimensions of sustainability influence and are interlinked with each other. This way, the relationships can be investigated in a systematic and transparent way [53].

The DEMATEL method was employed in this study to reveal the cause-and-effect relationships among facilitators after the ISM-MICMAC step. DEMATEL generates a cause-and-effect diagram representing centrality and relationship among the facilitators within the system. Among the strengths of the method is its capability to show not only direct effects but also the broader, indirect effects of these interactions. This comprehensive perspective provides useful insights in making strong and actionable strategic recommendations.

ISM Method

The ISM is an approach that finds interrelationships among factors of a complex system through expert opinion. It is also a step-by-step process of explaining the linkages of a system. These factors are then systematically grouped in a hierarchical order. The method becomes more useful when there are many variables that interact, and multi-level diagrams make visibility and understanding of these relationships easier. Basic steps in applying the ISM methodology are outlined as follows:

- Definition of the Problem and Determination of Objectives: The focus of the study and the variables to be analyzed are clearly defined. The boundaries and scope of the system under investigation are established.
- Identification of Variables (Elements): Key factors, variables, or elements relevant to the system are identified through expert input.
- Determination of Binary Relationships Between Variables: Experts assess the direct pairwise relationships between variables, typically by responding "Yes" or "No" to the question: "Does Variable A Influence Variable B?"
- Construction of the Structural Self-Interaction Matrix (SSIM): The experts' evaluations are put into a matrix, using predefined symbols to show whether a relationship exists and its direction.
- Development of the Reachability Matrix and Conversion to a Binary Matrix: The SSIM is converted into a binary reachability matrix. This matrix shows the direct connections between the variables.
- Calculation of the Transitive Closure: Indirect links between variables are found and added by calculating the transitive closure. This way, the system shows both direct and indirect influences.
- Level Partitioning of Variables: Variables are sorted into different levels. Ones that influence others the most are placed higher, while those that depend more on others are placed lower.
- Development of the Structural Model: The hierarchical relationships among variables are graphically represented, resulting in an ISM model that visually depicts the system's structure.
- Model Review and Validation: Experts review the completed model to check its accuracy and relevance. Any needed changes are made based on their feedback.

MICMAC Method

MICMAC is an analytical method for the study of the interactions between the variables of a system based on the influence they exert and their dependence on the others. Based on an evaluation of these two dimensions, that is, driving power and dependence, the method classifies variables into four distinct groups [54].

The first group, driving variables, are elements that strongly influence others and are themselves only minimally influenced. The second group, dependent variables, strongly influenced by other elements, themselves contribute little influence in return. The third group, called linkage variables, both strongly affect and are strongly affected by others, making them pivotal and often sensitive components of the system. Lastly, autonomous variables show low levels of both influence and dependence, indicating that they have little interaction with the system as a whole. The steps for applying the MICMAC method are described below.

- Identification of Variables: All relevant and significant variables (factors or agents) within the system under investigation are identified.
- Determination of Direct Interactions Among Variables: Utilizing expert judgments or empirical data, the direct influence exerted by each variable on others is assessed. These influences are typically quantified using a numerical scale (e.g., 0: no influence, 1: weak influence, 2: moderate influence, 3: strong influence).
- Construction of the Direct Influence Matrix: The quantified direct effects are organized into a matrix format, where each row corresponds to the influence of a specific variable on all other variables.

- Calculation of Indirect Effects: Through iterative matrix multiplication, indirect influences among variables are computed. This process yields the cumulative effects—both direct and indirect—within the system.
- Computation of Driving and Dependence Powers: For each variable, the total number of variables it influences (driving power) and the total number of variables influencing it (dependence power) are calculated.
- Classification and Clustering of Variables: Based on their driving and dependence powers, variables are classified into four categories: driving variables, dependent variables, linkage variables, and autonomous variables.
- Development of the Driver-Dependency Diagram: Variables are graphically represented according to their driving and dependence scores, providing a visual depiction of their roles and interactions within the system.
- Analysis and Interpretation: The classification and visualization facilitate the identification of system dynamics, critical leverage points, and strategic priorities for intervention or further study.

DEMATEL Method

DEMATEL represents a multi-criteria decision-making method used for analyzing and visualizing the cause-and-effect relationships between components in complex systems. This technique is designed to identify and understand the relationships and interactions that exist between influencing factors.

DEMATEL systematically identifies the causal relationships of variables according to expert opinions: their effects are then quantified and arranged in a structured matrix that considers the relationships through direct and indirect effects. The synthesized information forms a comprehensive map of the relationship between system elements.

This method classifies variables into two broad categories: cause factors and effect factors. Cause factors refer to the main driving forces that determine the value of other variables. Consequence factors are factors driven by other elements in the system and often generate secondary or indirect effects.

One of the key strengths of the method is that it can distinctly show cause-and-effect relationships in the form of a causal network. Such visualization allows identifying the most critical factors that need to be focused on strategically and intervened in. Thus, holistic analysis of system dynamics may be conducted if one considers both direct and indirect interactions. The visualization of the causal diagram is enhancing the interpretability and practical usability of the results.

In that respect, DEMATEL is a well-structured and sound method that is based on expert opinions. It unravels the entangled network of interrelations in a system and visually depicts the underlying causal structure. The steps in using the DEMATEL method are presented as follows.

- Problem Definition and Identification of Variables: Clearly define the scope of the problem and identify the key variables or factors to be analyzed within the system.
- Construction of the Direct Relationship Matrix: Collect expert judgments to evaluate the direct influence of each variable on all other variables. These influences are typically rated on a numerical scale (e.g., 0 = no influence, 1 = low influence, up to 4 = very high influence). The assessments are aggregated to form the direct relationship matrix.
- Normalization of the Direct Relationship Matrix: Normalize the matrix to ensure that all values fall within the interval [0,1]. This is usually achieved by dividing each element by the maximum row or column sum of the matrix.
- Calculation of the Total Relationship Matrix: Compute the total relationship matrix, which incorporates both direct and indirect effects among the variables, thereby capturing the overall influence within the system.
- Calculation of Prominence and Relation Values: For each variable, calculate:
  - Prominence (D + R): The sum of the corresponding row and column values in the total relationship matrix, representing the total involvement or significance of the variable within the system.
  - Relation (D - R): The difference between the row and column sums, indicating whether the variable functions primarily as a cause (positive value) or as an effect (negative value).
- Classification of Variables: Based on the prominence and relation values, classify the variables into cause-and-effect groups. Cause variables are those that drive system changes, whereas effect variables are influenced by others.
- Development of the Cause-Effect Diagram: Plot the variables on a two-dimensional graph using their prominence (D + R) and relation (D - R) values. This diagram visually represents the causal relationships and structural dynamics of the system.
- Interpretation and Decision-Making: Analyze the cause-effect diagram alongside matrix results to identify critical factors, understand the system's dynamic behavior, and support informed strategic planning and decision-making.

APPLICATION OF PROPOSED METHODOLOGY

This study analyzes the relationship and/or structure of the enablers emerging from the effects of AM technology and having impacts on supply chain sustainability. In this context, the driving forces and dependencies of these enablers brought by AM technology are examined. In this regard, the hierarchical interactions among different enablers are addressed through an ISM-based approach and MICMAC analysis and subsequently examined in detail using the DEMATEL method. The results of the study have the potential to enable decision-making mechanisms to effectively utilize the integration of AM technology, which triggers the aforementioned enablers, in ensuring supply chain sustainability. Thus, the related study may serve as a guide in improving the performance of supply chain sustainability.

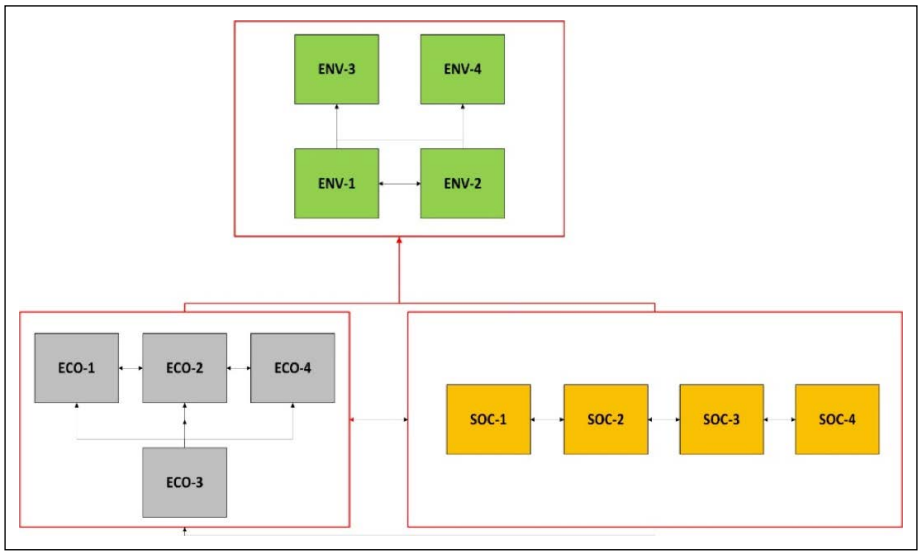

Figure 3. Hierarchical structure of supply chain sustainability sub-criteria affected by additive manufacturing identified through ISM (without inter-dimensional interactions).

This section discusses the output obtained through the combined use of the ISM-MICMAC and DEMATEL methods.

ISM MICMAC Results

ISM Analysis

In the ISM analysis, firstly, the three dimensions of supply chain sustainability were considered as the main criteria. The hierarchy of these criteria was revealed, and then the sub-criteria were evaluated among themselves. In the second stage, the interactions of all sub-criteria were addressed, and a holistic hierarchical structure was presented.

The ISM analysis has revealed a clear hierarchical relationship structure among the elements of supply chain sustainability influenced by AM technology. As shown in Figure 3, the economic and social sustainability main criteria at Level 2 affect the environmental sustainability at Level 1. Looking at the sub-criteria of economic sustainability, the Job Creation (ECO-3) criterion at Level 2 influences the other economic sustainability criteria. In other words, job creation emerges as a driving factor. This criterion is the root driver of the system, having a direct impact on cost reduction (ECO-1), product innovation (ECO-2), and supply chain efficiency (ECO-4). The strong directional links from ECO-3 to these economic enablers indicate that job creation not only strengthens the economic foundation but also triggers innovation and operational performance improvements.

From the perspective of social sustainability, it is observed that all criteria are located at the same level. However, these enablers also have mutual effects on each other at the same level. The environmental sustainability enablers at Level 1 are divided into two levels among themselves. ENV-1 (Material Efficiency) and ENV-2 (Energy Savings) take on the role of influencers from the second level. In other words, Material Efficiency and Energy Savings act as triggers for the criteria ENV-3 (Emission Reduction) and ENV-4 (Recycling & Circular Economy). In addition, ENV-1 (Material Efficiency) and ENV-2 (Energy Savings) also interact with each other. The mutual interaction between ECO-1 and ECO-2 reflects the synergy between cost optimization and product innovation and strengthens their combined capacity to increase resource efficiency. At Level 1, Emission Reduction (ENV-3) and Recycling & Circular Economy (ENV-4) are located. These criteria are highly dependent enablers, receiving cumulative effects from all lower levels. This situation emphasizes their role as final sustainability outcomes in the AM-enabled supply chain context.

Overall, the integrated ISM structure shows that job creation and improvement of health services provide the strongest leverage points for developing economic and social capacity, which also increase resource efficiency. In this way, it can be seen that the goals of reducing emissions and achieving circularity become reachable as a result of coordinated improvements across all sustainability dimensions. This finding strongly shows that decision makers should give priority to the fundamental and intermediate level enablers instead of focusing only on the final environmental outcomes.

In the second stage of the ISM analysis, the interactions among all sub-criteria are considered. The results of the relevant analysis are shown in Figure 4 (Appendix 1). Taking into account the levels and interactions obtained from the ISM analysis, a complex but distinct network of interactions emerges among the economic (ECO), social (SOC), and environmental (ENV) sustainability sub-criteria. This indicates that the sub-criteria establish strong connections not only within their own dimensions but also across other sustainability dimensions. At the lowest level, Community Empowerment (SOC-4) directly influences Job Creation (ECO-3), activating the root driver of the economic dimension, while ECO-3 contributes to strengthening economic performance by feeding into Cost Reduction (ECO-1), Product Innovation (ECO-2), and indirectly Supply Chain Efficiency (ECO-4). In the middle tier, Customization (SOC-2) and

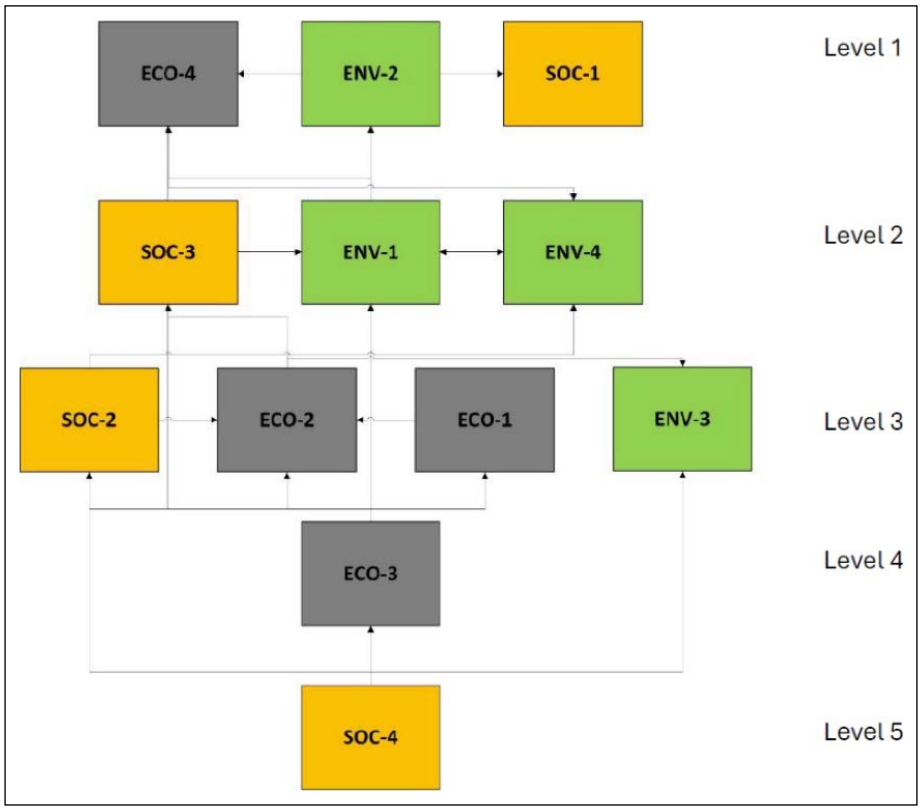

Figure 4. Hierarchical structure of supply chain sustainability sub-criteria affected by additive manufacturing identified through ISM (with inter-dimensional interactions).

Education & Skills Development (SOC-3) stand out; SOC-2 directly influences ECO-2, increasing product design flexibility capacity, while SOC-3 establishes strong connections with the environmental dimension by triggering Material Efficiency (ENV-1). Among the economic sub-criteria, ECO-1 influences ECO-2, clearly revealing the interaction between cost optimization and innovation.

The environmental sustainability criteria are dependent yet critical output areas that are fed by both economic and social factors, with ENV-1 and ENV-2 forming transition points toward environmental outcomes, interacting respectively with SOC-3 and SOC-1. At the top level, Energy Savings (ENV-2), Supply Chain Efficiency (ECO-4), and Improved Healthcare (SOC-1) are located, and they are directly or indirectly influenced by various sustainability criteria from different dimensions in the middle tier. These criteria are positioned in the affected dimension of the system.

MICMAC Analysis

When examining the MICMAC analysis results at the main criteria level, it is observed that the economic criterion has a high driving power and relatively low dependence (Fig. 5). This indicates that the economic sustainability dimension plays a fundamental driving role that influences the other dimensions. The social criterion, on the other hand, is positioned at a medium-high level in terms of both driving power and dependence and is located close to the linkage area, indicating a bidirectional relationship structure in which it both influences and is influenced by other dimensions. The environmental criterion has higher dependence and a moderate level of driving power, positioning it close to the "dependent" area, and is thus evaluated as an output dimension that is strongly influenced by the other dimensions.

At the economic sub-criteria level, Job Creation (ECO-3), with its high driving power and low dependence, is located in the driving area and is the most important trigger of the economic sustainability dimension. Product Innovation (ECO-2), Cost Reduction (ECO-1), and Supply Chain Efficiency (ECO-4) have relatively lower driving power and are positioned close to each other in the dependent area. However, they are also located close to the linkage area. This shows that they are intermediate variables that mutually influence each other and other criteria.

In the environmental sub-criteria, Material Efficiency (ENV-1) and Energy Savings (ENV-2) have high driving power and low dependence, placing in the "driving" area, so they stands out as main leverage points for improve environmental performance. Emission Reduction (ENV-3) and Recycling & Circular Economy (ENV-4) are positioned in the "dependent" area with high dependence, therefore showing that they are final environmental outcomes shaped by effects coming from other criteria.

In the social sub-criteria, Education & Skills Development (SOC-3) with its high driving power is located in the driving power area and plays an important role in the development of social dimension. Customization (SOC-2), Improved Healthcare (SOC-1) and Community Empowerment (SOC-4) have medium level of driving power and dependence and are positioned close to the linkage area. This

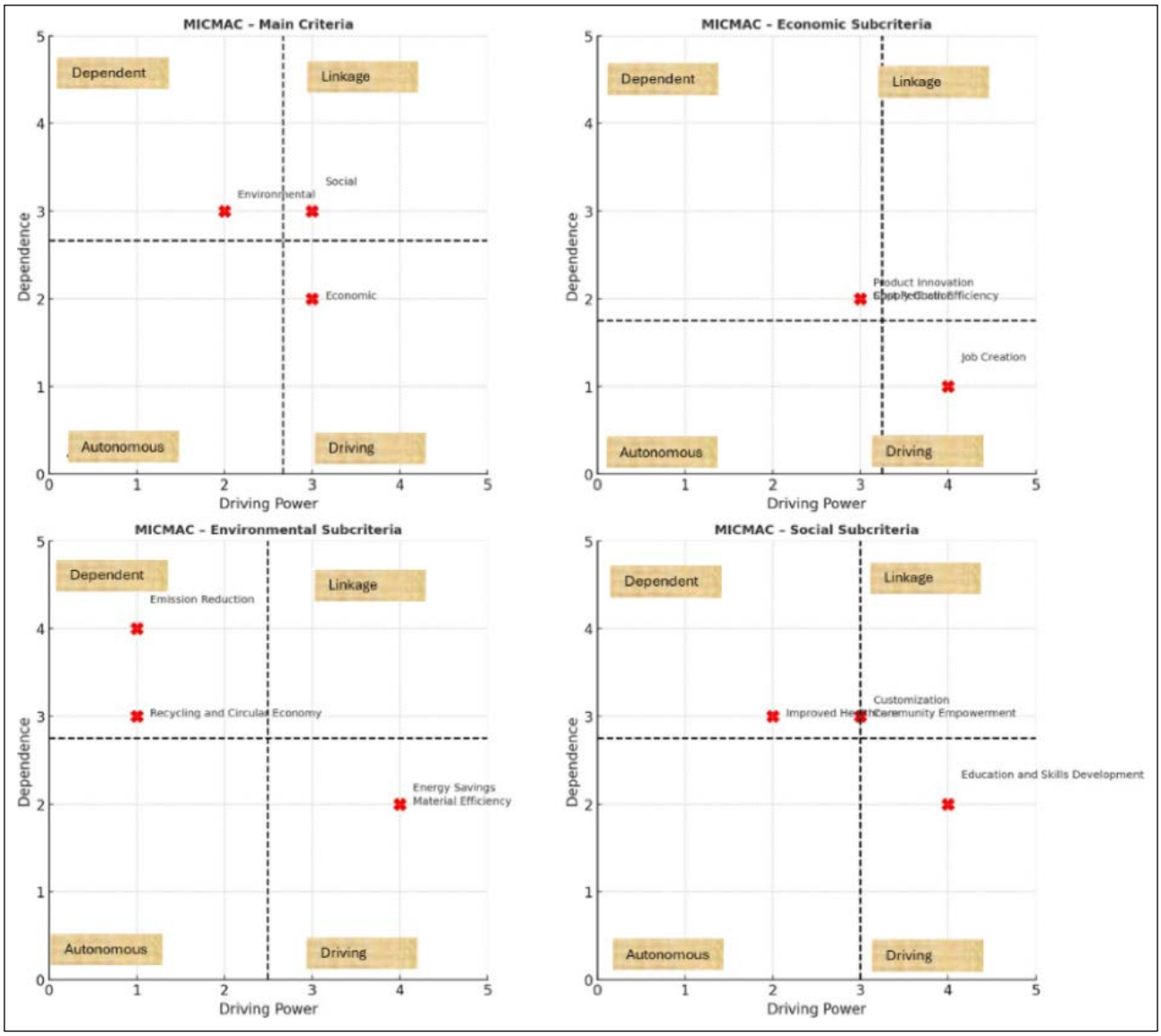

Figure 5. MICMAC analysis results of supply chain sustainability criteria affected by additive manufacturing.

situation shows that these criteria have bidirectional effect both on the social and other sustainability dimensions. When these results are evaluated in general, it is clearly seen that certain sub-criteria in the economic and social dimensions play a critical triggering role in shaping the environmental sustainability outcomes.

The final MICMAC diagram (Fig. 6) clearly reveals how all sub-criteria are positioned when evaluated within a single structure (For the final MICMAC diagram starting point, see the reachability matrix example in Appendix 2). In addition, it presents a holistic view of the interactions between the criteria. Based on Figure 6, Job Creation (ECO-3) and Community Empowerment (SOC-4) are located in the driving area. They have high driving power and relatively low dependence. In particular, Job Creation is the root trigger of economic sustainability. Community Empowerment stands out as the base factor that activates other criteria in the social dimension. These two criteria are strategic leverage dimensions that directly affect other dimensions of the system.

In the linkage area, Supply Chain Efficiency (ECO-4) and Product Innovation (ECO-2) have both high driving power and high dependence. This position shows that these criteria not only influence other sub-criteria but also are influenced by them, therefore they take an intermediate role where mutual dependencies are intense in the system. In the same way, Recycling & Circular Economy (ENV-4) is also placed here and indicate that the circular economy is fed by both economic and environmental inputs, making a significant contribution to the final outcomes.

In the dependent area, Energy Savings (ENV-2), Emission Reduction (ENV-3) and Material Efficiency (ENV-1) stand out, these criteria have high dependence and are shaped by the effects coming from other criteria. Especially Emission Reduction and Material Efficiency are strongly affected by both environmental and economic-social factors, forming the output dimension of the system. Improved Healthcare (SOC-1) and Education & Skills Development (SOC-3) also have relatively high dependence levels, and they are usually affected by triggers from social initiatives and capacity development processes.

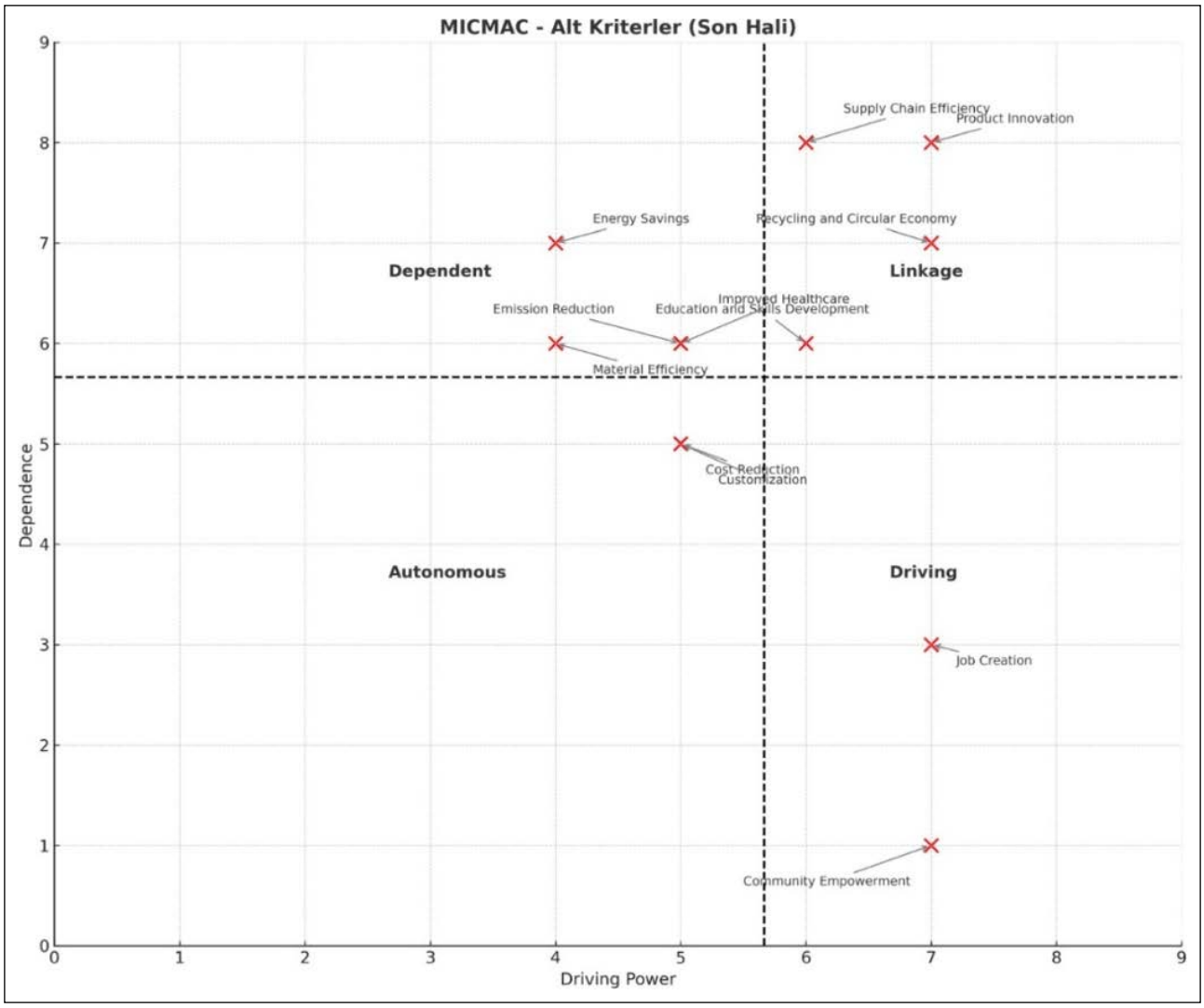

Figure 6. MICMAC analysis – sub-criteria.

In the autonomous area, there is almost no criteria, which shows that all the criteria in the system are affected by others in some way and the system is fully based on mutual dependency. This structure reveals that focusing on only one dimension in sustainability strategies is not enough, and that economic, social and environmental dimensions should be considered together. Especially focusing on high driving power criteria such as Job Creation, Community Empowerment, Product Innovation and Supply Chain Efficiency have potential to create chain and positive effects throughout the system.

The MICMAC and ISM results show a high degree of consistency. While MICMAC analyzes the driving–linkage–dependent classification of the criteria numerically, ISM places these criteria within a lower–middle–upper level hierarchy, visually supporting the identification of which criteria play a triggering role. In particular, ECO-3 and SOC-4 are identified as core factors in both analyses, criteria such as ECO-4, ECO-2, and ENV-4 appear as strategic linkage elements, and criteria like ENV-1, ENV-2, ENV-3, SOC-1, and SOC-3 are positioned as final outcomes.

DEMATEL Analysis

The findings of the DEMATEL analysis at the main criteria level indicate that the economic sustainability (ECO) criterion, with a positive D–R value, represents a strong element of the cause group, and it can be said that the social sustainability (SOC) criterion also shows influencing characteristics (Fig. 7). In addition, economic sustainability and social sustainability interact with each other. Furthermore, the environmental sustainability (ENV) criterion, with a negative D–R value, is revealed to be in the position of a result dimension with high dependence.

At the sub-criteria level, in the economic sustainability dimension, Job Creation (ECO-3) is identified as the root driver with the highest driving power and has a direct influence on Supply Chain Efficiency (ECO-4). Supply Chain Efficiency (ECO-4), with high D+R values, stands out as a linkage criterion that both influences and is influenced, while Cost Reduction (ECO-1), with a lower D–R value, is placed in the result group.

In the social sustainability dimension, Education & Skills Development (SOC-3), with a positive D–R value, is positioned in the cause group and constitutes the main

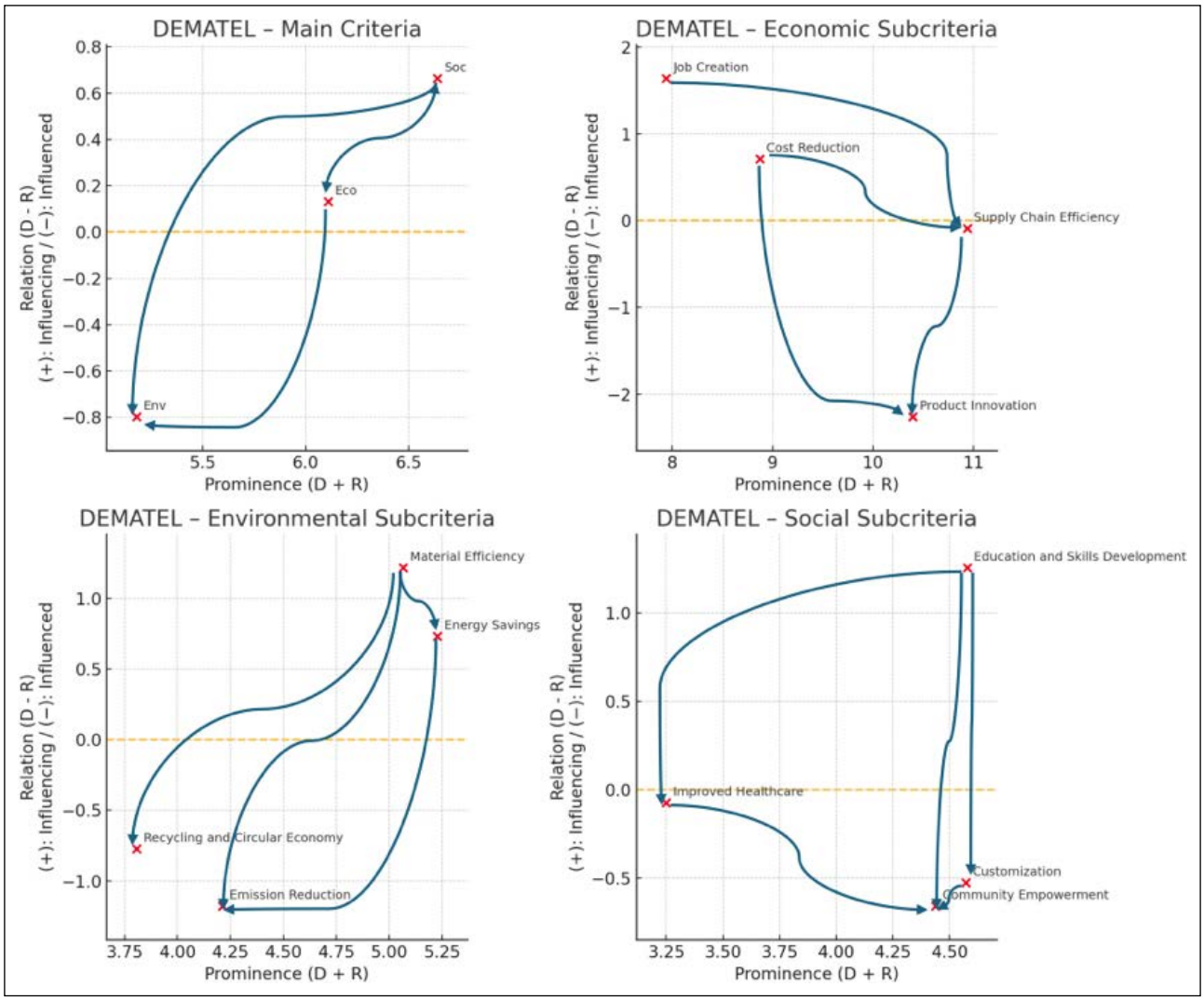

Figure 7. DEMATEL Analysis – Main Criteria and Sub-Criteria (Economic, Environmental, Social).

trigger of the social system. Customization (SOC-2), with its intermediary-oriented relationships, plays the role of a linkage criterion, while Improved Healthcare (SOC-1) and Community Empowerment (SOC-4), with negative D–R values, are included in the result group.

In the environmental sustainability dimension, Material Efficiency (ENV-1) and Energy Savings (ENV-2) are in the cause group and serve as intermediate levers for improving environmental performance. In contrast, Emission Reduction (ENV-3) and Recycling & Circular Economy (ENV-4), with negative D–R values, are located in the result group, positioned as the final outcomes of efficiency and process improvements. These results reveal that the cause–effect relationships identified by DEMATEL show a high level of consistency with the lower–middle–upper level hierarchy in the ISM analysis. In this context, strategies focusing on strong drivers such as ECO-3 and SOC-4 have the potential to create cascading and lasting effects on the top-level result criteria ENV-3, ENV-4, and SOC-1 through linkage criteria such as ECO-2, ECO-4, SOC-2, ENV-1, and ENV-2.

When examining the overall DEMATEL evaluation graph, it is evident that the interaction network of all main and sub-criteria is clearly revealed within a single integrated structure (Fig. 8 and Appendix 3, 4). According to the D–R axis, criteria with positive D–R values are in the "cause group" and represent the driving forces of the system. Among these, Job Creation and Community Empowerment stand out as root drivers with high driving power. Interestingly, Community Empowerment emerges as a triggering factor across all criteria, whereas within the social criteria set it was previously positioned as an influenced element. The criteria positioned as "linkage" have both high driving power and high dependence. At this point, Supply Chain Efficiency (ECO-4), Product Innovation (ECO-2), Recycling & Circular Economy (ENV-4), and Customization (SOC-2) are notable. These criteria represent the points where intermediary interactions are most intense in the system, being influenced by lower-level drivers while also feeding the upper-level result criteria. From a managerial perspective, these criteria can be considered as intermediate levers that play a key role in transferring cascading effects throughout the system.

Criteria with very low negative D–R values are placed in the "result group" and are defined as outcomes shaped by the effects coming from other criteria. In this group, Energy

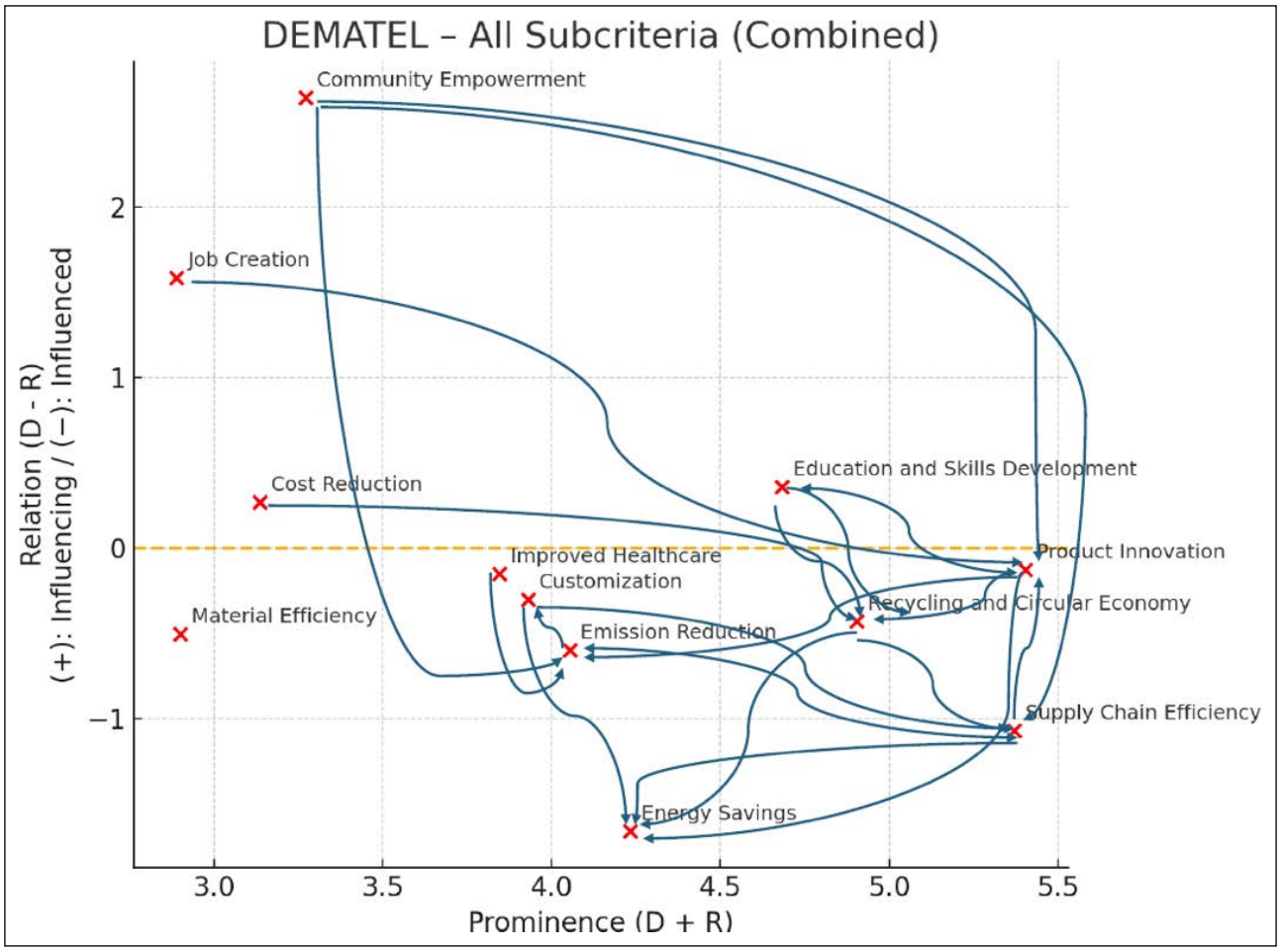

Figure 8. DEMATEL analysis – all sub-criteria (combined).

Savings and Material Efficiency stand out. Rather than triggering these criteria directly, strengthening the cause and linkage group criteria that influence them would be more effective in achieving long-term and lasting improvements. In particular, Material Efficiency is not observed to be in interaction within the overall evaluation system.

When evaluated in terms of importance level (D+R), linkage criteria such as Product Innovation and Supply Chain Efficiency have the highest centrality values and are the strategic transition points of the network. Strengthening these criteria accelerates the flow of information, resources and benefits between multiple dimensions, creating synergy across the system. Therefore, in the priority investment and improvement plans, considering together both the driver criteria with high driving power and the linkage criteria with high centrality values will make possible to increase the system performance in a holistic way.

DISCUSSIONS AND MANAGERIAL IMPLICATIONS

When the integrated ISM–MICMAC–DEMATEL results are considered together, it becomes evident that AM transforms supply chain sustainability through a layered and sequential mechanism operating across direct technical efficiencies (material/energy), economic building blocks (employment, innovation, process efficiency), and social capacity (community empowerment, education/skills, healthcare). The findings do not merely indicate where each criterion is positioned; they also reveal the channels of influence transmission: (i) Root drivers (e.g., ECO-3, and in certain contexts SOC-4/SOC-3) trigger economic and social capacity; (ii) Linkage nodes (e.g., ECO-2, ECO-4, SOC-2, and in some contexts ENV-4) propagate this trigger across operations and design; (iii) Dependent/output criteria (ENV-3, and depending on context SOC-1 and some environmental indicators) make this cumulative effect visible as environmental and societal performance. This sequencing strongly suggests that AM investments should not be approached as "isolated technology acquisitions" but rather as system-level flow design [46, 55].

The first critical managerial framing is the matter of prioritization and sequencing. The results indicate that instead of "jumping directly to the most visible environmental gains," organizations should strengthen foundational drivers (capacity expansions related to employment such as ECO-3; and depending on the context SOC-4/SOC-3 for community and skills capital), integrate these into organizational processes through linkage nodes (ECO-2 product innovation, ECO-4 process/supply chain efficiency, SOC-2 customization), and finally scale up environmental outcomes (ENV-3 emissions, ENV-4 circularity). In managerial terms, this is the driver-linkage-outcome roadmap. Without following

this sequence, AM-based gains in energy/material efficiency (ENV-1/ENV-2) risk being short-lived or failing to localize because the economic and social infrastructure that sustains them remains underdeveloped [56, 57].

The second framing is the leverage–centrality tension. Some criteria may have high driving power but only moderate centrality. Conversely, some linkage criteria (e.g., supply chain efficiency and product innovation) possess very high centrality, acting as key transition hubs in the network. The strategic approach involves managing both types of nodes simultaneously: driver nodes indicate the initiation points, whereas linkage nodes determine the pathways and mechanisms through which the flow is maintained within the organization. Without this integration, isolated investments either remain local (drivers exist but spread is weak) or become fragile (linkages are strong but lack input from drivers).

The third framing concerns governance and capability architecture. To make AM's impact on sustainability visible and repeatable, capabilities in (i) design–engineering (product modularity, repairability, recyclability), (ii) operations–supply (on-demand production, digital inventory, localized spare parts), and (iii) people–community (skill transformation, workforce planning, SME supplier development) must be developed in parallel. The findings show that especially community empowerment and skills development exert indirect but lasting impacts on both economic and environmental lines, making HR/L&D programs as strategically important as technical investments. In other words, AM should be treated not merely as a "production technology" but as an organizational transformation platform [10, 58].

The fourth framing addresses the risk–resilience–outcome balance. By nature, linkage nodes that both influence and are influenced are also carriers of systemic risks. For instance, if supply chain efficiency and product innovation are simultaneously highly central, disruptions in these nodes can cascade across the entire system. Therefore, managerial advice includes embedding resilience-enhancing measures (such as operational redundancy, standardization–modularization, supplier base diversification, critical spare capacity, and cyber-physical traceability) into the program. This ensures that the gains generated by drivers are transferred to top-level outcomes without dissipation [59].

The fifth framing is measurement and feedback architecture. The findings imply that environmental outcomes (emissions, circularity) form cumulatively and with delays. Thus, indicator sets must be designed in multiple layers: early-warning KPIs for drivers (employment quality, skill acquisition, innovation cycle time), flow and centrality KPIs for linkage nodes (supply cycle time, scrap/rework ratio, value per revision), and impact KPIs for outcomes (such as recycled content ratio, life-cycle cost). Linking these three layers through A/B testing and causal tracing makes it possible to demonstrate the effect of specific investments on specific outcomes with evidence.

The sixth framing is scaling and contextual adaptation. ISM–MICMAC–DEMATEL provides a flexible roadmap for which node to pull in which context [53, 60, 61]: in capital-constrained environments, start with the 2–3 nodes with the highest leverage-to-centrality ratio; in regulation/incentive-driven sectors, early-stage emphasis can be placed on policy-aligned nodes like ENV-4 circularity; in regions with acute skilled labor shortages, a human-centric scaling focused on SOC-3/SOC-4 can yield faster returns. In short, the same topology can be orchestrated differently—the key is preserving the driver–linkage–outcome sequence.

These framings taken together detail the managerial roadmap: (1) Establish the drivers, employment/capacity, community/skills; (2) institutionalize the linkage nodes, innovation, supply efficiency, customization; process-design integration; (3) scale the environmental outcomes, emissions, and circularity; (4) secure continuity of flows through resilience measures; (5) close the causal feedback loop through multi-layered measurement; and finally, (6) Periodically recalibrate orchestration according to context. More than anything else, this turns AM investments from a one-off technology project into a lasting transformation program anchored around organizational capability architecture and sustainable value creation.

Effective implementation of an AM management roadmap requires that additive manufacturing investments be considered an organizational transformation process rather than a technological innovation. In this respect, it is important that continuous training and skill renewal programs be designed in order to develop a qualified workforce, while establishing digital infrastructure, process standardization, and data integrity systems that will increase the efficiency of supply chains. The integration of AM technologies into existing production structures should be tested for the scalability of processes through pilot applications and with the support of a digital twin-supported design-production cycle. However, this transformation should not be limited to internal sources but should also be supported by external incentive mechanisms such as publicly supported R&D grants, green production credits, tax incentives, and sustainable innovation funds. Businesses should develop performance-based incentive systems in their organizations that will facilitate the encouragement of employee participation in innovative practices and process improvements. Finally, to ensure the lasting social impact of AM, there is a need for cooperation in joint development projects with local suppliers and SMEs, thus turning economic, social, and environmental sustainability into a self-reinforcing whole.

CONCLUSION

The paper presents a critical review of how AM technology influences supply chain sustainability based on the integrated approaches of ISM, MICMAC, and DEMATEL methods. In integrating the methods, the research reveals not just the hierarchical position of the criteria but also the causal and dependency relationships that define how economic, social, and environmental enablers interact. The results identify that the impact of AM on sustainability is not some simple direct outcome; rather, it is a result of a multi-layered and sequenced mechanism wherein root

drivers, such as job creation and community empowerment, start off transformative processes transmitted through linkage criteria like product innovation and supply chain efficiency to dependent outcomes like emission reduction and circular economy achievements. This systemic perspective provides important guidance for managers to design interventions that target both the source and transmission channels of sustainability impacts and thus assure long-term and scalable improvements. Further, the focus on driving power and centrality together underlines the need to balance investment between fundamental triggers and high-centrality connectors in order to maximize system-wide synergy.

From a practical standpoint, the results recommend that organizations approach investments in AM as a strategic transformation program rather than an isolated technology acquisition. This calls for strengthening the foundational economic and social capabilities necessary to make those gains strong and scalable and also for embedding measures of resilience at key network points. The multi-layered measurement and feedback framework proposed here provides decision-makers with the tools to track causal linkages and validate, with empirical evidence, the impact of their strategies.

The findings of this study contribute uniquely to the literature by showing how additive manufacturing transforms sustainable supply chain performance through direct environmental impacts and a dynamic systemic mechanism that connects economic and social capacity. In this respect, the study develops a holistic methodological framework that integrates AM's sustainability impacts with hierarchical, causal, and centrality-based analyses, enabling decision-makers to link technology investments to multi-layered sustainability outcomes.

Despite the contributions made, the following shortcomings are associated with this study. First, this analysis is based on the evaluation of experts and could therefore be subjective; larger and more diverse respondent groups might enhance its reliability. Second, the findings are context-specific to the AM-enabled supply chain and may thus need adaptation prior to being generalized to other technological or industrial contexts. Third, although the combined approach using ISM–MICMAC–DEMATEL offers powerful structural insights, it lacks information about dynamic temporal changes; integrating system dynamics or longitudinal data would be an exciting future research avenue. Finally, other exogenous factors that may alter these identified interaction patterns, such as changed policies, market volatility, and disruption to global supplies, have not been explicitly modeled.

Data Availability Statement

The authors confirm that the data that supports the findings of this study are available within the article. Raw data that support the finding of this study are available from the corresponding author, upon reasonable request.

Author's Contributions

Cihat Öztürk: Conception, Design, Supervision, Data Collection and Processing, Analysis and Interpretation, Writer, Critical Review.

Nurullah Güleç: Conception, Design, Literature Review, Analysis and Interpretation, Writer.

Conflict of Interest

The authors declared no potential conflicts of interest with respect to the research, authorship, and/or publication of this article.

Statement on the Use of Artificial Intelligence

The authors acknowledge the use of ChatGPT for ensuring language clarity and correcting grammatical mistakes.

Ethics

There are no ethical issues with the publication of this manuscript.

REFERENCES

[1] Mani, M., Lyons, K. W., & Gupta, S. K. (2014). Sustainability characterization for additive manufacturing. *Journal of Research of the National Institute of Standards and Technology, 119*, Article 419. [CrossRef]

[2] Berman, B. (2012). 3-D printing: The new industrial revolution. *Business Horizons, 55*(2), 155-162. [CrossRef]

[3] Ersoy, K. (2023). Supply chain management in defense industry with additive manufacturing. *Makina Tasarım ve İmalat Dergisi, 21*(2), 63-73. [Turkish] [CrossRef]

[4] Bigliardi, B., Bottani, E., Gianatti, E., Monferdini, L., Pini, B., & Petroni, A. (2023). Sustainable Additive Manufacturing in the context of Industry 4.0: a literature review. *Procedia Computer Science, 232*, 766-774. [CrossRef]

[5] Hegab, H., Khanna, N., Monib, N., & Salem, A. (2023). Design for sustainable additive manufacturing: A review. *Sustainable Materials and Technologies, 35*(23), e00576. [CrossRef]

[6] Ghobakhloo, M. (2018). The future of manufacturing industry: a strategic roadmap toward Industry 4.0. *Journal of Manufacturing Technology Management, 29*(6), 910-936. [CrossRef]

[7] Hozdić, E., & Butala, P. (2020). Concept of socio-cyber-physical work systems for Industry 4.0. *Tehnički vjesnik, 27*(2), 399-410. [CrossRef]

[8] Sarı, T., Güleş, H. K., & Yiğitol, B. (2020). Awareness and readiness of Industry 4.0: The case of Turkish manufacturing industry. *Advances in Production Engineering & Management, 15*(1), 57-68. [CrossRef]

[9] Kellens, K., Baumers, M., Gutowski, T. G., Flanagan, W., Lifset, R., & Duflou, J. R. (2017). Environmental dimensions of additive manufacturing: mapping application domains and their environmental implications. *Journal of Industrial Ecology, 21*(Suppl 1), S49-S68. [CrossRef]

[10] Kunovjanek, M., Knofius, N., & Reiner, G. (2022). Additive manufacturing and supply chains - a systematic review. *Production Planning & Control, 33*(13), 1231-1251. [CrossRef]

[11] Woldesilassiea, T. L., Lemu, H. G., & Gutema, E. M. (2024). Impacts of adopting additive manufacturing process on supply chain: Systematic literature review. *Logistics, 8*(3), 1-24. [CrossRef]

[12] Bouchenine, A., & Abdel-Aal, M. A. M. (2023). Towards supply chain resilience with additive manufacturing: A bibliometric survey. *Supply Chain Analytics, 2*, Article 100014. [CrossRef]

[13] Tuck, C., Hague, R., & Burns, N. (2007). Rapid manufacturing: impact on supply chain methodologies and practice. *International Journal of Services and Operations Management, 3*(1), 1-22. [CrossRef]

[14] Petrovic, V., Vicente Haro Gonzalez, J., Jordá Ferrando, O., Delgado Gordillo, J., Ramón Blasco Puchades, J., & Portolés Griñan, L. (2011). Additive layered manufacturing: sectors of industrial application shown through case studies. *International Journal of Production Research, 49*(4), 1061-1079. [CrossRef]

[15] Thomas, D. (2016). Costs, benefits, and adoption of additive manufacturing: A supply chain perspective. *The International Journal, Advanced Manufacturing Technology, 85*(5-8), 1857-1876. [CrossRef]

[16] Javaid, M., Haleem, A., Singh, R. P., Suman, R., & Rab, S. (2021). Role of additive manufacturing applications towards environmental sustainability. *Advanced Industrial and Engineering Polymer Research, 4*(4), 312-322. [CrossRef]

[17] Kunovjanek, M., & Reiner, G. (2020). How will the diffusion of additive manufacturing impact the raw material supply chain process? *International Journal of Production Research, 58*(5), 1540-1554. [CrossRef]

[18] Attaran, M. (2017). The rise of 3-D printing: The advantages of additive manufacturing over traditional manufacturing. *Business Horizons, 60*(5), 677-688. [CrossRef]

[19] Baumers, M., Tuck, C., Wildman, R., Ashcroft, I., Rosamond, E., & Hague, R. (2013). Transparency built-in. *Journal of Industrial Ecology, 17*(3), 418-431. [CrossRef]

[20] Khajavi, S. H., Holmström, J., & Partanen, J. (2018). Additive Manufacturing in the Spare Parts Supply Chain: hub Configuration and Technology Maturity. *Rapid Prototyping Journal, 24*(7), 1178-1192. [CrossRef]

[21] Tosello, G., Charalambis, A., Kerbache, L., Mischkot, M., Pedersen, D. B., Calaon, M., & Hansen, H. N. (2019). Value chain and production cost optimization by integrating additive manufacturing in injection molding process chain. *The International Journal of Advanced Manufacturing Technology, 100*(1-4), 783-795. [CrossRef]

[22] Ghuge, S., Dohale, V., & Akarte, M. (2022). Spare part segmentation for additive manufacturing-A framework. *Computers & Industrial Engineering, 169*, Article 108277. [CrossRef]

[23] Ullah, A. S., Hashimoto, H., Kubo, A., & Tamaki, J. I. (2013). Sustainability analysis of rapid prototyping: material/resource and process perspectives. *International Journal of Sustainable Manufacturing, 3*(1), 20-36. [CrossRef]

[24] Baumers, M., Tuck, C., Bourell, D. L., Sreenivasan, R., & Hague, R. (2011). Sustainability of additive manufacturing: measuring the energy consumption of the laser sintering process. *Proceedings of the Institution of Mechanical Engineers, Part B: Journal of Engineering Manufacture, 225*(12), 2228-2239. [CrossRef]

[25] Ford, S., & Despeisse, M. (2016). Additive Manufacturing and Sustainability: An Exploratory Study of the Advantages and Challenges. *Journal of Cleaner Production, 137*, 1573-1587. [CrossRef]

[26] Murmura, F., & Bravi, L. (2018). Additive manufacturing in the wood-furniture sector: Sustainability of the technology, benefits and limitations of adoption. *Journal of Manufacturing Technology Management, 29*(2), 350-371. [CrossRef]

[27] Kumar, S., & Czekanski, A. (2018). Roadmap to sustainable plastic additive manufacturing. *Materials Today Communications, 15*, 109-113. [CrossRef]

[28] Böckin, D., & Tillman, A.-M. (2019). Environmental assessment of additive manufacturing in the automotive industry. *Journal of Cleaner Production, 226*, 977-987. [CrossRef]

[29] Yang, S., Min, W., Ghibaudo, J., & Zhao, Y. F. (2019). Understanding the sustainability potential of part consolidation design supported by additive manufacturing. *Journal of Cleaner Production, 232*, 722-738. [CrossRef]

[30] Baechler, C., DeVuono, M., & Pearce, J. M. (2013). Distributed Recycling of Waste Polymer into RepRap Feedstock. *Rapid Prototyping Journal, 19*(2), 118-125. [CrossRef]

[31] Despeisse, M., Baumers, M., Brown, P., Charnley, F., Ford, S. J., Garmulewicz, A., & Knowles, S. (2017). Unlocking Value for a Circular Economy through 3D Printing: A Research Agenda. *Technological Forecasting and Social Change, 115*, 75-84. [CrossRef]

[32] Ingarao, G., Priarone, P. C., Deng, Y., & Paraskevas, D. (2018). Environmental Modelling of Aluminium Based Components Manufacturing Routes: Additive Manufacturing versus Machining versus Forming. *Journal of Cleaner Production, 176*, 261-275. [CrossRef]

[33] Parry, E. J., Best, J. M., & Banks, C. E. (2020). Three-dimensional (3D) scanning and additive manufacturing (AM) allows the fabrication of customised crutch grips. *Materials Today Communications, 25*, Article 101225. [CrossRef]

[34] Hohn, M. M., & Durach, C. F. (2021). Additive manufacturing in the apparel supply chain-impact on supply chain governance and social sustainability. *International Journal of Operations & Production Management, 41*(7), 1035-1059. [CrossRef]

[35] Kianian, B., Tavassoli, S., & Larsson, T. C. (2015). The role of additive manufacturing technology in job creation: an exploratory case study of suppliers of additive manufacturing in Sweden. *Procedia CIRP, 26*, 93-98. [CrossRef]

[36] Ekren, B. Y., Stylos, N., Zwiegelaar, J., Turhanlar, E. E., & Kumar, V. (2023). Additive manufacturing integration in E-commerce supply chain network to improve resilience and competitiveness. *Simulation Modelling Practice and Theory, 122*, Article 102676. [CrossRef]

[37] Delic, M., & Eyers, D. R. (2020). The effect of additive manufacturing adoption on supply chain flexibility and performance: an empirical analysis from the automotive industry. *International Journal of Production Economics, 228*, Article 107689. [CrossRef]

[38] Khajavi, S. H., Partanen, J., & Holmström, J. (2014). Additive manufacturing in the spare parts supply chain. *Computers in Industry, 65*(1), 50-63. [CrossRef]

[39] Liu, P., Huang, S. H., Mokasdar, A., Zhou, H., & Hou, L. (2014). The impact of additive manufacturing in the aircraft spare parts supply chain: supply chain operation reference (SCOR) model based analysis. *Production Planning & Control, 25*(13-14), 1169-1181. [CrossRef]

[40] Naghshineh, B., & Carvalho, H. (2022). The implications of additive manufacturing technology adoption for supply chain resilience: A systematic search and review. *International Journal of Production Economics, 247*, Article 108387. [CrossRef]

[41] Yosofi, M., Kerbrat, O., & Mognol, P. (2019). Additive manufacturing processes from an environmental point of view: a new methodology for combining technical, economic, and environmental predictive models. *The International Journal of Advanced Manufacturing Technology, 102*(9), 4073-4085. [CrossRef]

[42] Bäckström, H. K. (2024). Navigating the intersection: cost reduction and sustainability in logistics strategies [Master thesis]. Jonkoping University.

[43] Al-Meslemi, Y., Anwer, N., & Mathieu, L. (2018). Environmental performance and key characteristics in additive manufacturing: a literature review. *Procedia CIRP, 69*, 148-153. [CrossRef]

[44] Hertwich, E. G., Ali, S., Ciacci, L., Fishman, T., Heeren, N., Masanet, E., Asghari FN, Olivetti E, Pauliuk S, Tu Q, & Wolfram, P. (2019). Material efficiency strategies to reducing greenhouse gas emissions associated with buildings, vehicles, and electronics-a review. *Environmental Research Letters, 14*(4), Article 043004. [CrossRef]

[45] Fruggiero, F., Lambiase, A., Bonito, R., & Fera, M. (2019). The load of sustainability for additive manufacturing processes. *Procedia Manufacturing, 41*, 375-382. [CrossRef]

[46] Agnusdei, L., & Del Prete, A. (2022). Additive manufacturing for sustainability: A systematic literature review. *Sustainable Futures, 4*, 100098. [CrossRef]

[47] Bhatt, S., Joshi, D., Rakesh, P. K., & Godiyal, A. K. (2023). Advances in additive manufacturing processes and their use for the fabrication of lower limb prosthetic devices. *Expert Review of Medical Devices, 20*(1), 17-27. [CrossRef]

[48] Wang, Z., & Yang, Y. (2021). Application of 3D printing in implantable medical devices. *BioMed Research International, 2021*(2021), Article 6653967. [CrossRef]

[49] Fianko, S. K., Dzogbewu, T. C., Agbamava, E., & de Beer, D. J. (2025). Mass Customisation Strategies in Additive Manufacturing: A Systematic Review and Implementation Framework. *Processes, 13*(6), Article 1855. [CrossRef]

[50] Singh, A., Wu, P., Okwudire, C., & Banu, M. (2025). Advancing workforce development through additive manufacturing education and training. *Manufacturing Letters, 44*, 1637-1648. [CrossRef]

[51] Ben-Ner, A., & Siemsen, E. (2017). Decentralization and localization of production: The organizational and economic consequences of additive manufacturing (3D printing). *California Management Review, 59*(2), 5-23. [CrossRef]

[52] Wang, L., Cao, Q., & Zhou, L. (2018). Research on the influencing factors in coal mine production safety based on the combination of DEMATEL and ISM. *Safety Science, 103*, 51-61. [CrossRef]

[53] Öztürk, C. (2025). Digitalization as a catalyst for social sustainability in supply chains: an ISM-fuzzy MICMAC and DEMATEL approach. *Environment, Development and Sustainability*, 1-61. [CrossRef]

[54] Jung, S., Kara, L. B., Nie, Z., Simpson, T. W., & Whitefoot, K. S. (2023). Is additive manufacturing an environmentally and economically preferred alternative for mass production? *Environmental Science & Technology, 57*(16), 6373-6386. [CrossRef]

[55] Alinezhad, A., & Khalili, J. (2019). DEMATEL method. In *New Methods and Applications in Multiple Attribute Decision Making (MADM)* (pp. 103-108). Cham: Springer International Publishing. [CrossRef]

[56] Kravchenko, M., Pigosso, D. C. A., & McAloone, T. C. (2020). Circular economy enabled by additive manufacturing: Potential opportunities and key sustainability aspects. *DS 101: Proceedings of NordDesign 2020*. Lyngby, Denmark, 12th - 14th August 2020.

[57] Ponis, S., Aretoulaki, E., Maroutas, T. N., Plakas, G., & Dimogiorgi, K. (2021). A systematic literature review on additive manufacturing in the context of circular economy. *Sustainability, 13*(11), Article 6007. [CrossRef]

[58] Barati, A. A., Azadi, H., Dehghani Pour, M., Lebailly, P., & Qafori, M. (2019). Determining key agricultural strategic factors using AHP-MICMAC. *Sustainability, 11*(14), Article 3947. [CrossRef]

[59] Priyadarshini, J., Singh, R. K., Mishra, R., Chaudhuri, A., & Kamble, S. (2025). Supply chain resilience and improving sustainability through additive manufacturing implementation: a systematic literature review and framework. *Production Planning & Control, 36*(3), 309-332.

[60] Vishwakarma, A., Dangayach, G. S., Meena, M. L., & Gupta, S. (2022). Analysing barriers of sustainable supply chain in apparel & textile sector: A hybrid

ISM-MICMAC and DEMATEL approach. *Cleaner Logistics and Supply Chain, 5*, Article 100073. [CrossRef]

[61] Ozturk, C., & Gulec, N. (2025). Leveraging IoT, Big Data, and AI for Sustainable Supply Chains: A Strategic Analysis with ISM, MICMAC, and GREY-DEMATEL. In *International Conference on Intelligent and Fuzzy Systems* (pp. 550-557). Cham: Springer Nature Switzerland. [CrossRef]

Appendix 1. ISM levels

Levels	Criteria
Level-1	Eco-4, Env-2, Soc-1
Level-2	Env-1, Env-4, Soc-3
Level-3	Eco-1, Eco-2, Env-3, Soc-2
Level-4	Eco-3
Level-5	Soc-4

Appendix 2. MICMAC reachability matrix

	Eco-1	Eco-2	Eco-3	Eco-4	Env-1	Env-2	Env-3	Env-4	Soc-1	Soc-2	Soc-3	Soc-4
Eco-1	1	1	0	0	0	1	0	1	1	0	0	0
Eco-2	0	1	0	1	0	1	1	1	1	0	1	0
Eco-3	1	1	1	1	1	0	0	0	1	1	0	0
Eco-4	0	1	1	1	0	1	1	0	0	1	0	0
Env-1	0	0	0	1	1	1	0	1	0	0	0	0
Env-2	0	0	0	1	0	1	0	1	1	0	0	0
Env-3	0	0	0	1	1	0	1	0	0	1	1	0
Env-4	1	0	0	1	1	1	1	1	0	0	1	0
Soc-1	1	1	0	0	0	0	1	0	1	0	0	1
Soc-2	0	1	0	0	0	1	0	1	0	1	1	0
Soc-3	0	1	0	1	1	0	0	1	0	1	1	0
Soc-4	1	1	1	0	1	0	1	0	1	0	1	0

Appendix 3. MICMAC reachability matrix

	ECO-1	ECO-2	ECO-3	ECO-4	ENV-1	ENV-2	ENV-3	ENV-4	SOC-1	SOC-2	SOC-3	SOC-4
ECO-1	0.0897	0.2153	0.0211	0.1605	0.0670	0.2816	0.1325	0.2709	0.2564	0.0723	0.1080	0.0270
ECO-2	0.1041	0.1975	0.0423	0.3596	0.1304	0.3463	0.3277	0.3338	0.2696	0.1814	0.3153	0.0283
ECO-3	0.1847	0.2807	0.0340	0.2799	0.2229	0.2124	0.1550	0.1801	0.2730	0.2585	0.1273	0.0287
ECO-4	0.0632	0.3020	0.1290	0.2059	0.0934	0.3256	0.2786	0.1705	0.1308	0.2860	0.1500	0.0138
ENV-1	0.0427	0.0830	0.0293	0.2685	0.0434	0.2571	0.0856	0.1782	0.0657	0.0738	0.0632	0.0069
ENV-2	0.0671	0.1106	0.0302	0.2537	0.0498	0.1064	0.1122	0.1734	0.2096	0.0778	0.0730	0.0220
ENV-3	0.0380	0.1512	0.0337	0.3104	0.1773	0.1668	0.0994	0.1499	0.0621	0.2805	0.2511	0.0065
ENV-4	0.2101	0.1704	0.0402	0.3643	0.1982	0.2973	0.2282	0.1787	0.1145	0.1558	0.2665	0.0120
SOC-1	0.2218	0.2855	0.0354	0.1599	0.0901	0.1508	0.2809	0.1430	0.1218	0.1036	0.1352	0.1180
SOC-2	0.0686	0.2682	0.0223	0.1950	0.0859	0.3031	0.1234	0.3035	0.1056	0.1014	0.2266	0.0111
SOC-3	0.0807	0.3329	0.0427	0.3878	0.2492	0.2572	0.1711	0.3574	0.1138	0.3416	0.1731	0.0120
SOC-4	0.2620	0.3691	0.1912	0.2751	0.2946	0.2423	0.3315	0.2282	0.2761	0.1835	0.2740	0.0290

Appendix 4. DEMATEL cause-effect table

	D	R	D+R	D-R
ECO-1	1.702371	1.432726	3.135098	0.269645
ECO-2	2.63635	2.766288	5.402638	-0.12994
ECO-3	2.237225	0.651322	2.888547	1.585903
ECO-4	2.148693	3.22067	5.369363	-1.07198
ENV-1	1.197558	1.702355	2.899913	-0.5048
ENV-2	1.285912	2.947032	4.232945	-1.66112
ENV-3	1.726873	2.326079	4.052952	-0.59921
ENV-4	2.236284	2.667541	4.903826	-0.43126
SOC-1	1.846048	1.999203	3.845251	-0.15316
SOC-2	1.814728	2.116155	3.930883	-0.30143
SOC-3	2.51935	2.163246	4.682596	0.356104
SOC-4	2.956616	0.31539	3.272006	2.641226

J Adv Manuf Eng, Vol. 6, Issue. 2, pp. 111–120, December, 2025

Journal of Advances in Manufacturing Engineering
Web page info: https://jame.yildiz.edu.tr
DOI: 10.14744/ytu.jame.2025.00012

Original Article

Tensile testing of polylactic acid (PLA) samples produced with a 3D printer and finite element analysis

Yunus Zübeyir TURGUT[1], Sıtkı AKINCIOĞLU[2], Gülşah AKINCIOĞLU[*1]

[1]*Department of Machine and Metal Technology, Düzce University, Düzce, Türkiye*
[2]*Department of Industrial Design, Düzce University, Faculty of Art, Design and Architecture, Düzce, Türkiye*

ARTICLE INFO

Article history
Received: 29 July 2025
Revised: 07 December 2025
Accepted: 08 December 2025

Key words:
3D printer, finite element analysis, PLA filament, tensile test.

ABSTRACT

Polylactic acid (PLA) is increasingly vital in 3D printing due to its sustainability and versatility in applications ranging from product packaging to medical implants. Ensuring its mechanical reliability under load is critical for expanding its industrial use. This study evaluated the mechanical properties of fully loaded samples produced from PLA filament using a 3D printer, through experimental tensile tests and finite element analysis (FEA). The samples were designed in accordance with the ASTM D638 Type I standard and fabricated using a 3D printer. Unlike prior studies, this work uniquely combines the ANSYS Explicit Dynamics module with the Johnson–Cook material model to simulate high-deformation behavior in fully loaded specimens, addressing gaps in the literature regarding comprehensive mechanical analysis of 3D printed PLA. Fracture zones were examined with a digital microscope. Experimental tensile tests on fully loaded PLA samples accurately simulated the stress distribution using FEA. These findings offer insights into optimizing 3D printing parameters to improve interlayer bonding, reduce defects, and enhance PLA's reliability in industrial applications.

Cite this article as: Turgut, Y. Y., Akıncıoğlu, S., & Akıncıoğlu, G. (2025). Tensile testing of polylactic acid (PLA) samples produced with a 3D printer and finite element analysis. *J Adv Manuf Eng*, 6(2), 111–120.

INTRODUCTION

3D printing, also known as additive manufacturing, is a rapidly developing technology [1–3]. This manufacturing method is based on the principle of melting the material and adding layers on top of each other to produce the object [4]. PLA, acrylonitrile butadiene styrene (ABS), polyethylene terephthalate glycol (PETG) can be used as raw materials [5, 6]. PLA has attracted significant attention in recent years. The growing need for sustainable material solutions, in particular, has led PLA to emerge as a significant alternative in both research and applications. PLA material can be used in product packaging, medical applications such as implants, textile products, as a 3D printing raw material and many other applications [7–14]. However, for PLA material to be used safely, its behavior under load must be examined and defined. Therefore, tensile test results, either experimentally or using the finite element analysis, are important for determining the material's mechanical behavior [15]. FEA stands out as a powerful tool for evaluating the mechanical behavior of 3D printed parts. To enhance the reliability of sustainable materials, particularly PLA, in industrial applications, FEA precisely models stress distributions and deformations, providing results consistent with experimental tests [16]. This analysis enables the simulation of complex geometries and load conditions, contributing to design optimization and material strength prediction.

***Corresponding author.**
*E-mail address: gulsahakincioglu@gmail.com

Kumar and Narayan [17] investigated the mechanical behavior of tensile test specimens made of PLA material in accordance with ASTM D638 Type IV. They compared the results with those obtained using the computer-aided analysis program ANSYS. They concluded that the results were consistent and that the maximum tensile strength was 54.46 MPa. Alharbi et al. [18] performed tensile tests using finite element analysis to simulate the mechanical properties of 3D printed PLA samples. They found that the resulting values deviated from the experimental values by 2% for yield strength and 6.7% for tensile strength. Özmen et al. [19] produced tensile test specimens from PLA material with different infill patterns and different raster angles. They selected grid, concentric, triangular, hexagonal, and zigzag infill patterns, and 0°, 45°, and 90° raster angles. When examining the tensile test results, they determined that higher strength was achieved in the concentric and zigzag patterned specimens with 90° raster angles. These studies establish FEA as a robust analysis for understanding the mechanical performance of 3D printed PLA; however, comprehensive analyses of fully loaded samples using advanced FEA modules such as Explicit Dynamics remain limited and this study aims to address this issue.

When the literature is reviewed, Ganeshkumar et al. [20] produced tensile test specimens with different infill patterns (hexagonal (honeycomb), gyroid, rhombile, circular, truncated octahedron) and infill ratios (20%, 40%, 60%, 80%) using PLA material via 3D printing. These specimens were subjected to tensile testing using experimental and finite element analysis. They investigated the effect of infill pattern and infill ratio parameters on the strength of PLA material. They concluded that the hexagonal infill pattern had better mechanical strength than the other infill patterns examined and that the strength improved as the infill ratio increased. Harpool et al. [21] investigated the effects of different infill patterns on mechanical properties using PLA material. They used tensile testing and finite element analysis in their study. They obtained the highest tensile strength with a hexagonal infill pattern. Auffray et al. [22] investigated the effects of parameters such as infill pattern, infill density, printing speed, and raster angles on mechanical properties using PLA. The experiments were conducted using the Taguchi design of experiments. They noted that the best strength was achieved with a triangular infill pattern, 50% infill density, printing speed of 3 m/min, and a 45° raster angle. They also concluded that layer height and extrusion temperature were less effective than other parameters. Brischetto and Torre [23] conducted compression and tensile tests using PLA material. The test results revealed that PLA exhibits different mechanical behavior in tension and compression. Evlen et al. [24] investigated the effect of infill ratio on mechanical properties using PLA and PET materials. They found that increasing the infill ratio increased the hardness and surface roughness of the materials. Kamer et al. [25] produced tensile test specimens from PLA and ABS materials at different printing speeds. They also conducted hardness and surface roughness tests. They found that as printing speed increased, hardness and tensile strength decreased in PLA samples, while surface roughness increased. When the same parameters were examined for ABS, no clear conclusions were reached. Aloyaydi et al. [26] subjected samples they produced using 3D printing in PLA material with different infill patterns to compression tests. The highest compressive strength was achieved with the grid pattern. Klossa et al. [27] conducted tensile tests using carbon fiber-reinforced nylon samples. The parameters used were carbon fiber content (0%, 10%, 15%, 20%) and infill angle (0°, 45°, 90°). The best results were obtained at a infill angle of 0° with 10% carbon fiber. Öztürk et al. [28] investigated the mechanical behavior of polycarbonate (PC) using both experimental and numerical analysis. They found that the highest strength was achieved at a 0° raster angle. They found the difference between the experimental and numerical results to be 11.98%, which they considered reasonable. In the literature, mechanical tests have been carried out on samples of many different materials produced by 3D printing method [29–34]. These studies establish FEA as a robust method for understanding the mechanical performance of 3D printed PLA; however, comprehensive analyses of fully loaded samples using advanced FEA modules such as Explicit Dynamics have been limited and this study aims to address this issue.

While the literature provides a rich foundation for understanding the mechanical properties of 3D printed PLA samples, it lacks areas such as the extensive use of fully loaded samples and finite element analysis. In this study, we conducted experimental and finite element analysis studies for tensile testing on fully loaded samples produced from 3D printed PLA filament. PLA samples were manufactured in accordance with the ASTM D638 Type I standard for rigid and semi-rigid materials. The ANSYS Explicit Dynamics module was used in the finite element analysis. Our study infills these gaps and makes a unique contribution from both scientific and practical perspectives. Analyses of fully loaded specimens and the integration of Explicit Dynamics and the Johnson-Cook model represent significant advances in better understanding the mechanical behavior of PLA and improving its reliability in industrial applications. By integrating experimental validation with advanced numerical simulations, this study offers significant scientific contributions to the literature and practical insights for enhancing the reliability of 3D printed PLA in industrial applications, paving the way for future research into optimized additive manufacturing processes.

MATERIALS AND METHODS

The workflow diagram for our study, which conducted tensile tests and finite element analyses using PLA filament, is shown in Figure 1. Tensile test specimens were 3D modeled in Solidworks 2024 for use in the production and analysis phases. The solid model was dimensioned in accordance with the ASTM D638 Type 1 standard [35], recommended for rigid and semi-rigid plastics. Figure 2 shows the sample dimensions according to the standard. The sample thickness was 3 mm.

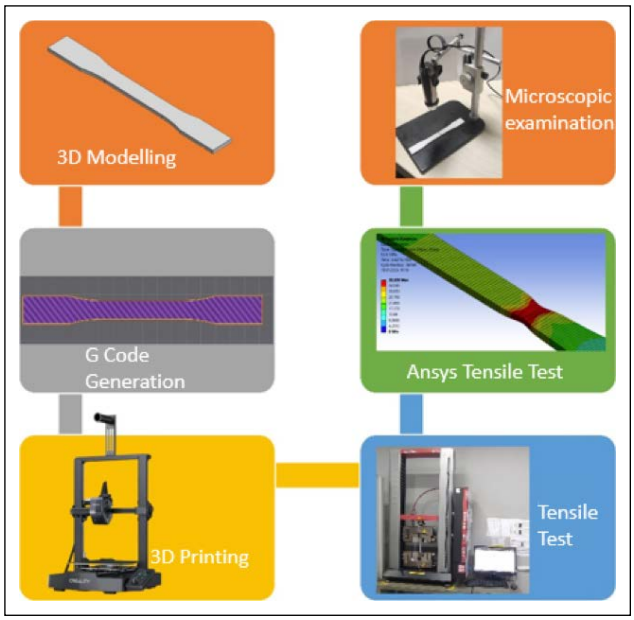

Figure 1. Workflow diagram.

G codes were obtained for the 3D modeled sample using the Creality Print slicing program. The slicing parameters prepared in the Creality Print program are listed in Table 1.

Samples with G codes were prepared using a 3D printer. The prints were obtained using a Creality brand Ender 3 V3 SE model 3D printer (origin: China) (Fig. 3).

Tensile tests of the samples were performed in accordance with the ASTM D638 standard on a Zwick/Roell Z010 tensile tester (Germany). The experimental setup for the tensile test is shown in Figure 4. Tensile tests were conducted at room temperature at a tensile speed of 5 mm/min. The Zwick/Roell Z010 tensile tester with a pneumatic gripper has a test height of 1050 mm, a maximum load capacity of 10 kN, and high-precision measurement with a deviation of 0.5%.

To validate the experimental data and avoid the need for further experiments in future studies, tensile tests were performed in a computer environment using Ansys 2024 R2. The Johnson-Cook material model was used to accurately reflect the plastic deformation and material behavior occurring in the tensile test. The Johnson-Cook material model is preferred in situations with high plastic deformation, such as machining, explosion, and impact. Table 2 shows the Johnson-Cook parameters for PLA material [36, 37].

Table 1. Slicing parameters

Parameters	Values	Unit
Filament type	PLA	
Infill pattern	Grille	
Infill density	100	%
Raster angle	45	°
Layer height	0.2	mm
Wall thickness	0.8	mm
Nozzle diameter	0.2	mm
Print temperature	190	°
Table temperature	50	°
Print speed	180	mm/s

PLA: Polylactic acid.

Table 2. Johnson-Cook parameters [38]

Johnson-Cook parameters	Values
Initial yield stress	40.16 MPa
Hardening constant	16.55 MPa
Hardening exponent	0.374
Strain Rate constant	0.05

Table 3. Information about the mesh structure

Properties	Value	Unit
Element Quality (Average)	0.96	
Element size	1	mm
Nodes	13040	
Elements	9234	

The boundary conditions and mesh structure defined in the Ansys program on the tensile test specimen are shown in Figure 5. The specimen was fixed in the blue section (A). A perpendicular displacement was applied to the specimen section in the yellow section (B). Information on the mesh structure is given in Table 3.

The mesh was generated using tetrahedral elements. The element type used in ANSYS Explicit Dynamics is SOLID168, a 10-node quadratic tetrahedron element suitable for large deformation and explicit analysis.

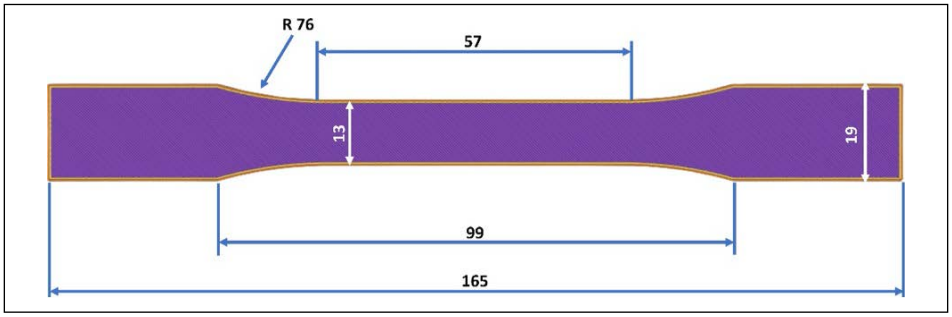

Figure 2. Sample dimensions according to ASTM D638 Type 1 standard.

Figure 3. Obtaining samples using a 3D printer.

A Dino-Lite brand digital microscope (origin Taiwan) was used to examine the fractured areas of the samples (Fig. 6). Images of the fractured areas were obtained using Dino-Lite software.

RESULTS AND DISCUSSION

Table 4 shows the experimental and FEA results of tensile tests performed on fully loaded samples made from PLA (polylactic acid) filament produced with a 3D printer. The table compares the tensile strength values obtained from the experimental and FEA.

According to the data in the table, both the experimental and FEA results are close to each other. Specifically, a tensile strength of around 38 MPa was observed. This reflects the expected mechanical properties of the PLA material. Furthermore, the Explicit Dynamics module used in the FEA is considered a suitable analysis for simulating the dynamic behavior of the material. The standard deviations of the experimental results were calculated according to Formula (1).

Table 4. Comparison of experimental and FEA tensile strength

	Experimental tensile strength values (MPa)	FEA tensile strength values (MPa)
PLA 1	34.845	38.639
PLA 2	37.943	38.639
PLA 3	38.445	38.639
PLA 4	38.126	38.639
Average	37.340	38.639

Table 5. Comparison of experimental and FEA yield strength

	Experimental yield strength values (MPa)	FEA yield strength values (MPa)
PLA 1	29.565	32.773
PLA 2	32.962	32.773
PLA 3	29.629	32.773
PLA 4	32.727	32.773
Average	31.221	32.773

FEA: Finite element analysis.

Standard deviation (σ) measures how far the data deviates from the mean. Its formula is:

$\sigma = \sqrt{[\Sigma(xi - \mu)^2 / N]}$ Formula (1)

Here:

σ: Standard deviation

xi: Each data point

μ: Average

N: Number of data

Confidence interval $= \mu \pm \left(t \times \frac{\sigma}{\sqrt{n-1}}\right)$ Formula (2)

Here:

μ: Sample mean

t: Degrees of freedom, df = n - 1

σ: Sample standard deviation

n: Sample size

$\frac{\sigma}{\sqrt{n}}$: Standard error

Experimental tensile strenght average ve standard deviation;

Average: 37.340

Standard Deviation: ≈ 1.676

Confidence interval (t-value (n=4, df=3. %95 confidence level) ≈ 34.673 MPa – 40.007 MPa

Margin of Error≈ 2.667%

The experimental tensile test results for PLA samples show a mean of 37.340 MPa and a standard deviation of 1.676 MPa, indicating consistent data. The 95% confidence interval ranges from 34.673 MPa – 40.007 MPa, suggesting that the true mean likely falls within this range. The margin of error of 2.667% indicates minimal deviation from the mean, confirming the reliability of the experimental results.

The tensile test FEA result is approximately 1.299 MPa higher than the experimental average, with an error rate of 3.48%. This indicates that the FEA exhibits little devia-

Figure 4. Tensile test experimental setup.

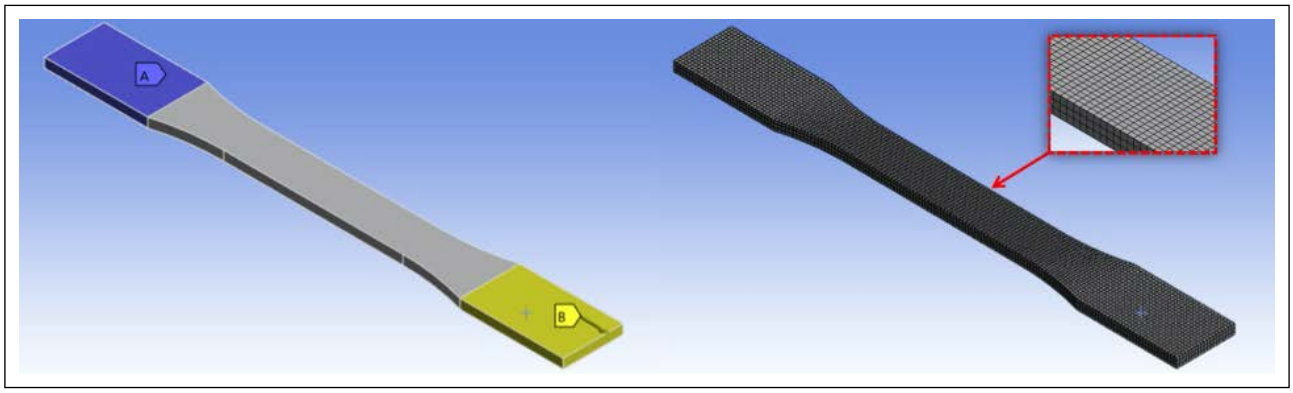

Figure 5. Boundary conditions and mesh image of the test sample.

tion compared to the experimental results and is generally consistent. This study, which used experimental and tensile FEA, achieved successful results in verifying the tensile strength of PLA materials using both experimental and numerical analysis. It can be said that the ANSYS Explicit Dynamics module offers a reliable approach in tensile test analyses, especially since the FEA results are in great agreement with the experimental results.

Table 5 shows the experimental and FEA yield strength results obtained from tensile tests on four different fully loaded samples produced from PLA filament using a 3D printer.

Yield strength represents the maximum stress a material can withstand before beginning plastic deformation and is measured here in MPa. Experiments revealed a yield strength of 30 MPa for PLA1 and PLA3, 33 MPa for PLA2 and PLA4. This suggests that differences between samples may be due to manufacturing or testing conditions. Based on Finite Element Analysis (FEA), the yield strength was calculated as a constant value of 32.773 MPa for all samples. The Finite Element Analysis (FEA) yield strength results are higher than the experimental results for PLA1, PLA3 and PLA4, but slightly lower than for PLA2. Overall, the differences are within an acceptable range (ranging from 0.14% to 10.85%), indicating that FEA is generally reliable, despite showing deviations in samples with manufacturing defects.

Experimental yield strength means and standard deviation values;

Average: 31.221 MPa

Standard Deviation: ≈ 1.877 MPa

Confidence Interval: 28.235 MPa-34.207 MPa

Margin of Error (percentage) ≈ 9.57 %

Yield strength standard deviation results show that the yield strength values of the samples vary from the mean by

Figure 6. Dino-Lite Digital microscope.

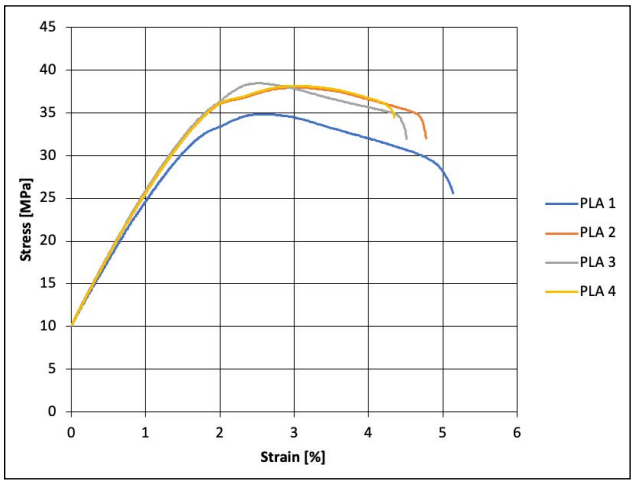

Figure 7. Experimental stress-strain curve.

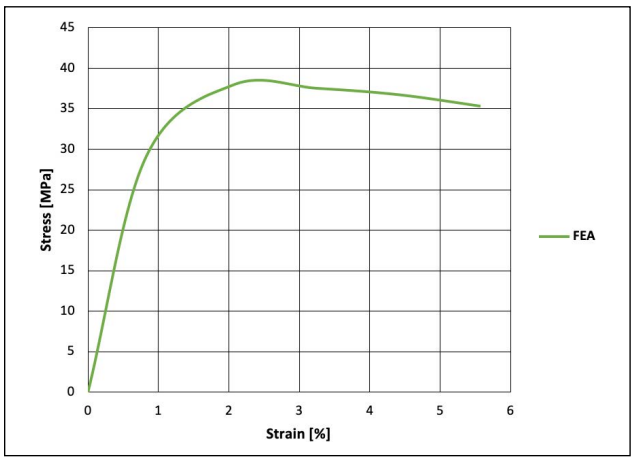

Figure 8. FEA stress-strain curve.

±1.877 MPa. The yield strength values clustered into two distinct groups (approx. 30 MPa and 33 MPa). The high consistency within these groups contributed to the reliable data distribution, despite the slight variation between the groups.The Margin of Error indicates a deviation of ±9.57% from the mean. This is acceptable for this type of experimental study. The confidence interval indicates that the average yield strength of the samples could be between 28.235 MPa and 34.207 MPa for the material. The margin of error indicates that the results are reliable with a moderate degree of deviation. The yield test FEA result is approximately 1.552 MPa higher than the experimental average, with an error rate of 4.97%. This indicates that the FEA exhibits little deviation compared to the experimental results and is generally consistent.

Figure 7 shows the experimentally obtained tensile test curves, and Figure 8 shows the tensile test curve obtained with FEA.

Figure 9 shows images of the fracture zones of PLA samples resulting from tensile tests. The fracture surface and surrounding deformation characteristics were analyzed for each sample. Polymeric materials such as PLA generally exhibit brittle fracture behavior; however, due to 3D printing layers, delamination or voids can occur at the fracture surface. The fracture surface of PLA1 appears rough. There is significant delamination between the layers, and small voids are observed at the fracture site. PLA1 exhibited lower tensile strength (34.845 MPa) and yield strength (29.565 MPa) than the other samples. The higher tensile strength of PLA2 indicates that the material has a more homogeneous structure and better stress distribution. The layer separation and voids seen in the PLA3 microscope image caused the sample to yield prematurely. However, its high tensile strength indicates that the material can sustain the stress for some time after yielding. This indicates that the sample has localized weaknesses in its internal structure but is generally durable. In PLA4, the microscope image shows strong interlayer bonds and minimal separation.

Layer separation seen in the microscope image indicates a weak bond within the sample's internal structure and insufficient fusion between layers. This can be caused by factors such as low temperature, rapid cooling, or insufficient extrusion during 3D printing. Furthermore, voids reduce the material's strength.

PLA is generally a brittle material, and the images show brittle fracture characteristics (irregular fracture surfaces, cracks) rather than ductile fracture. However, delamination (delamination) at the fracture surface due to the 3D printing layers plays a prominent role.

The FEA results (32.773 MPa for yield, 38.639 MPa for tensile) are generally higher than the experimental results. Microscope images show defects (voids, delamination) not considered in the FEA. These defects are the main reason why the experimental results are lower than the FEA results.

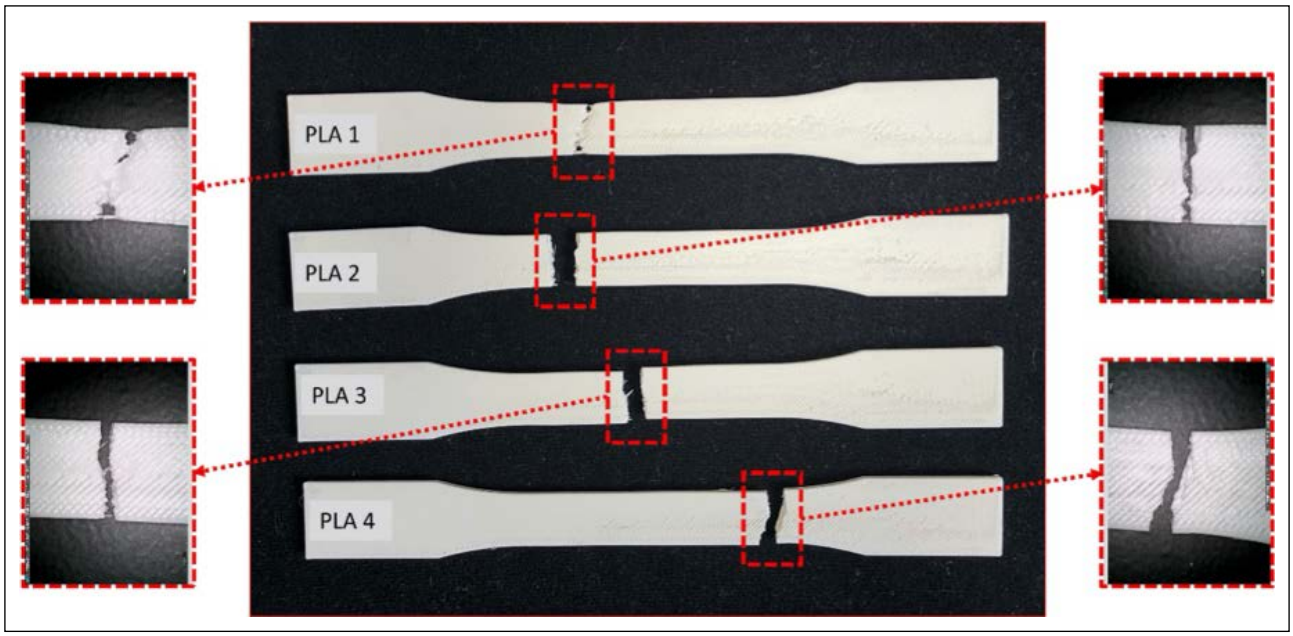

Figure 9. Experimental tensile strength resuts stereo microscop images.

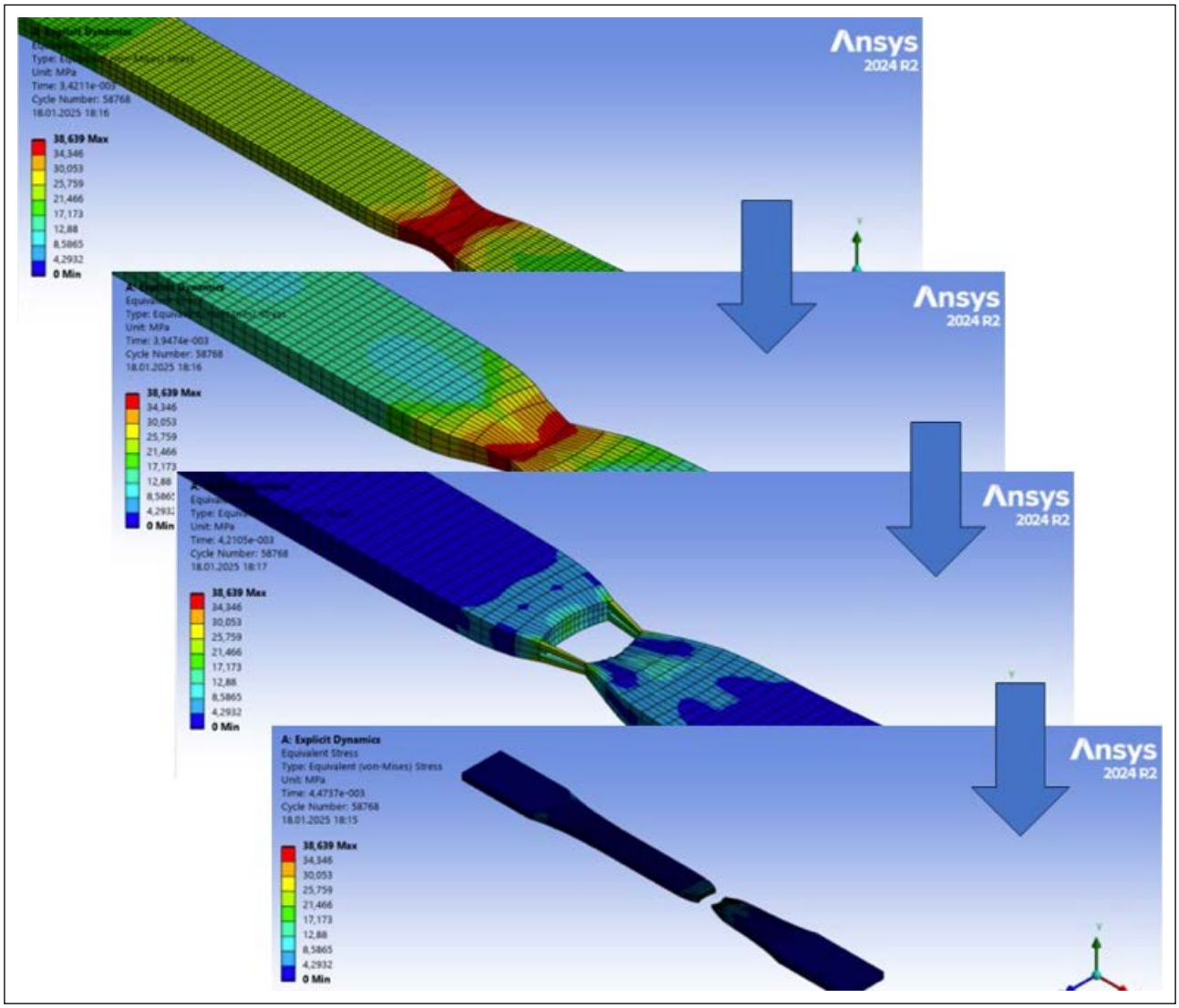

Figure 10. FEA image tensile strenght.

Figure 10 shows the stress distributions of the samples during tensile testing from FEA performed with ANSYS. The same model was used for all samples in the finite element analysis. In the color scale, blue regions represent low stress (0-5 MPa), and red regions represent high stress (36-38.639 MPa). The stress concentration is maximum in the central portion of the specimens (the contraction region), as expected in tensile testing. Fracture typically occurs in this region, where the stress is highest. The ANSYS images clearly show the stress concentration in the contraction region of the specimens. This confirms that the fracture occurred in this region in the microscope images.

The fracture characteristics observed in the PLA samples revealed brittle fracture characteristics in 3D printed PLA samples, with delamination, rough surfaces, and voids primarily resulting from interlayer bonding issues. These brittle fracture features and interlayer delamination observations are also in good agreement with the fracture surface analyses reported by Bacak et al. on FDM-printed PLA specimens produced with different process parameters and infill geometries [33, 34]. Tensile tests using digital image correlation on FDM-printed PLA samples reported similar rough fracture profiles and delamination, attributing these to manufacturing parameters such as infill density and printing speed. They noted a decrease in overall ductility and an increase in brittle behavior. This is consistent with our findings that voids and delamination led to premature yielding in PLA1 and PLA3, while PLA2 and PLA4 exhibited stronger bonds and higher strength. Furthermore, studies of tensile and fracture properties, influenced by parameters such as raster angle and layer height, demonstrate the dependence on print quality. Looking at the experimental and FEA results, the average tensile strength of 37.340 MPa and yield strength of 31.221 MPa are within the commonly reported ranges for 3D printed PLA. This has been seen in extensive characterizations of PLA composites, where variations infillers and additives yield similar mechanical properties. The low error rates between experimental and FEA results (2.667% for tensile strength, 4.97% for yield) support previous comparisons showing 2–6.7% deviations in yield and tensile strengths [18] and stress-strain curve fits with deviations below 5% for architectural cellular PLA composites. These fits validate the use of the Johnson-Cook model in Explicit Dynamics for high-deformation simulations and highlight the need to include microscopic defects such as voids in future FEA models.

CONCLUSION

The present study investigated the tensile behavior of 3D-printed PLA specimens produced with 100% infill according to ASTM D638 Type I standard using both experimental tests and finite element analysis with ANSYS Explicit Dynamics.

The key findings are as follows:

- The average experimental ultimate tensile strength was 37.340±1.676 MPa and the yield strength was 31.221±1.877 MPa.
- FEA using the Johnson–Cook material model in Explicit Dynamics module predicted an ultimate tensile strength of 38.639 MPa and a yield strength of 32.773 MPa, with deviations of 3.48% and 4.97%, respectively, from the experimental mean values.
- The Explicit Dynamics approach successfully simulated stress distribution and correctly predicted the fracture location in the gauge section.
- Microscopic examination of fracture surfaces revealed brittle fracture characteristics accompanied by interlayer delamination and voids, which explain the slightly lower experimental strengths compared to FEA results.

These results confirm that ANSYS Explicit Dynamics combined with the Johnson–Cook model is a reliable tool for predicting the tensile behavior of fully infilled 3D-printed PLA parts. The findings contribute to improving the confidence in using PLA in load-bearing applications through better understanding and optimization of printing parameters.

Data Availability Statement

The authors confirm that the data that supports the findings of this study are available within the article. Raw data that support the finding of this study are available from the corresponding author, upon reasonable request.

Author's Contributions

Yunus Zübeyir Turgut: Analysis, Writer, Data Collection, Critical Review.

Sıtkı Akıncıoğlu: Supervision, Conseption, Writer, Design.

Gülşah Akıncıoğlu: Literatür Review, Writer, Critical Review.

Conflict of Interest

The authors declared no potential conflicts of interest with respect to the research, authorship, and/or publication of this article.

Statement on the Use of Artificial Intelligence

The authors acknowledge the use of Scite for assistance in drafting parts of the introduction and ensuring language clarity.

Ethics

There are no ethical issues with the publication of this manuscript.

REFERENCES

[1] Chadha, U., Abrol, A., Vora, N. P., Tiwari, A., Shanker, S. K., & Selvaraj S. (2022). Performance evaluation of 3D printing technologies: a review, recent advances, current challenges, and future directions. *Progress in Additive Manufacturing, 7*(5), 853-886. [CrossRef]

[2] Aslan, E., & Akıncıoğlu, G. (2024). Investigation of the wear and friction profile of TPU-based polymers at different infill ratios. *International Journal of Automotive Science and Technology, 8*(1), 125-131. [CrossRef]

[3] Akıncıoğlu, G., Şirin E., & Aslan, E. (2023). Tribological characteristics of ABS structures with different infill densities tested by pin-on-disc. *Proceedings of the Institution of Mechanical Engineers, Part J: Journal of Engineering Tribology, 237*(5), 1224-1234. [CrossRef]

[4] Shahrubudin, N., Lee, T. C., & Ramlan, R. J. P. (2019). An overview on 3D printing technology: Technological, materials, and applications. *Procedia Manufacturing, 35*, 1286-1296. [CrossRef]

[5] Iftekar, S. F., Aabid, A., Amir, A., & Baig, M. (2023). Advancements and limitations in 3D printing materials and technologies: a critical review. *Polymers, 15*(11), Article 2519. [CrossRef]

[6] Toktaş, I., & Akıncıoğlu, S. (2025). Investigation of tribological properties of industrial products with different patterns produced by 3D printing using polylactic acid. *Rapid Prototyping Journal, 31*(2), 371-378. [CrossRef]

[7] Jiménez, L., Mena, M. J., Prendiz, J., Salas, L., & Vega-Baudrit, J. (2019). Polylactic acid (PLA) as a bioplastic and its possible applications in the food industry. *Journal of Food Science&Nutrition, 5*(2), 2-6. [CrossRef]

[8] Abd Alsaheb, R. A., Aladdin, A., Othman, N. Z., Abd Malek, R., Leng, O. M., Aziz, R., & El Enshasy, H. A. (2015). Recent applications of polylactic acid in pharmaceutical and medical industries. *Journal of Chemical and Pharmaceutical Research, 7*(12), 51-63.

[9] Avinc, O., & Khoddami, A. (2009). Overview of poly (lactic acid)(PLA) fibre: Part I: production, properties, performance, environmental impact, and end-use applications of poly (lactic acid) fibres. *Fibre Chemistry, 41*(6), 391-401. [CrossRef]

[10] Arockiam, A. J., Subramanian, K., Padmanabhan, R. G., Selvaraj R., Bagal D. K., & Rajesh S. (2022). A review on PLA with different fillers used as a filament in 3D printing. *Materials Today: Proceedings, 50*(5), 2057-2064. [CrossRef]

[11] Hussain, M., Maqsood Khan, S., Shafiq, M., & Abbas, N. (2024). A review on PLA-based biodegradable materials for biomedical applications. *Giant, 18*, Article 100261. [CrossRef]

[12] Aslan, E., & Akıncıoğlu, G. (2026). *3D printing in automotive component development*, in Sustainable Composites for Automotive Engineering (p. 321-338). Elsevier. [CrossRef]

[13] Şirin, Ş., Aslan, E., & Akincioğlu, G. (2023). Effects of 3D-printed PLA material with different filling densities on coefficient of friction performance. *Rapid Prototyping Journal, 29*(1), 157-165. [CrossRef]

[14] Akıncıoğlu, G., & Aslan, E. (2021). Investigation of tribological properties of amorphous thermoplastic samples with different filling densities produced by an additive manufacturing method. *Gazi Journal of Engineering Sciences, 8*(3), 540-546. [CrossRef]

[15] Pezer, D., Vukas, F., & Butir, M. (2022). Experimental study of tensile strength for 3D printed specimens of HI-PLA polymer material on in-house tensile test machine. *Technium, 4*(1), 197-206. [CrossRef]

[16] Ayrilmis, N., Kariz, M., Heon Kwon, J., & Kuzman, M. K. (2019). Effect of printing layer thickness on water absorption and mechanical properties of 3D-printed wood/PLA composite materials. *The International Journal of Advanced Manufacturing Technology, 102*(5), 2195-2200. [CrossRef]

[17] Anand Kumar, S., & Shivraj Narayan, Y. (2019). Tensile testing and evaluation of 3D-printed PLA specimens as per ASTM D638 type IV standard. In *Innovative Design, Analysis and Development Practices in Aerospace and Automotive Engineering (I-DAD 2018) Volume 2*. Chennai, India. [CrossRef]

[18] Alharbi, M., Kong, I., & Patel, V. I. (2020). Simulation of uniaxial stress-strain response of 3D-printed polylactic acid by nonlinear finite element analysis. *J Applied Adhesion Science, 8*(5), 1-10. [CrossRef]

[19] Özmen, Ö., Sürmen, H. K., & Sezgin A. (2023). The effect of infill pattern in 3-dimensional printing on tensile strength. *Journal of Engineering Sciences and Design, 11*(1), 336-348. [CrossRef]

[20] Ganeshkumar, S., Dharani Kumar, S., Magarajan, U., Rajkumar, S., Arulmurugan, B., Sharma, S., Li, C., Ilyas, R. A., & Badran, M. F. (2022). Investigation of tensile properties of different infill pattern structures of 3D-printed PLA polymers: analysis and validation using finite element analysis in ANSYS. *Materials, 15*(15), Article 5142. [CrossRef]

[21] Harpool, T. D., Alarifi, I. M., Alshammari, B. A., Aabid, A., Baig, M., Malik, R. A., Sayed, AM., Asmatulu, R., & Ali EL-Bagory, T. M. A. (2021). Evaluation of the infill design on the tensile response of 3D printed polylactic acid polymer. *Materials, 14*(9), Article 2195. [CrossRef]

[22] Auffray, L., Gouge, P.-A., & Hattali, L. (2022). Design of experiment analysis on tensile properties of PLA samples produced by fused filament fabrication. *The International Journal of Advanced Manufacturing Technology, 118*, 4123-4137. [CrossRef]

[23] Brischetto, S., & Torre, R. (2020). Tensile and compressive behavior in the experimental tests for PLA specimens produced via fused deposition modelling technique. *Journal of Composites Science, 4*(3), Article 140. [CrossRef]

[24] Evlen, H., Özdemir, M. A., & Çalışkan, A. (2019). Effects of filling percentage on mechanical properties of PLA and PET materials. *Journal of Polytechnic, 22*(4), 1031-1037. [Turkish] [CrossRef]

[25] Kamer, M. S., Temiz, Ş., Yaykaşlı, H., Kaya, A., & Akay, O. E. (2022). Comparison of mechanical properties of tensile test specimens produced with ABS and PLA material at different printing speeds in 3D printer. *Journal of the Faculty of Engineering Architecture of Gazi University, 37*(3), 1197-1211. [CrossRef]

[26] Aloyaydi, B., Sivasankaran, S., &. Mustafa, A. (2020). Investigation of infill-patterns on mechanical response of 3D printed poly-lactic-acid. *Polymer Testing, 87*, Article 106557. [CrossRef]

[27] Klossa, C. M., Chatzidai, N., & Karalekas, D. (2023). Tensile properties of 3D printed carbon fiber reinforced nylon specimens. *Materials Today: Proceedings, 93*, 571-574. [CrossRef]

[28] Öztürk, F. H., Marques, E. A. S., Carbas, R. J. C., & da Silva, L. F. M. (2024). Experimental and numerical study on mechanical behavior of 3D printed adhesive joints with polycarbonate substrates. *Journal of Applied Polymer Science, 141*(29), Article e55657. [CrossRef]

[29] Bacak, S. (2022). Investigation of the tensile strength properties of samples produced using different parameters from ABS, PLA, TPU(Flex) materials. *Journal of Yekarum, 7*(2), 58-64.

[30] Alarifi, I. M. (2023). Mechanical properties and numerical simulation of FDM 3D printed PETG/carbon composite unit structures. *Journal of Materials Research Technology, 23*, 656-669. [CrossRef]

[31] Akhoundi, B., Behravesh, A. H., & Bagheri Saed, A. (2019). Improving mechanical properties of continuous fiber-reinforced thermoplastic composites produced by FDM 3D printer. *Journal of Reinforced Plastics Composites, 38*(3), 99-116. [CrossRef]

[32] Shakor, P., Sanjayan, J., Nazari, A., & Nejadi, S. (2017). Modified 3D printed powder to cement-based material and mechanical properties of cement scaffold used in 3D printing. *Construction Building Materials, 138*, 398-409. [CrossRef]

[33] Bacak, S., Özkavak, H. V., & Sofu, M. M. (2021). Comparison of Mechanical Properties of 3D-Printed Specimens Manufactured Via FDM with Various Inner Geometries. *Journal of the Institute of Science and Technology, 11*(2), 1444-1454. [CrossRef]

[34] Bacak, S., Özkavak, H. V., & Tatlı, M. (2021). Investigation of the effect of processing parameters on tensile properties of PLA samples produced by FDM method. *Mühendislik Bilimleri ve Tasarım Dergisi, 9*(1), 209-216. [Turkish]. [CrossRef]

[35] Sola, A., Chong, W. J., Simunec, D. P., Li, Y., Trinchi, Y., Kyraatzis, I. L., & Wen, C. (2023). Open challenges in tensile testing of additively manufactured polymers: A literature survey and a case study in fused filament fabrication. *Polymer Testing, 117*, 107859. [CrossRef]

[36] Sirigiri, V.K.R., Gudiga, V. Y., Gattu, U. S., Suneesh, G., & Buddaraju, K. M. (2022). A review on Johnson Cook material model. *Materials Today: Proceedings, 62*, 3450-3456. [CrossRef]

[37] Burley, M., Campbell, J. E., Dean, J., & Clyne, T. W. (2018). Johnson-Cook parameter evaluation from ballistic impact data via iterative FEM modelling. *International Journal of Impact Engineering, 112*, 180-192. [CrossRef]

[38] Pyka, D., Słowiński, J. J., Kurzawa, A., Roszaki, M., Stachowicz, M., Kazimierczak, M., Stępczak, M., & Grygier, D. (2024). Research on basic properties of polymers for fused deposition modelling technology. *Applied Sciences, 14*(23), Article 11151. [CrossRef]